The internal structure of α-accretion discs

A thesis submitted to

The University of Leicester

for the degree of

Doctor of Philosophy

by

Daniel Anthony Westwood Heron BSc (Durham)

Department of Physics & Astronomy

University of Leicester

August 1997

ProQuest LLC
789 East Eisenhower Parkway
P.O. Box 1346
Ann Arbor, MI 48106-1346

D.A.W.Heron

The internal structure of α-accretion discs

Abstract

In this thesis we develop a mathematical model to describe the internal structure of an α-accretion disc. The method is to consider the standard thin disc as a zero order approximation to a disc with vertical structure. The order of the approximation is controlled by the parameter $1/M^2$, where M is the Mach number of the azimuthal flow at a fiducial point. The theory is developed analytically as far as possible, using numerical solutions for the final system of ordinary differential equations only.

The model expands upon the work of other authors by assuming a disc surface defined by the condition of pressure balance between the disc and its environment. Vertically transported angular momentum is extracted by coupling to these surroundings. In the absence of an external couple, the vertical transport of angular momentum is ignored, as in the standard thin disc.

The internal structure and stability of the disc is investigated in both the gas and radiation pressure dominated regions, and the effects of including vertical transport of angular momentum is discussed. An application of the disc model is presented whereby external heating from X-rays associated with a radio jet are shown to induce mass loss from the disc surface. Such a configuration may undergo symmetry breaking to an asymmetric state in which one jet dominates. This is therefore a possible model for intrinsically one-sided radio sources.

Acknowledgements

I would like to thank Derek Raine for his supervision over the last three years and Ted Thomas for his input during the early stages of the project. I acknowledge the receipt of a SERC studentship and the use of STARLINK facilities. Additional thanks are due to Andrew King, Gordon Stewart and Juhan Frank for useful discussions.

My time in Leicester would not have been the same without the company of Norma, Ray, my fellow shunned and despised members of the Underpass, crosswords, Treasure, homepages, talkers, ghostbusting and planetarium wars with Ken.

I would like to thank my family for their help and encouragement. Finally, this work would not have been completed without the consistent support and patience of Janine Westwood. Thank you Janine for everything.

Contents

Chapter One

Accretion discs

1.1 Introduction

Active galactic nuclei (AGN) are the most luminous objects in the known Universe. Accretion of matter on to a supermassive black hole ($\sim 10^8 M_0$) is widely believed to be the source of power for this enormous outflow of radiation ($\sim 10^{46} erg\, s^{-1}$) (c.f. Frank et al., 1992). For galactic material to accrete on to the black hole it must lose its angular momentum. The most efficient way to achieve this is by the formation of an accretion disc.

Accretion discs around black holes are of special interest because the disc radiation seems to be the basic observational effect of black holes (Shakura & Sunyaev, 1973; Novikov & Thorne, 1973; Lynden-Bell & Pringle, 1974). Therefore, analysis of the disc structure as well as the disc radiation is of great importance. The pioneering work on disc accretion was done in the early 1970's and in 1973 Shakura and Sunyaev produced what is now the standard model in describing accretion discs. This is known as the *thin disc model* (Shakura & Sunyaev, 1973).

1.2 The thin disc model

Galactic material will orbit a supermassive black hole as a ring of matter with Keplerian motion. Within the ring dissipative processes, such as viscous dissipation and particle collisions, will convert some of the material's energy into internal, heat energy. In due course, a fraction of this energy will radiate

away and the material will move closer to the gravitational source, requiring it to lose angular momentum. As a Kepler orbit has the least energy for a given angular momentum, it is efficient for the material to move towards the black hole in a series of near Kepler orbits. In this way an accretion disc is formed. In many cases the material lies mainly close to the orbital plane and the disc can be thought of as two-dimensional. This is the thin disc approximation.

In cylindrical co-ordinates (R,ϕ,z) the material lies close to $z=0$ and circles the central black hole with an approximate Kepler orbit

$$\Omega=\Omega_K(R)=(\frac{GM}{R})^{1/2}. \tag{1.1}$$

The material is also assumed to have a small radial 'drift' velocity υ_R that is negative near the black hole so that matter is accreted. This radial velocity comes about because of the dissipative processes active in the disc. One of the main problems in the theory of disc accretion is the exact nature of the dissipative mechanisms that transport angular momentum within the disc.

1.2.1 The viscous mechanism

Within an accretion disc only a fraction of the gravitational energy of the infalling matter can be transformed into orbital kinetic energy: this fraction is $1/2$ when the rotation is exactly Keplerian. Since the remainder cannot be stored in a stationary disc, it must leave the system, and this can only be achieved through radiation. The same conclusion may be drawn from the virial theorem. To summarise, the extra energy must be converted into heat in order to be radiated into space.

Turbulent motions between fluid particles on neighbouring orbital flowlines are usually assumed to be the mechanism that transports angular momentum by viscous shearing. Unfortunately, no rigorous theory exists to

describe the mutual interaction of random and average quantities in turbulent flows. Hence the description of turbulence in the accretion disc seems to be rather approximate.

The turbulent viscosity can be written in terms of the velocity $\tilde{\upsilon}$ and the size λ of the largest viscous 'eddy' that can effectively participate in the energy dissipation:

$$\nu = \tilde{\upsilon}\lambda . \tag{1.2}$$

Since the largest eddies ought to be smaller than the disc scale-height H (i.e. $\lambda \leq H$), and the speed of the turbulent motion is not likely be supersonic, then (1.2) can be rewritten as

$$\nu = \alpha c_s H . \tag{1.3}$$

This is the well-known α-prescription first defined by Shakura & Sunyaev, (1973). This parameterization means that the dissipation of the extra energy can be achieved by turbulence that remains subsonic, and our ignorance of the viscous mechanism can be hidden in the constant $\alpha \leq 1$.

It is useful to define a viscous timescale $t_{visc} \sim R / \upsilon_R \sim R^2 / \nu$ over which changes in the radial structure will occur. In most systems studied, external conditions change on much longer timescales. Therefore the disc will settle down to a steady state structure. This simplifies the calculation of the disc structure.

1.2.2 The local structure of thin discs

To investigate the internal structure of the thin disc, the Euler equation for the conservation of momentum in a fluid is used

$$\rho\frac{\partial \underline{v}}{\partial t}+\rho \underline{v}.\underline{\nabla v}=-\nabla P+\underline{f}. \tag{1.4}$$

Here $\underline{f}$ specifies forces other than pressure gradients acting upon the fluid; in this case important contributions arise from the gravitational force of the central object and viscosity.

First the vertical structure of the disc. If the disc is thin (i.e. $z << R$), then any vertical flow will be small. Therefore, the vertical component of (1.4) reduces to hydrostatic equilibrium:

$$\frac{1}{\rho}\frac{\partial P}{\partial z}=-\frac{GMz}{R^3}. \tag{1.5}$$

Using $P=\rho c_s^2$ for a perfect gas, where c_s is the sound speed, equation (1.5) can be integrated to give

$$\rho(R,z)=\rho_c(R)\exp(-z^2/2H^2) \tag{1.6}$$

where $\rho_c(R)$ is the density on the centre line $z=0$, and H is the scale height of the disc in the z-direction defined by

$$H=c_s(\frac{R}{GM})^{1/2}R. \tag{1.7}$$

By investigating the viscous torques in the disc it can be shown that the radial velocity $\upsilon_R \sim \nu/R$. When the α-prescription is adopted to describe the viscosity this becomes

$$\upsilon_R \sim \alpha c_s H/R. \tag{1.8}$$

In deriving the equations (1.6)-(1.8) it was assumed that the disc was thin (i.e. $H << R$). Therefore to check self-consistency it necessary to insist that, from (1.7), the local Kepler velocity is highly supersonic

$$c_s << (\frac{GM}{R})^{1/2} \tag{1.9}$$

and, from (1.8), that the radial velocity is highly sub-sonic.

If the thin disc approximations hold, calculating the disc structure becomes relatively easy, as Shakura & Sunyaev (1973) showed. The radial and vertical structures within the disc decouple because the pressure and temperature gradients are basically vertical. Therefore each radial component can be treated separately and its vertical structure determined. Each radial part is related to another by the local energy generation rate $D(R)$ only.

The sound speed is give by

$$c_s^2 = dP / d\rho \tag{1.10}$$

where the total pressure in the disc is the sum of gas and radiation pressures:

$$P = \frac{\rho k T_c}{\mu m_p} + \frac{4\sigma}{3c} T_c^4 . \tag{1.11}$$

It is assumed that the temperature $T(R,z)$ is close to the central temperature $T_c(R)$.

There should be an energy equation that relates the vertical transport of energy flux to the rate of energy generation by the viscous dissipation. This vertical transport mechanism can be either radiative or convective depending on whether or not the temperature gradient required for radiative transport is smaller or greater than the gradient given by the adiabatic assumption

$P\rho^{-\gamma} = const.$ where γ is the ratio of specific heats. If the disc is optically thick, in that, if each element of the disc face radiates as a blackbody, i.e.

$$\tau = \rho H \kappa_R(\rho, T_c) >> 1, \tag{1.12}$$

the flux of radiant energy through a surface z-constant is given by

$$F(z) = -\frac{16\sigma T^3}{4\kappa_R \rho}\frac{\partial T}{\partial z}. \tag{1.13}$$

κ_R is the Rosseland mean opacity. Once the optical depth of the disc material $\tau \leq 1$, it is optically thin, equation (1.13) breaks down and the radiation can escape directly.

The energy balance equation gives the volume rate of energy production by viscous dissipation Q^+ as

$$Q^+ = \frac{\partial F}{\partial z}. \tag{1.14}$$

Integrating therefore gives the dissipation rate per unit face area $D(R)$

$$F(H) - F(0) = \int_0^H Q^+(z)dz = D(R). \tag{1.15}$$

If the rotation of the disc is exactly Keplerian then half of the disc's gravitational energy will be dissipated. Thus, $D(R)$ can be calculated

$$D(R) = \frac{3GM\dot{M}}{8\pi R^3}[1 - (\frac{6GM}{Rc^2})^{1/2}]. \tag{1.16}$$

where $\dot{M}$ is the accretion rate in the disc

$$\dot{M} = 2\pi R\Sigma(-\upsilon_R) \qquad (1.17)$$

(remembering that $\upsilon_R < 0$) and Σ is the disc's surface density. The last term on the right of (1.16): $[1-(\frac{6GM}{Rc^2})^{1/2}]$, comes from the inner boundary condition. This states that the viscous torque vanishes at three Schwarzschild radii, which is the last stable orbit for a Schwarzschild black hole.

The important thing to note is that the energy flux through the face of the disc is independent of viscosity. $D(R)$ is an observationally measurable quantity, and our ignorance of the viscosity mechanism is hidden by the fact that υ adjusts itself to give the correct $\dot{M}$.

From (1.13) and (1.12) an alternative expression for the emitted flux can be obtained

$$F(z) \sim (\frac{4\sigma}{3\tau})T^4(z). \qquad (1.18)$$

Assuming that $T_c^4 >> T^4(H)$ equation (1.18) can be equated with (1.15) to give the thin disc energy equation

$$\frac{4\sigma}{3\tau}T_c^4 = D(R). \qquad (1.19)$$

1.2.3 The thin disc equations

Using the equations of §1.2.2, a complete set of thin disc equations can be derived (see Frank et al., 1992 for full details).

$$H = c_s(\frac{R}{GM})^{1/2}R$$

$$c_s^2 = P/\rho$$

$$P = \frac{\rho kT_c}{\mu m_p} + \frac{4\sigma}{3c}T_c^4$$

$$\frac{4\sigma}{3\tau}T_c^4 = \frac{3GM\dot{M}}{8\pi R^3}[1-(\frac{6GM}{Rc^2})^{1/2}] \tag{1.20}$$

$$\tau = \rho H \kappa_R(\rho, T_c)$$

$$\nu\rho H = \frac{\dot{M}}{3\pi}[1-(\frac{6GM}{Rc^2})]$$

$$\nu = \nu(\rho, T_c, \alpha, ...)$$

The disc structure can now be solved for the seven unknowns ρ, H, c_s, P, T_c, τ and ν.

1.3 The thin disc solution

To obtain the standard thin disc model derived by Shakura & Sunyaev (1973), the equations from the previous section are solved using the α-prescription (1.3) for viscosity, and by specifying the opacity function. Equation (1.13) assumes that the disc is optically thick and radiates flux as a blackbody. In the regions of the disc where this holds the source of opacity is dominated by absorption. For pure hydrogen and free-free processes the Rosseland mean opacity is best approximated by Kramers' law

$$\kappa_R = 6.6\times10^{22}\rho T_c^{-7/2}\ cm^2 g^{-1}. \tag{1.21}$$

It is also assumed that in this region the gas pressure term in (1.11) will dominate and so the radiation pressure term is dropped. The assumptions made here will be tested later.

Taking $\mu = 0.615$ for a fully ionizes mixture of gases, and $\Sigma = \rho H$, the Shakura - Sunyaev disc solutions are (Frank et al., 1992)

$$\Sigma = 5.2\times10^6 \alpha^{-4/5} \dot{M}_{26}^{2/10} M_8^{1/4} R_{14}^{-3/4} f^{14/5}\ g\ cm^{-2}$$

$$H = 1.7\times10^{11} \alpha^{-1/10} \dot{M}_{26}^{3/10} M_8^{-3/8} R_{14}^{9/8} f^{7/5}\ cm$$

$$\rho = 3.1\times10^{-5}\alpha^{-7/10}\dot{M}_{26}^{11/20} M_8^{5/8} R_{14}^{-15/8} f^{11/5} g\ cm^{-3}$$

$$T_c = 1.4\times10^{6}\alpha^{-1/5}\dot{M}_{26}^{3/10} M_8^{1/4} R_{14}^{-3/4} f^{6/5} K \qquad (1.22)$$

$$\tau = 3.3\times10^{3}\alpha^{-4/5}\dot{M}_{26}^{1/5} f^{4/5}$$

$$\nu = 1.8\times10^{18}\alpha^{4/5}\dot{M}_{26}^{3/10} M_8^{-1/4} R_{14}^{3/4} f^{6/5}\ cm^2\ s^{-1} s^{-1}$$

$$\upsilon_R = 2.7\times10^{4}\alpha^{4/5}\dot{M}_{26}^{3/10} M_8^{-1/4} R_{14}^{-1/4} f^{-14/5}\ cm\ s^{-1}$$

with $f = 1-(6GM/Rc^2)^{1/2}$. As mentioned above, this takes the last stable orbit for a Schwarzschild black hole as the inner radius. It is encouraging that the quantities are reasonably insensitive to the particular value of α, although this means that it will be difficult to predict the size of α by comparing this model with observations.

It is now possible to check the assumptions made earlier. Kramers' opacity was used and from (1.21) this becomes

$$\kappa_R(Kramers) = 6.3\times10^{-4}\dot{M}_{26}^{-1/2} M_8^{-1/4} f^{-2}\ cm^2\ g^{-1}. \qquad (1.23)$$

For an ionized gas in the inner regions of the disc electron scattering becomes an important source of opacity:

$$\kappa_R(electron\ scattering) \cong \sigma_T / m_p \cong 0.4\ cm^2\ s^{-1}. \qquad (1.24)$$

Therefore using (1.22) it is clear that Kramers' opacity dominates over electron scattering if

$$R \geq 5.4\times10^{17}\dot{M}_{26}^{2/3} M_8^{1/3} f^{8/3}\ cm. \qquad (1.25)$$

Turning to the disc pressure, (1.22) shows that the ratio of radiation to gas pressure is

$$\frac{P_r}{P_g} = 2.7\alpha^{1/10}\dot{M}_{26}^{7/20} M_8^{1/8} R_{14}^{-3/8} f^{7/5} \tag{1.26}$$

which is small over the region that (1.25) holds. In fact radiation pressure becomes even more important when electron scattering dominates the opacity. Shakura & Sunyaev (1973) show that radiation pressure exceeds gas pressure at radii

$$R \leq 5.2\times 10^{14}\alpha^{8/30}\dot{M}_{26}^{14/15} M_8^{1/3} f^{56/15}\, cm. \tag{1.27}$$

Therefore, this disc can actually be split into three distinct zones. Zone A where the radiation pressure P_r is dominant and opacity is determined by electron scattering, zone B where the gas pressure P_g plays the main role and electron scattering gives the main contribution to the opacity, and zone C where $P_g > P_r$ and opacity is determined using Kramers' equation (1.21).

1.4 The disc spectrum

In the last section, solutions were found for the thin disc equations in zone C: gas pressure dominant with opacity given by free-free transitions. In deriving the energy equation (1.13) it was an important assumption that the disc was optically thick in the z-direction. If this holds then each element of the disc face radiates roughly as a blackbody with a temperature $T(R)$, where

$$\sigma T^4(R) = D(R). \tag{1.28}$$

Therefore using (1.16):

$$T(R) = \left(\frac{3GM\dot{M}}{8\pi R^3\sigma}[1-(\frac{6GM}{Rc^2})^{1/2}]\right)^{1/4}. \tag{1.29}$$

Now, the emitted spectrum from each element of the area of the disc can be approximated as

$$I_\nu = B_\nu[T(R)] = \frac{2h\nu^3}{c^2(e^{h\nu/kT(R)}-1)} \ (erg\,s^{-1}\,cm^{-2}\,Hz^{-1}\,sr^{-1}). \tag{1.30}$$

This approximation neglects any contribution or effect from the atmosphere of the disc (i.e. regions of the disc that are optically thin, $\tau \leq 1$) in redistributing the radiation over the frequency ν. For an observer at a distance D whose line of sight makes an angle i to the normal to the disc plane, the flux at frequency ν from the disc is

$$F_\nu = \frac{2\pi \cos i}{D^2}\int_{R_*}^{R_{out}} I_\nu R dR \tag{1.31}$$

where R_{out} is the outer radius of the disc. Using the blackbody assumption (1.30) this becomes

$$F_\nu = \frac{4\pi \cos i \nu^3}{c^2 D^2}\int_{R_*}^{R_{out}} \frac{RdR}{e^{h\nu/kT(R)}-1}. \tag{1.32}$$

Once again it is worth noting that the flux (an observable quantity) is independent of the disc viscosity. The expression obtained for the flux emitted from the disc surface (1.32) is a product of a steady-state disc, in the region where the conditions for zone C are valid, assuming that it is optically thick. Even though this gives a somewhat simplified picture of the disc structure, the spectrum from (1.32) should give a crude representation of the observed spectrum for some systems.

The spectrum given by (1.32) is shown in figure 1. The spectrum of the disc as a whole varies as $F_\nu \propto \nu^{1/3}$ until it peaks at a frequency that corresponds to the maximum effective temperature. At greater frequencies there is an

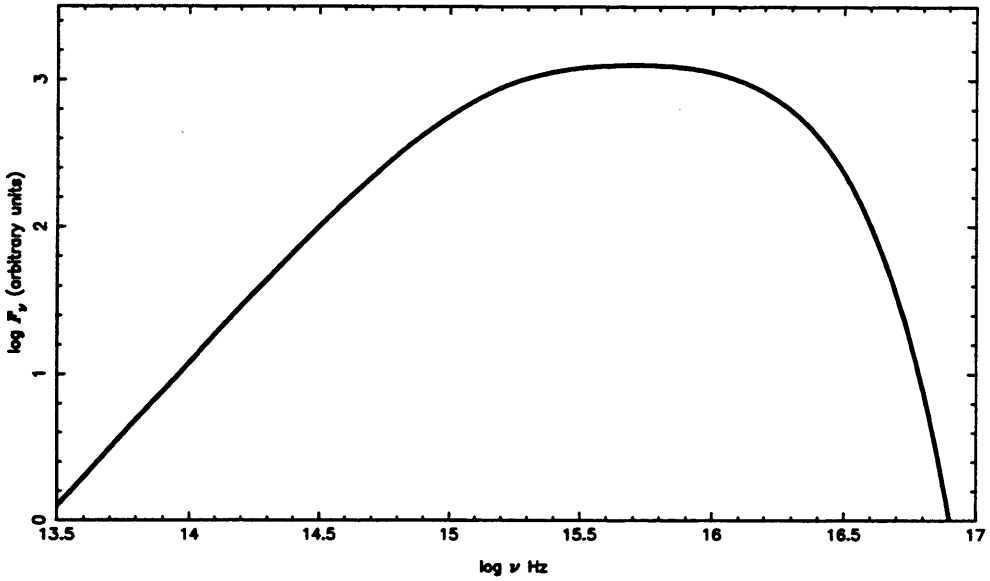

Figure 1
The continuum spectrum F_ν of a steady optically thick accretion disc radiating locally as a blackbody.

exponential cut-off where F_ν declines rapidly as a Wien law. For massive black holes, the maximum temperature from the optically thick area of the disc is situated in the UV region of the electromagnetic spectrum.

1.5 AGN spectra and the accretion disc

Having developed an emission spectrum for the standard thin disc, the next step is to see if this can be linked to the observed spectrum of an AGN. This will provide evidence that accretion discs are the primary source of power in AGNs.

The strongest evidence for the existence of accretion discs in AGN is the spectral feature called the UV-bump. Figure 2 shows the spectral distribution of AGN. It can be divided up into three parts: an infrared bump, a UV-bump (blue bump), separated by a gap at about $1\mu m$, and a X-ray power law continuum with a positive index. The $1\mu m$ gap is probably due to the superposition of two different components dominating respectively the infrared and UV emission

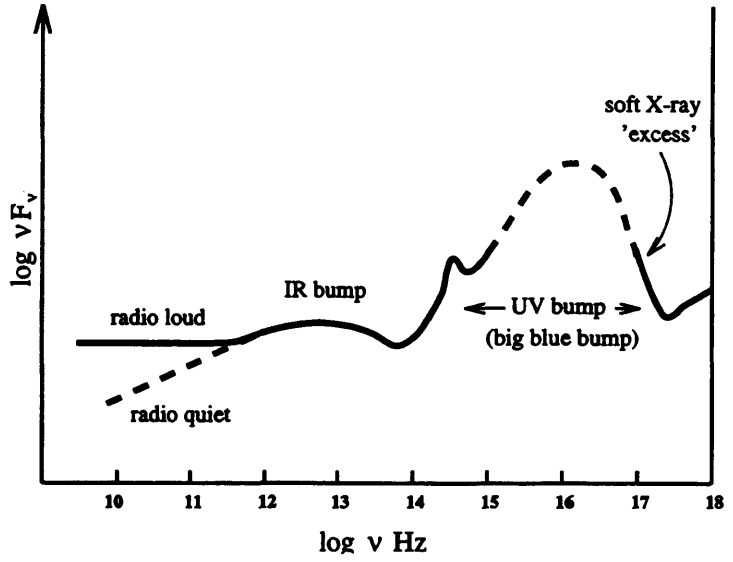

Figure 2
Schematic AGN spectrum

and fading at 1μm (Elvis et al., 1986). The optical-UV flux varies by factors of two or more in time scales of weeks for Seyfert galaxies and of months for quasars. These timescales correspond to a dimension for the emitting region of smaller than, or of the order of $1000R_s$, where R_s is the Schwarzschild radius of the central black hole. The variation timescales are smaller in the X-ray region, suggesting a smaller dimension for the emitting region. Variations of the infrared flux above a few microns have not credibly been detected so far.

1μm is the minimum wavelength at which hot dust just below the sublimation temperature can radiate. Therefore the infrared bump is often attributed to dust thermal radiation reprocessed from the central UV source. However, this is a controversial problem and an infrared synchrotron power law continuum is not dismissed by the observations (Collin-Souffrin, 1994).

Although the EUV is not observed, it can be guessed from the shape of the soft X-ray continuum that νf_ν reaches its maximum between 10 and 100 eV. Indeed the slope of the soft X-ray continuum is strongly negative, which translates into the so-called soft X-ray excess (Arnaud et al., 1985).

The UV-bump

Once the Broad Line emission has been subtracted from the optical-UV spectrum, the UV bump appears as a smooth continuum increasing towards small wavelengths. Two thermal mechanisms can give rise to such a featureless and increasing continuum: an optically thin gas radiating mainly by free-free processes, or an optically thick gas radiating as a blackbody.

- Optically thin free-free emission

  This has been invoked by various authors (e.g. Ferland at al., 1990) but it certainly cannot account for the UV bump in the majority of objects. For free-free to dominate free-bound emission, temperatures of at least 4×10^6 K are required. The emissive surface must be large, since the surface emissivity of an optically thin medium is small. Malkan (1991) showed that the dimension of the emissive medium would then be larger than that given by the variation timescale in the UV range.

- Blackbody emission

  The only way to account for the small variation time scale of the UV flux is therefore to assume a blackbody emission. To produce a maximum in the 10 - 100 eV range, the temperature of this blackbody should be of the order of $10^5 K$.

Apart from the accretion disc model, there is one other model that is based on blackbody emission. In the 'cold cloud model' (Celotti et al., 1992) cold clouds (with temperatures $\sim 10^5 K$) are formed and confined in a hot spherical accretion flow and reprocess as the UV bump a large fraction of a primary hard X-ray continuum. The clouds are very small ('room size') and must be located at a small radii. This means that they should be intimately mixed with the X-ray source and the UV flux should vary on the same timescale as the X-ray flux. This is not observed.

This leaves the accretion disc model, which was shown to dissipate its gravitational energy mainly in the UV range (§1.4). The shape of the blue

bump is suggestive of an accretion disc. The optical part of the bump has a slope of ~1/3 (once the power law is subtracted) and the UV indicates a turnover toward short wavelengths. The standard thin disc model has a low frequency slope of ~1/3 and a turnover at the maximum temperature (figure 2). Caditz (1993) found that AGNs over the limited range of redshifts $0.4 < z < 0.75$ occupy a well defined region of the colour-magnitude plane. It was found that the standard thin disc model accurately replicated the observed colour-magnitude distribution, and that the low and high colour cut-offs were defined by the Eddington limit and a maximum central mass $M \sim 10^{9.5} M_0$ respectively. This result provides real evidence for accretion discs as the power source for AGNs in the redshift range investigated.

However, there is a problem with the accretion disc origin for the UV bump. Malkan (1983) found that in the objects he studied, the UV turndown suggested a uniform maximum temperature in the disc of 20,000-30,000 K which is in contradiction to the temperatures implied from EUV observations made by Betchtold et al. (1984). Also, the most extreme high temperature cases are those AGN with soft excesses in their X-ray spectra (Elvis et al., 1985), which as mentioned earlier are generally interpreted as shortward extensions of the blue bump. In an accretion disc, this corresponds to a peak temperature of ~500,000 K. The thin disc interpretation of this is that it becomes highly super-Eddington which is both implausible and inconsistent with the thin disc model (Betchtold et al., 1987). Unless these problems can be resolved then the accretion disc model may have to be abandoned for the UV bump. Therefore it is necessary to develop more sophisticated models to describe the observed AGN spectra.

There have been many attempts to improve upon the thin disc model in order to obtain a more realistic emission spectrum. These include the influence of relativity on the emission spectrum, relaxation of the blackbody

approximation, investigations into the soft X-ray emission and the importance of external irradiation.

1.6 Relativistic thin discs

The standard thin disc developed by Shakura & Sunyaev (1973) emitted a blackbody spectrum at the effective temperature at each radius. The effective temperature was determined by the local dissipation rate. The spectrum in the UV range depends on two parameters, the mass of the central black hole and the accretion rate (1.32) and (1.29). This is only true for UV though, since the optical spectrum depends also on the value of the outer radius R_{out}.

However, the disc is accreting onto a supermassive black hole and therefore relativistic effects are important, especially for rotating black holes seen at large inclinations. Space-time around a rotating black hole is described by the Kerr metric and the structure of the thin disc in this metric was investigated by Novikov & Thorne (1973). Cunningham (1975) calculated its spectrum for both a non-rotating and maximally rotating ($a/M = 0.998$) black hole. Here the observed spectrum depends on four parameters, the disc inclination, the black hole mass and angular momentum, and the accretion rate (plus external radius for the optical spectrum). In spite of these unknowns the model did show emission in the EUV range.

1.7 Modified blackbody approximations

The models considered so far have all insisted upon a locally emitted blackbody. This is only the case when the opacity mechanism is given by the Rosseland opacity. In §1.3 it was shown that other zones could exist in an accretion disc. A gas pressure dominated region with electron scattering, and a radiation pressure dominated region where once again electron scattering

outweighs free-free opacity. When electron scattering becomes the dominant mechanism departures from a local blackbody spectrum are expected.

The relative importance of electron scattering and absorption is a function of frequency υ. The emitted radiation flux can be described by a modified blackbody approximation (Rybicki & Lightman, 1979),

$$I_\nu = B_\nu \sqrt{\frac{\kappa_{abs}}{\kappa_{abs}+\kappa_{es}}} \tag{1.33}$$

where

$$\kappa_{es} = 0.4\ cm^2\ s^{-1} \tag{1.34}$$

$$\kappa_{abs} = 1.4\times10^{25}\rho T^{-3.5}\frac{1-e^{-h\nu/kT}}{(h\nu/kT)^3}\ cm^2\ s^{-1}. \tag{1.35}$$

Therefore, in the spectral range $\kappa_{abs} > \kappa_{es}$, the spectrum can be described as a blackbody (1.33) (cf. (1.30)). If electron scattering dominates, the emitted radiation flux is lower ($I_\nu < B_\nu$) for the same value of temperature and so causes a flattening of the spectrum. The frequency ν_0 which divides these two ranges can be calculated from the condition $\kappa_{abs} = \kappa_{es}$:

$$\frac{h\nu_0}{kT} \approx 6.3\times10^{12}T^{-7/4}\rho^{1/2} \tag{1.36}$$

(Shakura & Sunyaev, 1973). Therefore, if a significant part of the energy is emitted at $\nu > \nu_0$ then the departure of the spectrum from blackbody will be quite significant.

Computing the emission spectrum is made significantly easier if a vertically averaged radial structure is used in the calculations. The disc is divided into rings allowing the vertical structure to be computed independently.

Using a vertically averaged model, Czerny & Elvis (1987) state that when electron scattering is included the radiation spectrum above $\log \nu \sim 15.0$ will be modified which means that the UV region is flattened whilst the X-ray flux increases.

This assumes only electron scattering and free-free absorption are important in the disc. There will also be some contribution from heavy elements through bound-free processes. The important sources being bound-free from hydrogen $n=1$ to $n=5$, bound-free from He^0 $n=1,2$, and bound-free from He^+ $n=1,2$ for $T>10^4 K$ (Laor & Netzer, 1989). Their effect can be estimated using the Rosseland mean opacity. So far Kramers' approximation for the Rosseland mean value of the absorption coefficient has been used (1.21). This can be thought of as the first approximation with the contribution from bound-free processes represented as a change by some small factor in the numerical coefficient of κ_{abs}. Czerny & Elvis (1987) and Madau (1988) show that the effect decreases the role of electron scattering and predicts a flattening of the spectrum around $\log \nu \sim 15.3$ which is close to that found by Malken & Sargent (1982) for 3C 273. This strongly suggests that the observed spectrum of AGN should be described using a modified blackbody (or better) approximation.

1.8 Comptonization

High frequency photons are scattered many times before they leave the disc since the last thermalization surface at high frequencies lies deep within the disc. For photons with frequency greater than a frequency ν_c, the disc becomes effectively thin (i.e. transparent to absorption), but the thermalization of photons proceeds as a result of energy changes in multiple scatterings. The importance of this process is represented by the Comptonization parameter y (see Rybicki & Lightman, 1979 for details),

$$y = \frac{4kT}{m_e c^2}\tau^2 \tag{1.37}$$

where the first factor approximates the energy increase per scattering (if $h\nu < 4kT$) and the second factor describes the number of scatterings for photons originating at the optical depth for scattering τ ($\tau > 1$). Therefore, the Comptonization effect is greater for photons at optical depths greater than

$$\tau_c = \sqrt{\frac{m_e c^2}{4kT}}\,. \tag{1.38}$$

Photons emitted between the disc surface and τ_c contribute to the spectrum as thermal brehmsstrahlung since the geometrical depth of this region does not depend on photon frequency.

Photons emitted from regions at $\tau > \tau_c$, but above the last thermalization surface, are shifted in frequency by Comptonization and form a Wien peak around $3kT$ (Maraschi & Molendi, 1990). Below a frequency ν_c, absorption removes photons completely. Above ν_c Comptonization is important and that corresponds to frequencies higher than $\log\nu \sim 16.1$ (Wandel & Petrosian, 1988, Czerny & Elvis, 1987) for a disc where opacity contributions from heavy elements are accounted for.

Polarisation and frequency variability of the induced scattering should be observable in AGN in the radio-infrared region of the spectrum (Coppi et al., 1993) and although none of these effects have been unambiguously observed, sharp turnovers in frequencies $\sim 10^{12}$ Hz imply the existence of Compton scattering (de Kool & Begelman, 1989). Therefore Comptonization is an effect that must be considered in accretion theory especially when trying to model objects with observed soft X-ray excesses.

It has been shown that the inner regions of accretion discs in AGN are actually strong emitters of soft X-rays, which is contrary to expectations from

the standard blackbody disc approximation. By considering Comptonization effects in radiation pressure dominated discs Ross et al. (1992) found that the closer the luminosity to the Eddington limit and the lower the mass of the central black hole, the greater the fraction of the emission in soft X-rays. Their accretion disc model produced a steep soft X-ray component in the spectrum which was similar to that observed for MKN 841. Similar results were found by Laor & Netzor (1989).This strongly hints that the harder X-ray emission is due to relativistic electrons which do not cool to the extent that a substantial population of thermal electrons accumulate (i.e. the Lorentz factor of the electrons always exceeds ~2).

1.9 Addition of atmospheres

When the optical depth of the material in a region of the disc becomes ≤ 1 that area of the disc is described as optically thin. In this region radiation escapes freely once produced and the material itself reabsorbs very little. Equation (1.13) can no longer be used to describe the flux of radiant energy and instead the volume loss of energy is

$$-\underline{\nabla}.\underline{F} = -4\pi \int j_{\nu} d\nu \,. \tag{1.39}$$

For a hot gas radiating thermal brehmsstrahlung (or free-free radiation), this has the approximate form

$$-\underline{\nabla}.\underline{F} = const\ \rho^2 T^{1/2}. \tag{1.40}$$

In reality the free-free emission in the optically thin region will be enhanced by Compton scattering. The luminosity enhancement of radiation from thermal

electrons Comptonizing their own brehmsstrahlung can be approximated using an appropriate amplification factor (Dermer et al., 1991).

In the inner most parts of the disc where radiation pressure and electron scattering dominate, the standard diffusion approximation says that if $\alpha \geq 0.1$ then the disc is optically thin for absorption, yet optically thick for scattering, and the radiation spectrum is that of saturated Comptonization. Calculations lead to a very high surface temperature (~ 10^9K) since there are only a small number of photons to carry the large energy flux generated. This implies a temperature inversion; there is a cool interior (~ 10^5K) and hot atmosphere (Callahan, 1977). The implicit assumption here is that almost all of the energy is transported to the upper atmosphere by non-radiative means. There are some consistency problems with this model. The region of strong temperature inversion must be optically thin for scattering because the pressure must decrease monotonically outward from the equatorial plane. Therefore, even if the disc has a hot corona the outgoing radiation cannot be thermalized to the high coronal temperature.

The correct solution for the problem must be to solve the equation of the vertical structure of the disc together with the radiative transfer equation. This can lead to some very complicated physics! As a solution to the problem of how to move smoothly between the optically thin and optically thick regimes, a number of flux-limiting diffusion equations have been introduced to replace the modified blackbody approximation (1.33), including Czerny & Elvis (1987), Wandel & Liang (1991) and Levermore & Pomraning (1981). As an example the diffusion equation used by Czerny & Elvis (1987) is shown:

$$\bar{F}_\nu = \frac{2(1-e^{-2\tau_\nu^*})}{1+[(\kappa_{abs}+\kappa_{es})/\kappa_{abs}]^{1/2}} \pi B_\nu(T_s). \qquad (1.41)$$

Here $\tau_\nu^* = [(\kappa_{abs} + \kappa_{es})\kappa_{abs}]^{1/2}$ and τ_ν^* is the effective optical thickness of the disc for absorption at frequency ν. For large τ_ν^* it reproduces the result from the modified blackbody approximation (1.33), while for low τ_ν^* it describes the thermal brehmsstrahlung from an optically thin medium.

Using this formalisation Czerny & Elvis (1987) found that even in ranges where the effective optical depth of the disc was small, the optical depth for electron scattering could be large. Photons generated by Brehmsstrahlung at large optical depths undergo many scatterings and change their energy as a result of Comptonizaton. The energy from these thermalized photons will be shifted to a mean value of $\sim 3kT$ which will be emitted with a Wien spectral shape. Czerny & Elvis (1987) find that the deviation of the emitted spectrum from a black body can be described as

$$f_\nu = \frac{2(1-e^{-2\tau_\nu^*})}{1+[(\kappa_\nu + \kappa_{es})/\kappa_\nu]^{1/2}}[1-f_{th}(\nu)] + C \qquad (1.42)$$

where f_{th} is the ratio of thermalized photons to all generated photons and C is a normalization constant.

In hot optically thin regions, Coulomb coupling often fails to equilibrate ion and electron temperatures, resulting in lower electron temperatures ($\sim 10^9 K$) which must be taken into account. The disc typically emits radiation as a power law in the X-rays with a prominent Wien peak and exponential cut-off at a few hundred keV. Wandel & Liang (1991) calculated a spectral index of ~ 0.3 - 2 and Maraschi & Molendi (1990) ~ 1. This is consistent with calculations using (1.42) (Czerny & Elvis, 1987) and Shimura & Takahara (1993). Wandel & Liang (1991) claim that their solutions are physically observable. However recent work has suggested that hot optically thin regions of the disc ($T > 10^7 K$) are thermally unstable against perturbations in the proton temperature (Kusonose & Mineshige, 1992). Therefore these discs are difficult

to observe, because they are only stable on timescale less than the thermal timescale.

If the electron temperature approaches the electron rest mass, then electron-positron pairs must also be included. The electron-positron pairs could become important within high accreting discs where they could escape from the disc to form a hot pair atmosphere or pair wind, or they could be advected to smaller radii with the accretion flow (White & Lightman, 1989). Here, pairs are being created faster than they can annihilate and all of the available energy including the thermal energy goes into creating the pairs and the disc cools down, stopping pair production until the disc heats again. Therefore the disc would undergo limit-cycle oscillations on a viscous time scale. In this case it may be possible to observe the disc/disc corona cycling around in a quasi-steady manner (Kusonose & Mineshige, 1992).

1.10 Disc irradiation

There are several lines of evidence to suggest that irradiation of the disc surface may be important. The disc thickness ratio H/R increases outwards (1.22) and hard radiation from an axial jet or ion torus at small radii (Rees et al., 1982), or radiation scattered by a hot atmosphere (§ 1.9) could irradiate the disc at various radii. Observations of Seyfert galaxies have shown no measurable time delay between the UV and optical continuum light curves (Clavel et al., 1992). The absence of a time lag is in contradiction with the standard thin disc model. The local temperatures must be causally linked with the transmission of information at the speed of light. This would be the case if the disc were radiatively heated by a central source (Molendi, Maraschi & Stella, 1992). This external supply of energy is reprocessed as thermal radiation at frequencies corresponding to the effective temperature of the disc, i.e. as UV and optical continuum emission.

The irradiation theory is backed up by X-ray observations of a high energy 'hump' which is associated with partial reprocessing of a hard X-ray continuum by Compton reflecting off an optically thick slab of effectively cool gas, such as an accretion disc (Pounds et al., 1990). A consequence of this is that if a fraction of the X-ray continuum is Compton reflected then another fraction should be absorbed in the disc itself and give rise to observable optical and UV flux variations. This would mean that in some cases the viscous UV flux could be up to an order of magnitude lower than was thought, and the majority of the flux could be provided by radiative heating of the disc (Collin-Souffrin, 1994).

Irradiated disc theories are still in their infancy and self-consistent calculations of the atmospheric structure are needed to determine what kind of corona may be created and how much energy is deposited below the optical photosphere. In a model considering non-thermal electron-positron pair cascades Zdziarski & Coppi (1991) investigated disc irradiation by the AGN's hard X-ray component. They predicted that soft excesses should be common in AGN and showed a correlation between large soft X-ray excesses and steeper hard X-ray slopes. This is backed to some degree by observations (Saxton et al., 1993). It is hoped that the reflecting spectrum will relate to the density in the disc and the ionizing flux. This will give information on the disc structure and geometry of the illumination and aid further research in this direction (Ross & Fabian, 1993).

1.11 Disc instabilities

In §1.2 the theory of a steady thin accretion disc was developed. There are several reasons for extending this theory to the study of time-dependent behaviour of discs. Disc stability against small perturbations can be investigated, and, as the time dependence of disc flow is likely to be controlled

by the size of viscosity, observations of time dependent disc behaviour can offer quantitative information about disc viscosity.

Typical disc timescales can be identified: the *dynamical* (hydrostatic) timescale, τ_z, which denotes the time taken for deviations from hydrostatic equilibrium in the z-direction to be smoothed out, the *thermal* timescale, τ_{th}, which gives the timescale for re-adjustment to thermal equilibrium, and the *viscous* timescale, τ_{visc}, which gives the timescale on which matter diffuses through the disc under the effect of the viscous torques. These timescales can be shown collectively as (Frank et al., 1992)

$$\tau_z \sim \alpha\tau_{th} \sim \alpha(H/R)^2\tau_{visc} \sim R/v_\phi \sim \Omega_K^{-1}. \tag{1.43}$$

Using the α-disc solutions (1.22):

$$\tau_z \sim \alpha\tau_{th} \sim 1\times10^4 M_8^{-1/2} R_{14}^{3/2}\ s \tag{1.44}$$

$$\tau_{visc} \sim 3\times10^9 \alpha^{-4/5} \dot{M}_{26}^{-3/10} M_8^{1/4} R_{14}^{5/4}\ s. \tag{1.45}$$

$\tau_z \sim \alpha\tau_{th} \sim 1\times10^4 M_8^{-1/2} R_{14}^{3/2}\ s$

$\tau_{visc} \sim 3\times10^9 \alpha^{-4/5} \dot{M}_{26}^{-3/10} M_8^{1/4} R_{14}^{5/4}\ s.$

Thus the dynamical and thermal timescales are of the order of hours, and the viscous timescale of the order of years for typical parameters.

A disc is unstable if a small perturbation is made to a putative equilibrium solution and this perturbation continues to grow rather than being damped. From (1.44) and (1.45) we see that, in general, a disc may suffer from two kinds of instability. The Lightman-Eardley (Lightman & Eardley, 1974) instability causes the surface density to clump into alternatively high and low density rings on a viscous timescale; a thermal instability causes the disc to expand and contract vertically on a thermal timescale while maintaining constant surface density. The viscous instability occurs if the stress is inversely related to surface density, i.e. $\partial(\nu\Sigma)/\partial\Sigma < 0$, which can be rewritten as

$$\frac{\partial \dot{M}}{\partial \Sigma} < 0, \tag{1.46}$$

and the thermal instability when there is an insufficient dependence of the rate of radiative cooling Q^- on temperature, to counteract the rate of viscous heating Q^+, i.e.

$$\frac{\partial \ln Q^-}{\partial T_c} < \frac{\partial \ln Q^+}{\partial T_c}. \tag{1.47}$$

An unstable structure will commonly be subject to both sorts of instability. The viscous evolution timescale is larger than the thermal timescale (1.43), so that wherever an annulus goes from one temperature to another because of a thermal instability, this transition is rapid compared to the subsequent viscous response of the disc in the *r*-direction.

If a viscously and thermally unstable regime (surface density decreasing with increasing effective temperature) connects to stable sequences (surface density increasing with effective temperature) at higher and lower temperatures, the resulting double-valued nature of the locus ensures that other stable solutions at higher and lower temperatures are accessible at fixed surface density. The unstable portion is inaccessible to evolving discs (Bath & Pringle, 1982) and, in general, the existence of an unstable sequence can give rise to limit cycle behaviour (Pringle, 1981).

In a plot of accretion rate versus surface density, the locus of steady state α-models at a single radius shows a characteristic 'S-shaped' curve (figure 3) containing an unstable portion with negative slope. This instability is related to the partial ionization of hydrogen which results in very temperature sensitive diffusion or convective flux (Meyer & Meyer-Hofmeister, 1983). Meyer & Meyer-Hofmeister proposed a limit cycle mechanism for dwarf novae based on this unstable sequence. In this model the viscosity in the disc varies:

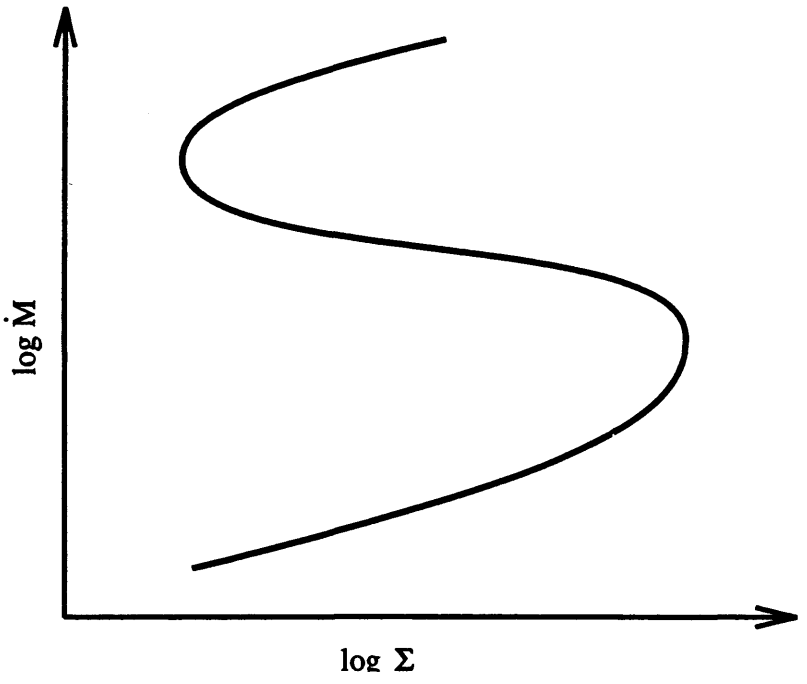

Figure 3
An illustration of an S-shaped $\dot{M}$ (Σ) curve.

between outbursts (at 'quiescence') the viscosity is low, so that the viscous timescale is long and matter accumulates in the disc; at outburst the viscosity suddenly rises, the viscous timescale becomes short and the matter previously stored in the disc is rapidly deposited on to the white dwarf.

Lightman & Eardley (1974) also found that the inner regions of a standard thin disc was viscously and thermally unstable. The rapid growths of these unstable modes may result in the breakdown of the thin accretion disc configuration, although there has been some research into mechanisms that quash these instabilities (see §1.11.1 and §1.11.2).

With regard to the perturbation of viscosity, Kato (1978) suggested that a local pulsational instability exists in a viscous disc. His suggestion was proved in subsequent investigations (Blumenthal et al., 1984). The existence of pulsational instabilities does not depend on what pressure and opacity dominates the disc, although they are likely to exist only in the innermost regions of the disc, with the oscillations trapped in this narrow area (Okazaki et

al., 1987). Kato et al. (1988) found that there are two kinds of instability in an isothermal disc when the viscosity parameter α is above a critical value. The pulsational instability in the inner part of the disc, and a sonic-point instability. The research into these instabilities continue, and recent work has included the investigation of different viscosity mechanisms (i.e. radial viscosity: Wu et al., 1994; Yu et al., 1994). Vertical shear instabilities set up by the resonant response of a disc with a slight tilt has been studied by Kumar & Coleman (1993), and instabilities in magnetized accretion discs have been discussed by Kumar et al. (1994).

1.11.1 Slim discs

It was stated above that Lightman & Eardley (1974) found that the inner region of the standard thin disc becomes thermally (and viscously) unstable. Here radiation pressure dominates over gas pressure. The rate of radiative cooling $Q^- \sim H$, while the rate of viscous heating $Q^+ \sim H^2$; thus overheating produces expansion that leads to a thermal runaway (Frank et al., 1992). Abramowicz (1981) noted that advective cooling (heat transport by the bulk motion of the disc material) at the inner edge could have a sufficiently steep dependence on H ($Q^-_{adv} \sim H^3$) to halt the thermal runaway. The extent of the stabilized region would depend on the accretion rate, and only for high accretion would there be sufficient cooling for no instability to occur. The inclusion of advective cooling, general relativistic effects, and to keep consistency, radial pressure gradients led to the construction of a new family of accretion discs known as 'slim discs' (Abramowicz et al., 1988) for moderately super-Eddington accretion rates. The discs are 'slim' because the usual assumption that the angular velocity of the disc material is Keplerian must be dropped. The resulting discs have a ratio of disc height to radius smaller than unity.

The slim disc theory is justified when investigating the very inner regions of accretion on to black holes where the radial motion is transonic. Abramowicz et al. (1988) found an S-shaped $\dot{M}(\Sigma)$ relation (c.f. figure 3) at a fixed R defining three regimes of accretion. There is a *lower* branch where gas pressure dominates radiation pressure and opacity is given by electron scattering. The cooling is provided by vertical radiative flux. A *middle* branch where the opacity and cooling mechanism are the same as the lower branch but radiation pressure dominates, and finally an *upper* branch where radiation pressure is greater than gas pressure and the cooling is provided by both vertical radiative flux and horizontal advection. This implies that non-stationary, quasi periodic behaviour should be expected in the innermost transonic parts of slim accretion discs.

1.11.2 Different viscosity prescriptions

Generally accretion discs models have used the α-prescription (1.3) to describe the viscous mechanism. An alternative form of (1.3) is

$$T_{r\phi} = \alpha P_{total} \tag{1.48}$$

where $T_{r\phi}$ is the component of viscous stress that drives the accretion and P_{total} is the sum of the gas pressure and radiation pressure. Very different radial structures could be obtained with other combinations of P_{rad} and P_{gas}. The β-prescription ($T_{r\phi} = \beta P_{gas}$) has been used by some authors (Wandel & Liang, 1991; Abramowicz et al., 1988) giving quite different results from the α-models. β-discs have different instability regions and change the S-shaped $\dot{M}(\Sigma)$ curve (Abramowicz et al., 1988).

The α/β parameter is generally assumed to be constant and of the order unity. This assumption has strong implications on the radial disc structure and on the EUV emitted spectrum, since a smaller value of α would lead to a larger

density, thus an opacity less easily dominated by electron scattering. Obviously more work is needed to understand the viscous mechanisms present in accretion discs.

In an attempt to understand dwarf novae outbursts it was described above how it was necessary to have the viscous parameter α vary from a low value in the quiescent state to a high value in the outburst state. Meyer & Meyer-Hofmeister (1983) approximated this variance by assuming a viscous mechanism with $\alpha = \alpha_0 (H/R)^n$. In a radiation pressure dominated disc Milsom et al. (1994) found that limits were imposed upon the disc scale height, resulting in thermally stable discs. As with slim discs, the disc solutions take the form of an S-shaped $\dot{M}(\Sigma)$ curve, with two stable branches corresponding to high and low accretion rates, and a viscously and thermally unstable middle branch for discs with intermediate $\dot{M}$.

1.12 Discs with vertical structure

As shown in the previous sections there have been many attempts to improve upon the standard thin disc and to obtain realistic disc emission spectra. With the exception of some particular cases (e.g. Madau, 1988) the comparison with observations has been carried using vertically averaged models of the disc. It is not at all clear that this averaging of the vertical structure is appropriate to a discussion of emission spectra.

A knowledge of the vertical structure of accretion discs is vital since spectral features departing from a pure blackbody are formed in the upper layers of the disc. Attempts to obtain a disc spectrum by solving the vertical structure of an accretion disc have been made (i.e. Shimura & Takahara, 1993), but the disc solutions are found at a fixed radius only. Inconsistencies may occur as the spectrum is not calculated from the global structure. Therefore in the following chapters a model will be presented which investigates both the

vertical and radial structure of an accretion disc and makes the first steps towards obtaining the emission spectrum of a disc with vertical structure.

Urpin (1983) was the first to study the internal structure of accretion discs. The disc equations (conservation of momentum, energy and the continuity equation) were solved using a parameterization similar to Shakura & Sunyaev (1973). Defining $\tilde{M}$ as the Mach number of the azimuthal flow at a fiducial point

$$\tilde{M}^2 = \frac{GM_{bh}}{\bar{r}\bar{c}^2}, \tag{1.49}$$

where $\bar{c}$ is the sound speed at $\bar{r}$ and M_{bh} is the mass of the central black hole, Urpin assumed $v_\phi \sim \tilde{M}c_s$, $v_R \sim \alpha\tilde{M}^{-1}c_s$, $v_z \sim \alpha\tilde{M}^{-2}c_s$ and $H \sim \tilde{M}^{-1}R$. The solutions showed an outwardly directed flow in the equatorial plane and inflow near the surface of the disc. However, Urpin's model was highly simplified. The disc equations did not include the full viscous stress tensor and a 'vertically isothermal' approximation was used to obtain solutions.

With a set of more realistic opacities and equations of state, Siemiginowska (1988) found similar results to Urpin. The calculations show a very large radial infall velocity near the disc surface, but lack in general the outflow in the midplane. Instead a few circulation cells occur in the equatorial plane. However, her inability to keep the accretion rate constant over a global region throws doubt into the validity of the results.

With improved numerical methods, Eggum et al. (1985) calculated the two-dimensional structure of an accretion disc around a black hole by solving the time dependent hydrodynamic equations, including radiation. Their simulations show a small convective cell slowly moving outwards, although this seems to be a result of the initial conditions. Otherwise they found no indication of any variation in radial infall velocity with height.

Kley & Lin (1992) developed a time-dependent, two-dimensional numerical radiative hydrodynamical scheme to calculate general two-dimensional flow. They solved the disc equations including the full viscous stress tensor. For low values of the viscosity parameter α their solutions show mass outflow in the central parts of the disc close to the equatorial plane, and inflow near the disc surface (similar to Urpin, 1983). However, for higher values of α (≥ 0.06), the flow throughout the disc is directed inward.

The most reliable results are those of Kley & Lin (1992). However, using a numerical finite difference method to solve the disc equations can mean that it is very difficult to interpret the physical reason behind the solutions. Therefore in the following chapters we will present a method that endeavours to develop the theory for the disc analytically as far as possible, resorting to numerical methods for the solution of the final system of ordinary differential equations only. The thin disc is treated as a zero order approximation to a disc with vertical structure. The order of this approximation is controlled by the parameter $1/\tilde{M}^2$, where $\tilde{M}$ is the Mach number of the azimuthal flow at a fiducial point (1.49). This work is therefore similar in intention to Urpin (1983).

The studies into the internal structure of an accretion disc mentioned above, have all assumed surface-less discs where vertical equations are integrated to infinity. In reality, in an AGN system, this is unlikely to be the case. We define a disc surface as a condition of pressure balance between the disc and its surrounding medium. This medium could consist of a corona or disc wind created by Compton heating of the disc through illumination by hard X-rays from the central regions of the disc near the black hole, or a radio jet (Begelman et al., 1983). Therefore, it is possible to imagine situations where the disc surroundings influence the internal structure of the disc.

In §2 the expansion method used to solve the disc equations is introduced. The zero order terms are identified and solved to produce global

solutions for an α-accretion disc. At this stage the vertical transport of angular momentum is ignored. The internal structure and stability of the disc is investigated in both the gas and radiation pressure dominated regions. The effects of applying an external pressure (varying with r as a power law) to the disc is also studied, and in §2.4 possible sources for this external pressure are discussed .

An application of the disc model is introduced in §3. External heating from X-rays associated with a radio jet are shown to induce mass loss from the disc surface. This mass provides the environment in which the jet is collimated. Assuming that the dissipation in the jet depends on the pressure of this external medium and hence the rate of the mass loss produced from the jet illumination, such a configuration may undergo symmetry breaking to an asymmetric state in which one jet dominates. This is therefore a possible model for intrinsically one-sided radio sources.

The effects of including the vertical transport of angular momentum within the disc is investigated in §4. Finally, conclusions are summarised in §5, and future work is discussed.

Chapter Two

The internal structure of an α-accretion disc

2.1 Introduction

In §1 we outlined some of the problems faced in predicting the disc spectrum. The calculation of the emitted radiation flux depends on an understanding of the radiative transfer processes occurring within the disc. This is often by-passed by using a modified blackbody approximation (i.e. equation (1.33), Rybicki & Lightman, 1979). For this approximation to be used correctly, all mechanisms that contribute to the opacity must be accounted for. This suggests that the use of vertically averaged models is not appropriate in the discussion of emission spectra. A specific knowledge of the vertical structure is required because departures from a pure blackbody are likely to occur in the upper layers of the disc (Collin-Souffrin, 1994). These regions will be 'smoothed' out in an averaged model.

Another problem associated with obtaining a disc spectrum surrounds the area of disc stability. As mentioned in §1.12, the thermal disc properties are determined by the requirement that viscous torques can dissipate the disc's mechanical energy at the required rate, and therefore cannot be prescribed without a knowledge of the viscosity within the disc. When α-viscosity (Shakura & Sunyaev, 1973) is used in a radiation pressure dominated disc viscous instabilities evolve (Lightman, 1974). These instabilities can induce

more rapidly evolving thermal instabilities (Shakura & Sunyaev, 1976). In these regions a steady state disc is untenable, and the disc becomes optically thin (Shapiro et al., 1976), or causes the expulsion of matter in a radiation driven wind (Meier, 1979; Jones & Raine, 1980). It is important to investigate for which disc parameters and radial regions these instabilities occur, as it is likely to alter any predicted disc spectrum. To do this correctly requires a knowledge of the internal structure of the disc.

There have been a number of attempts to calculate the internal structure of an accretion disc. Urpin (1983) investigated the internal structure of the thin disc. His results implied that the vertically averaged solutions were a good approximation. The most notable result associated with Urpin's disc was the existence of an outflow of material near the equatorial plane away from the central black hole. This outflow of material has also been predicted by Siemiginowska (1988) and Kley & Lin (1992). However, there is some doubt to the validity of these results. Urpin solves the vertical structure of the disc assuming a pseudo-isothermal solution, Siemiginowska's model suffers from poor ordering of the disc equations which is confirmed in the inability to keep the accretion rate constant, and the accretion disc developed by Kley & Lin assumes that the vertical transport of angular momentum is of the same order as the radial transport. This is probably only true in a thin disc if an external torque is applied that can 'carry' the angular momentum away (a torque of this kind was not included in Kley & Lin). All of these models will be discussed in more detail in §2.5.1.

Clearly, a model is needed that can provide the large scale internal structure self-consistently. If an outflow of material is indeed obtained then this may significantly affect the disc solutions, because for a given accretion rate, there is more material in a disc with both inflow and outflow than in a disc with just inflow.

In this chapter we endeavour to obtain the internal structure of a 'thin' accretion disc, by considering the standard thin disc as a first order approximation to a disc with vertical structure. We seek to develop the theory for a steady state disc analytically as far as possible, resorting to numerical methods for the solution of the final system of ordinary differential equations only. The basis of the method is an expansion of the equations of motions in the parameter $1/\tilde{M}^2$, where $\tilde{M}$ is the Mach number of the azimuthal flow at a fiducial point. We restrict ourselves to $z/r < 1$ and impose boundary conditions at the disc surface corresponding to no loss of angular momentum and mass. We also incorporate a disc surface defined by a pressure balance between the disc and its environment in a special case of zero net torque (see §2.2.3).

An accretion disc is unlikely to 'sit' in a vacuum. The surrounding medium could consist of an optically thin, hot corona or disc wind (Begelman et al., 1983), which will apply a pressure upon the disc (see §2.4) The external pressure applied by the surrounding medium can have an important effect on the internal structure of a disc. According to Kippenhahn & Thomas (1982) an accretion disc cannot be in hydrostatic and thermal equilibrium simultaneously if the rotation velocity is a function of radius only. They suggest, that as in stars (Tassoul 1978), this problem can be resolved by small meridional circulations within the disc. However, we find that when a disc is under the influence of an external pressure, its effect allows the disc to adopt the correct surface height to remain in both hydrostatic and thermal equilibrium, and no meridional circulations are found.

We also find that when the applied pressure is small, our disc solutions are similar to that of Urpin's (1983); we have an outwardly directed flow in the equatorial plane and inflow near the surface of the disc. The disc is also unstable when radiation pressure dominates. However, when a significant external pressure is placed on the disc (of order $\sim 1-10\%$ of the disc central pressure), the disc structure is compressed, and the solutions depart from that

expected by Urpin and the standard thin disc. Most notably, the outflow of material along the equatorial plane $z = 0$ ceases, and the possibility of a thermally stable (although viscously unstable) radiation pressure dominated disc arises. We will show that this could be of some importance in the study of disc stability and disc spectra variability.

In §2.2 we introduce the disc equations and describe our computational method. The results are presented in §2.3. Possible sources of external pressure are discussed in §2.4 and we investigate whether any of these sources could provide a large enough 'push' to alter the disc structure (as described above). Concluding comments on the model are given in §2.5.

2.2 The disc model

2.2.1 Basic equations for disc accretion

In developing this disc model we consider a two-dimensional system in cylindrical co-ordinates (r, ϕ, z) with azimuthal symmetry assumed, i.e. physical quantities are allowed to vary in r and z, but not in ϕ. Symmetry about the mid-plane $(z = 0)$ is also assumed, although this condition will be dropped in § 4.

The gravitational potential for the disc is provided by a central black hole ($M_{bh} \sim 10^8 M_O$). This means that the effect of self-gravity is ignored. At the disc height H, at radius r from the centre, the z-component of gravitational force due to the black hole is $g_c \sim GMH / r^3$. This compares to the self-gravity contribution $g_s \sim G\Sigma$, treating the disc as an infinite uniform plane. Discs in which $g_s > g_c$ are gravitationally unstable, with the end result being possibly non-interacting cloudlets or angular momentum transporting spiral arms (Lin & Pringle, 1987). The condition for the neglect of self-gravitation is

$$\rho << M / R^3 \qquad (2.1)$$

which from (1.22) is satisfied for all disc radii up to ~ $10^{17-18} cm$, although this limit can decrease for lower values of the viscosity parameter α (see §1.2.1 and equation (1.3)). In more accurate studies investigating the regimes of self-gravity, Cannizzo & Reiff (1992) and Cannizzo (1992) (using vertically averaged and vertically explicit disc models respectively) parameterized the region for which $g_c > g_s$ as $R \leq 5\times10^{17}\alpha^{2/3} cm$, for a black hole mass $M = 10^8 M_0$ and an accretion rate $\dot{M} = 0.01 M_0 yr^{-1}$. This is in agreement with limits presented in Clarke (1988) and Mineshige & Shields (1990). Including the effects of self-gravity is beyond the scope of this work; therefore results corresponding to the very outer regions of the disc need to be treated cautiously.

To describe the gravitational effects of a rotating black hole the equations of motion for the disc should be solved within a Kerr metric. Relativistic models to describe discs around rotating black holes have been produced: the relativistic thin disc (Novikov & Thorne, 1973) and the relativistic slim disc (Lasota, 1994). However using the Kerr metric can become difficult and cumbersome, and the solutions require an enormous numerical effort. There have been some attempts to describe orbits in the Kerr metric by a pseudo-potential (Chakrabarti & Khanna, 1992) but the result is not very satisfactory since it is a poor approximation of the full Kerr treatment. The majority of models (e.g. Madau, 1988; Abramowicz et al., 1988; Cao, 1992) describing the disc properties close to the central black hole use the pseudo-Newtonian potential of the form

$$\Phi = -\frac{GM}{(r^2+z^2)^{1/2} - r_s} \tag{2.2}$$

which has been shown by Paczynski & Wiita (1980) to mimic the essential features of a Schwarzschild spacetime with regard to accretion flows.

The nearest region to the central black hole we shall investigate in our model will correspond to radii where radiation pressure dominates gas pressure. From (1.27) it is noted that this occurs at a minimum distance of $\sim 35R_s$ in the standard thin disc model. At these distances the effects of general relativity are small, therefore for the present time the gravitational potential of the black hole will be described by the simple Newtonian form

$$\Phi = -\frac{GM_{bh}}{(r^2+z^2)^{1/2}}. \tag{2.3}$$

Considering special relativity, Novikov & Thorne (1972) show that if the orbital motion of the disc material is assumed to be very nearly geodesic, then although general relativistic effects are very important near the hole, one can ignore special relativistic corrections to the local thermodynamic, hydrodynamic, and radiative properties of the disc at all r and z - even near the black hole. Special relativity can become important when a disc becomes optically thin and takes a two-temperature state in which the electron temperature differs from the ion temperature. However, we are only considering one-temperature discs, where the electron and ion temperatures are equal, and therefore all relativistic effects remain small.

As mentioned in §1.2.1 the fundamental problem associated with the study of accretion discs is the uncertainty of the form and magnitude of the viscous stress which drives the accretion. The traditional remedy is the semi-empirical theory; that the total pressure P is proportional to the component of viscous stress $\bar{T}_{r\phi}$ which drives the accretion (which means that the turbulent length scales are no larger than a scale height). This gives rise to the α-disc where

$$\alpha = \frac{\bar{T}_{r\phi}}{P}, \tag{1.48}$$

is taken to be a constant. This prescription will be adopted for our disc model.

To obtain the internal structure of the α-accretion disc, the conservation equations of momentum, mass and energy in a fluid must be solved. These are given in covariant derivative form and are solved using a flat space-time metric in cylindrical polar co-ordinates. The conservation of momentum is described by the Euler equation (§1.2.2 and (1.4)). To include the effects of gravity and viscous stress, the Euler equation is used in the Navier-Stokes form (Eggum et al., 1987)

$$\frac{\partial}{\partial t}(\rho\upsilon^i)+(\rho\upsilon^i\upsilon^j)_{;j}=-\overline{T}^{ij}_{;j}-(P\delta^{ij})_{;j}-\rho\Phi_{;i} \tag{2.4}$$

where $i=1,2,3,$ and υ_i is velocity of the fluid. This equation differs from Eggum et al. (1987) in the fact that the stress energy tensor here includes only the viscous stresses (because the pressure is written explicitly) and is given by

$$\overline{T}_{ij}=-\nu\rho(\upsilon_{i;j}+\upsilon_{j;i}-\frac{2}{3}\delta_{ij}\upsilon^k_{;k}). \tag{2.5}$$

The conservation of mass is described by the continuity equation

$$\frac{\partial\rho}{\partial t}+(\rho\upsilon^i)_{;i}=0. \tag{2.6}$$

The vertical energy transport mechanism in accretion discs may be either radiative or convective, depending on whether or not the temperature gradient required for radiative transport is smaller or greater than the gradient given by the adiabatic assumption

$$P\rho^{-\gamma}=const. \tag{2.7}$$

Convective energy transport is generally ignored; Shakura et al. (1978) showed that convection amounts to less than half the total energy transport in radiation pressure dominated discs. More recent studies have shown that for sub-Eddington thin discs the effect of convection on the structure of the disc is relatively benign, causing only small perturbations (Eggum et al., 1987). This is in marked contrast to the situation within thick super-Eddington discs in which convective cell activity dominates the dynamics within a significant fraction of the disc volume (Eggum et al., 1985). The theory of convective discs are discussed in works such as Clarke et al. (1985), Meyer & Meyer-Hofmeister, (1983) and Kley (1994). For now all energy transport will be assumed to be via radiative mechanisms. Our work could be expanded to include convection at a later date.

Energy conservation requires that the rate at which a fluid element increases its heat energy equals the rate at which heat is delivered to the element minus the rate at which the element does work against its surroundings (1st law of thermodynamics). Using Eggum et al. (1987) this is written as

$$\frac{\partial E}{\partial t}+(E\upsilon^{k})_{;k}+P\upsilon^{k}_{;k}+T^{k\lambda}\upsilon_{k;\lambda}+D_{r}(E_{0}^{k})_{;k}=0 \tag{2.8}$$

where

$$E=\frac{3\rho kT}{2\mu m_{H}} \tag{2.9}$$

is the gas energy density and

$$E_{0}=aT^{4} \tag{2.10}$$

is the radiative energy density, both at temperature T .

Within the equation of energy conservation is the contribution of the radiative transport to the energy flow within the disc. This can be expressed in terms of the radiation energy density E_0 and the radiation flux F_0. In the optically thick case

$$F_0 = -D\nabla E_0 \tag{2.11}$$

where, in the diffusion approximation

$$D = \frac{cl}{3}.$$

Here l is the photon mean free path. This relation is not strictly accurate for the accretion disc problem because optically thin regions must be treated, and the use of the diffusion approximation for D leads to violation of causality. Solutions to this problem have been found and expressed in the many variations of radiative transport by flux limited diffusion (FLD). An example of FLD was shown in §1.9 (1.41) with the algorithm developed by Czerny & Elvis (1987). A similar approximation was developed by Levermore & Pomraning (1981) in which the diffusion algorithm is replaced by

$$\begin{aligned} D_r &= \frac{cl(2+R)}{6+3R+R^2} \\ R &= -\frac{l|\nabla E_0|}{E_0}. \end{aligned} \tag{2.12}$$

This reduces (2.11) to its correct optically thick form $F_0 = -\frac{cl}{3}\nabla E_0$ when $l|\nabla E_0| << E_0$ and gives the limit of freely streaming radiation $|F_0|/E_0 = c$ when optically thin $l|\nabla E_0| >> E_0$. FLD algorithms have been used in other

astrophysical contexts (e.g. supernova shockwave calculations; Chevalier & Klein, 1979) with good results.

There is a problem implementing any flux limited algorithm into our disc model. This is linked to our method of solving the disc equations and in particular the diffusion equation (see §2.2.4 for details). Therefore we shall use the energy equation corresponding to a fully optically thick disc (2.11) as an approximation which we will justify in §2.3.1.

The equation of state is given by the sum of the gas pressure and radiation pressure

$$P_{tot} = P_{gas} + P_{rad} = \frac{\rho kT}{\mu m_H} + \frac{1}{3} aT^4, \tag{2.13}$$

where μ=0.6 is taken for an ionised gas with cosmic abundance.

2.2.2 Thin disc expansion

In the previous section the equations governing the structure of the accretion disc were defined (equations (2.3), (1.43), (2.4), (2.6), (2.8) and (2.13)). To obtain solutions, these equations are expanded in terms of a small parameter so that the thin disc is treated as a zero order approximation to a disc with vertical structure. The parameter that controls the ordering of this approximation is $1/\tilde{M}^2$, where $\tilde{M}$ is the Mach number of the azimuthal flow at a fiducial point

$$\tilde{M}^2 = \frac{GM_{bh}}{\bar{r}\bar{c}^2}. \tag{2.14}$$

$\bar{c}$ is the sound speed at $\bar{r}$, and M_{bh} is the mass of the central black hole.

The expansion parameter $1/\tilde{M}^2$ reaches of order 1/10 only if the gas temperature approaches 1/10× the proton virial temperature. Thus, this

expansion will be valid over most of the disc, except possibly in the atmosphere of the inner region, or radii where general relativity is important. For the present however, we restrict ourselves to the case that the components of velocity are of the order of the thin disc values. In this case the expansion parameter is of order 10^{-6}.

In the thin disc it is assumed that the disc material circles the central black hole with an approximate Kepler orbit (1.1). At the fiducial point f

$$\frac{[\upsilon_\phi]_f}{[c_s]_f} = \left(\frac{GM_{bh}}{\bar{r}\bar{c}^2}\right)^{1/2} = \tilde{M}. \tag{2.15}$$

Therefore we can define a dimensionless azimuthal velocity V :

$$V = \frac{\upsilon_\phi}{[\upsilon_\phi]_f} = \frac{\upsilon_\phi}{\bar{c}\tilde{M}}. \tag{2.16}$$

From (1.7) and (1.8) the thin disc value of the radial velocity υ_r is

$$[\upsilon_r]_f = \frac{\alpha\bar{c}H}{\bar{r}} = \frac{\alpha\bar{c}^2\bar{r}^{1/2}}{(GM_{bh})^{1/2}} = \frac{\alpha\bar{c}}{\tilde{M}}. \tag{2.17}$$

Hence a dimensionless radial velocity U can be defined as

$$U = \frac{\upsilon_r}{[\upsilon_r]_f} = \frac{\upsilon_r\tilde{M}}{\alpha\bar{c}}. \tag{2.18}$$

We complete the velocity scalings by assuming $\upsilon_r \approx \tilde{M}\upsilon_z$ (Urpin, 1983; Siemiginowska, 1988), and thus our z -component of velocity, W , is

$$W = \frac{\upsilon_z\tilde{M}^2}{\alpha\bar{c}}. \tag{2.19}$$

Finally we choose a vertical scale, $\bar{z}$, such that, at the fiducial radius,

$$\frac{\bar{z}}{\bar{r}} = \frac{1}{\tilde{M}}. \tag{2.20}$$

We also define dimensionless quantities

$$\begin{aligned} \zeta &= z/\bar{z} \qquad \omega = r/\bar{r} \\ \sigma &= \rho/\bar{\rho} \qquad c^2 = c_s^2/\bar{c}^2. \end{aligned} \tag{2.21}$$

Note that c^2 is the dimensionless speed of sound, not the speed of light which we shall not need.

The equations of motion and energy transport (2.4), (2.6) and (2.8) give five equations for U, V, W, σ and c^2. These are

$$\begin{aligned} \sigma UU_{,\omega} + \sigma WU_{,\zeta} - \frac{\tilde{M}^4 \sigma V^2}{\alpha^2 \omega} = &-\frac{\sigma\nu\tilde{M}}{\alpha\bar{c}\bar{r}}\left(\frac{4}{3}U_{,\omega\omega} + \tilde{M}^2 U_{,\zeta\zeta} + \frac{1}{3}W_{,\omega\zeta} - \frac{4U}{3\omega^2} + \frac{4U_{,\omega}}{3\omega}\right) \\ &+\left(\frac{\sigma\nu\tilde{M}}{\alpha\bar{c}\bar{r}}\right)_{,\omega}\left(\frac{4}{3}U_{,\omega} - \frac{2}{3}W_{,\zeta} - \frac{2U}{3\omega}\right) \\ &+\frac{\tilde{M}}{\alpha\bar{c}\bar{r}}(\nu\sigma)_{,\zeta}\left(\tilde{M}^2 U_{,\zeta} + W_{,\omega}\right) \\ &-\frac{\tilde{M}^2}{\alpha^2}(\sigma c^2)_{,\omega} - \frac{\tilde{M}^2\sigma\bar{r}}{\bar{c}^2\alpha^2}\Phi_{,r} \end{aligned} \tag{2.22}$$

$$\begin{aligned} \sigma UV_{,\omega} + \sigma WV_{,\zeta} + \frac{\sigma VU}{\omega} = &\frac{\sigma\nu\tilde{M}}{\alpha\bar{c}\bar{r}}\left(\tilde{M}^2 V_{,\zeta\zeta} + V_{,\omega\omega} + \frac{1}{\omega}V_{,\omega} - \frac{1}{\omega^2}V\right) \\ &+\left(\frac{\sigma\nu\tilde{M}}{\alpha\bar{c}\bar{r}}\right)_{,\omega}\left(V_{,\omega} - \frac{1}{\omega}V\right) \\ &+\tilde{M}^2\frac{\tilde{M}}{\alpha\bar{c}\bar{r}}(\nu\sigma)_{,\zeta}V_{,\zeta} \end{aligned} \tag{2.23}$$

$$\begin{aligned} \sigma UW_{,\omega} + \sigma WW_{,\zeta} = &\frac{\sigma\nu\tilde{M}}{\alpha\bar{c}\bar{r}}\left(\frac{1}{3\omega}W_{,\omega} + \frac{\tilde{M}^2}{\omega}U_{,\zeta} + W_{,\omega\omega} + \tilde{M}^2 W_{,\zeta\zeta} + \tilde{M}^2 U_{,\omega\zeta}\right) \\ &+\left(\frac{\sigma\nu\tilde{M}}{\alpha\bar{c}\bar{r}}\right)_{,\omega}\left(W_{,\omega} + \tilde{M}^2 U_{,\zeta}\right) \end{aligned}$$

$$-\frac{2}{3}\frac{\tilde{M}}{\alpha\bar{c}\bar{r}}(\nu\sigma)_{,\zeta}(\tilde{M}^2U_{,\omega}-2\tilde{M}^2W_{,\zeta}+\frac{\tilde{M}^2U}{\omega})$$
$$-\frac{\tilde{M}^4}{\alpha^2}(c^2\sigma)_{,\zeta}-\frac{\tilde{M}^4\sigma\bar{z}}{\bar{c}^2\alpha^2}\Phi_{,z} \qquad (2.24)$$

$$(U\sigma\omega)_{,\omega}+(\sigma W\omega)_{,\zeta}=0 \qquad (2.25)$$

$$\frac{3}{2}[U(\sigma c^2)_{,\omega}+W(\sigma c^2)_{,\zeta}]+\frac{5}{2}\sigma c^2(U_{,\omega}+W_{,\zeta}+\frac{U}{\omega})-\frac{\nu\sigma\tilde{M}^3}{\alpha\bar{c}\bar{r}\omega^2}(\omega^2(V_{,\omega})^2-2\omega VV_{,\omega}+V^2)$$
$$-\frac{\bar{c}\nu\sigma\tilde{M}^4}{\alpha\bar{z}}V_{,\zeta}^2+\frac{\tilde{M}}{\alpha\bar{c}^3\bar{\rho}}[\frac{1}{\bar{r}}\frac{\partial}{\partial\omega}(D\frac{\partial E_0}{\partial\omega})+\frac{\tilde{M}}{\bar{z}}\frac{\partial}{\partial\zeta}(D\frac{\partial E_0}{\partial\zeta})+(\frac{1}{\bar{r}}\frac{D}{\omega}\frac{\partial E_0}{\partial\omega})]=0. \qquad (2.26)$$

To find approximate solutions, equations (2.22)-(2.26) are expanded in powers of $1/\tilde{M}^2$:

$$U=U_0(\omega,\zeta)+\frac{U_1(\omega,\zeta)}{\tilde{M}^2}+\ldots$$
$$V=V_0(\omega,\zeta)+\frac{V_1(\omega,\zeta)}{\tilde{M}^2}+\ldots \qquad (2.27)$$
$$W=W_0(\omega,\zeta)+\frac{W_1(\omega,\zeta)}{\tilde{M}^2}+\ldots$$
$$\sigma=\sigma_0(\omega,\zeta)+\frac{\sigma_1(\omega,\zeta)}{\tilde{M}^2}+\ldots$$
$$c^2=c_0^2(\omega,\zeta)+\frac{c_1^2(\omega,\zeta)}{\tilde{M}^2}+\ldots$$

The zero order terms from each equation can now be identified. These produce the expected thin disc equations as follows. For the radial component of (2.22), the lowest order terms give the Kepler approximation to the azimuthal velocity,

$$V_0=\frac{1}{\omega^{\frac{1}{2}}}. \qquad (2.28)$$

In the vertical direction (2.24) the lowest order terms correspond, as expected, to hydrostatic equilibrium:

$$(\sigma_0 c_0^2)_{,\zeta} = -\frac{\sigma_0 \zeta}{\omega^3}. \tag{2.29}$$

As both gas pressure and radiation pressure are being considered, it is useful to introduce the parameter β, which is the ratio of gas pressure to the total pressure. Writing $P_0 = \sigma_0 c_0^2$, then from (2.13):

$$\beta_0 = \frac{(P_0 - AT_0^4)}{P_0} \tag{2.30}$$

where β_0 is the zero order expression for β and A is the constant

$$A = \frac{a\bar{T}^4}{3\bar{\rho}\bar{c}^2}. \tag{2.31}$$

$\bar{T}$ is the temperature at the fiducial point and T_0 is the corresponding zero order dimensionless variable. The equation for hydrostatic equilibrium (2.29) can be rewritten in the form

$$\frac{\partial P_0}{\partial \zeta} = -\frac{\beta_0 P_0 \zeta}{T_0 \omega^3}. \tag{2.32}$$

As discussed in §1.11.2 various parameterizations for the viscous stress within the disc have been presented (for a review see Narayan & Goodman, 1989). We are assuming that the viscous stress tensor $\bar{T}_{r\phi}$ is proportional to the total pressure (1.48). Using the thin disc expansion defined in (2.15-2.21) this gives a lowest order

$$\nu = \frac{\alpha \bar{c} \bar{r} c_0^2 \omega^{-\frac{3}{2}}}{\tilde{M}}. \tag{2.33}$$

As a result of this we find that the lowest non-trivial order in the ϕ-component of the momentum equation (2.23) gives an expression for the radial velocity U_0,

$$\sigma_0 U_0 = -\frac{3}{\omega^{1/2}}(\sigma_0 c_0^2 \omega^2)_{,\omega} + 2\sigma_0 c_0^2 \omega^3 V_{1,\zeta\zeta} - 2\sigma_0 \zeta V_{1,\zeta}. \tag{2.34}$$

Here the final two terms represent the corrections from non-Kepler azimuthal motions; these terms are included by Urpin (1983) and Kley & Lin (1992) but ignored in the standard treatment where this equation is integrated vertically to give the radial velocity in terms of the surface density. Note that V_1 contributes to U_0 at the lowest order in this expansion. The departure from Kepler velocity, V_1, is obtained from the first order correction to the radial equation (2.22):

$$2\sigma_0 V_1 = \alpha^2 c_0^2 \sigma_0 \omega^3 U_{0,\zeta\zeta} + \alpha^2 \sigma_0 \zeta U_{0,\zeta} + \omega^{-\frac{3}{2}}(\sigma_0 c_0^2)_{,\omega} - \frac{3\sigma_0}{2\omega^{\frac{5}{2}}}\zeta^2. \tag{2.35}$$

Note that the third term on the right of (2.35) comes from the radial pressure gradients while the first two terms on the right represent the effects of the viscous transport of angular momentum vertically; the final term is from the vertical gradient of the gravitational field. These effects are fed into the radial motion through V_1 in (2.34). The $U_{0,\zeta}$ and $U_{0,\zeta\zeta}$ terms were included by Kley & Lin (1992), but omitted by Urpin (1983).

Both Kley & Lin and Urpin assume that there is no external torque being applied to the disc. In this case it is unlikely that there will be significant vertical transport of angular momentum. Angular momentum is transported principally by large scale eddies (and energy dissipated mainly by small scale ones). In the vertical transport of angular momentum, eddies of scale H would

be deposited in the disc environment. This would require an external torque to extract the angular momentum. We will investigate the effects of adding an external torque to an accretion disc in §5.

In this section we are not considering the vertical transport of angular momentum. Therefore we can neglect the z -derivatives of the velocity terms (i.e. set $U_{,\zeta}=V_{,\zeta}=W_{,\zeta}=0$) that appear in $\overline{T}_{\mu\nu}$, as it is these terms that carry the angular momentum in the z-direction.

Neglecting the vertical transport of angular momentum simplifies (2.34) to give an explicit expression for the radial velocity:

$$U_0=-\frac{1}{\beta_0}[6\omega^{\frac{1}{2}}T_0+3\omega^{\frac{3}{2}}\frac{P_{0,\omega}T_0}{P_0}]. \tag{2.36}$$

It can be seen that an outwardly directed flow of material ($U_0>0$) arises when

$$\frac{P_{0,\omega}}{P_0}<-\frac{2}{\omega}. \tag{2.37}$$

This is a simple expression that relates the direction of flow to the pressure within the disc. The thin disc solutions (1.22) shows that, for a gas pressure dominated disc with opacity given by Kramers' rule, the centre line pressure falls off radially as $r^{-21/8}$. Therefore we should expect fluid outflow near the equatorial plane (from 2.37). Similar velocity flows have been predicted by Urpin (1983), Siemiginowska (1988) and Kley & Lin (1992), however, until now a condition for outflow has not been presented. The derivation of (2.37) contradicts the suggestion made by Urpin (1983) that an outflow of disc material is linked to the vertical transport of angular momentum. We see that the radial velocity depends solely on the viscous transport of angular momentum in the radial direction.

Turning now to the equation of energy balance (2.26), the zero order equation relates the radiated flux to the rate of energy generated by viscous dissipation

$$\frac{\partial F_0}{\partial \zeta} = \frac{A_V P_0}{\omega^{3/2}} \tag{2.38}$$

where F_0 is the heat flux which, using (2.30), is given by

$$F_0 = -\frac{T_0^3}{\kappa_0 \sigma_0}\frac{\partial T_0}{\partial \zeta} = -\frac{T_0^4}{\kappa_0 \beta_0 P_0}\frac{\partial T_0}{\partial \zeta} \tag{2.39}$$

and

$$A_V = \frac{3\alpha \overline{\kappa c}^3 \overline{\rho r}}{16\sigma \overline{T}^4 \tilde{M}}.$$

From here on the viscosity parameter α has been absorbed into the constant A_V.

Understanding the physical processes that can contribute to the opacity within the disc is very important if a realistic disc spectrum is to be produced. A great deal of work has been done calculating the effects of electron scattering, free-free and bound-free processes (e.g. Cox & Stewart, 1970), which dominate at high temperatures $T > 10{,}000K$, and the effects of molecules and grains at cooler temperatures (e.g. Alexander et al., 1983; Pollack et al. , 1985). Models using these different opacities have been developed (Collin-Souffrin & Dumont, 1990; Cannizzo & Reiff, 1992; Cannizzo, 1992) but they have not included the correct radiative transfer effects.

Cannizzo (1992) showed that for temperatures $T > 6000K$ the disc could be modelled using standard thin disc opacities. Therefore, to gain an

understanding of the internal structure of the accretion disc, we will not over-complicate the model by including detailed opacity contributions, but simply consider the two main mechanisms apparent in the disc; namely free-free absorption κ_R (represented by Kramers' law, (1.23)) and electron scattering κ_{ES} (1.24). These have the zero order form:

$$\begin{aligned} \kappa_{R0} &= \beta_0 P_0 T_0^{-9/2} & \bar{\kappa} &= 6.6\times 10^{22}\bar{\rho}\bar{T}^{-7/2} \\ \kappa_{ES0} &= 1 & \bar{\kappa} &= 0.4. \end{aligned} \tag{2.40}$$

Finally, the continuity equation (2.25) gives

$$\left(\frac{\beta_0 P_0 U_0 \omega}{T_0}\right)_{,\omega} + \omega\left(\frac{\beta_0 P_0 W_0}{T_0}\right)_{,\zeta} = 0. \tag{2.41}$$

For the purpose of calculating the disc structure we find that (2.41) is easier to solve when integrated with respect to ω. This expresses mass conservation, to zero order, in the form of a mass flux Ξ:

$$\frac{\partial \Xi_0}{\partial \zeta} = \frac{\beta_0 P_0 U_0 \omega}{T_0}. \tag{2.42}$$

On integrating vertically this gives the accretion rate $\Xi_0 = \dot{M}$.

This completes the set of equations needed to obtain the disc structure: the hydrostatic equation (2.32), the energy equation (2.38 and 2.39) and the continuity equation (2.42).

2.2.3 Boundary conditions

For the conditions on the surface of the disc we integrate equation (2.4) over a pill-box spanning an element of surface (figure 4). This gives

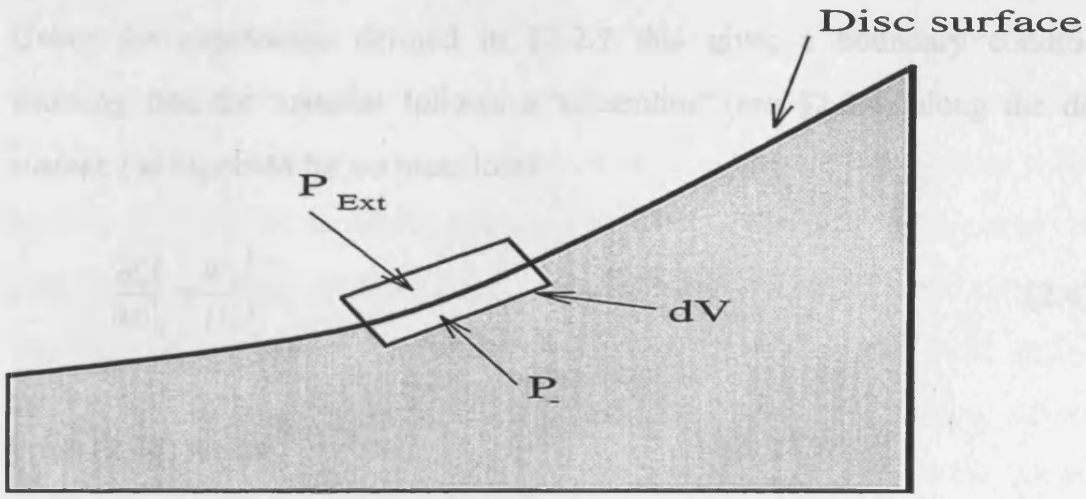

Figure 4
The boundary conditions on the disc surface are obtained by integrating the Navier Stokes equation over a pill-box spanning an element of surface.

$$\int \rho v^i v^j dS_j = -\int \bar{T}^{ij} dS_j - g^{ij} \int P dS_j - \int \rho (\Phi g^{ij})_{;j} dV \tag{2.43}$$

where the first term in equation (2.4) is zero in the steady state and the third term on the right of (2.43) is zero in the limit that the pill-box volume tends to zero. Labelling the surface values with the subscript s we obtain

$$[\bar{T}^{ij} n_j + \rho v^i v^j n_j + P n^i]_s = P_{ext} n_s^i \tag{2.44}$$

where P_{ext} is the pressure in the external medium surrounding the disc.

Assuming no mass-loss from the surface of the disc gives the condition

$$\frac{d\dot{M}_{loss}}{dr} = 0 = 2\pi r \rho v_n \left(1 + \left(\frac{dz}{dr}\right)_s^2\right)^{\frac{1}{2}} \tag{2.45}$$

where v_n is the velocity (at the surface) normal to the surface of the disc

$$v_n = [\frac{v_z dr - v_r dz}{(dr^2 + dz^2)^{1/2}}]_s . \tag{2.46}$$

Using the expansions defined in §2.2.2 this gives a boundary condition showing that the material follows a 'streamline' (see §2.2.4) along the disc surface (as expected for no mass loss)

$$\left.\frac{\partial\zeta}{\partial\omega}\right|_s = \left.\frac{W_0}{U_0}\right|_s . \tag{2.47}$$

From (2.44) we get

$$[\bar{T}^{11}n_1 + \bar{T}^{13}n_3 + \rho(\upsilon^1\upsilon^1 n_1 + \upsilon^1\upsilon^3 n_3)]_s = [(P_{ext} - P_+)n^1]_s \tag{2.48}$$

$$[\bar{T}^{21}n_1 + \bar{T}^{23}n_3 + \rho(\upsilon^2\upsilon^1 n_1 + \upsilon^2\upsilon^3 n_3)]_s = 0 \tag{2.49}$$

$$[\bar{T}^{31}n_1 + \bar{T}^{33}n_3 + \rho(\upsilon^3\upsilon^1 n_1 + \upsilon^3\upsilon^3 n_3)]_s = [(P_{ext} - P_+)n^3]_s \tag{2.50}$$

where n_i is the normal vector to the surface of the disc (from 2.47):

$$\frac{n_1}{n_3} = -[\frac{\upsilon_z}{\upsilon_r}]_s = -[\frac{W_0}{\tilde{M}U_0}]_s . \tag{2.51}$$

Expanding (2.48), (2.49) and (2.50)

$$\begin{aligned}[\tilde{M}^2\Delta P]_s = &-[c^2\omega^{3/2}\sigma(\frac{4}{3}U_{,\omega} - \frac{2}{3}W_{,\zeta})]_s \\ &+[c^2\omega^{3/2}\sigma(\tilde{M}^2U_{,\zeta} + W_{,\omega})\frac{U}{W}]_s\end{aligned} \tag{2.52}$$

$$[\tilde{M}^2 V_{,\zeta}]_s = [\frac{W}{U}(V_{,\omega} - \frac{1}{\omega}V)]_s \tag{2.53}$$

$$\begin{aligned}[\tilde{M}^4\Delta P]_s = &[c^2\omega^{3/2}\sigma(\tilde{M}^2U_{,\zeta} + W_{,\omega})\frac{W}{U}]_s \\ &-[c^2\omega^{3/2}\sigma(\frac{4\tilde{M}^2}{3}W_{,\zeta} - \frac{2\tilde{M}^2}{3}U_{,\omega})]_s .\end{aligned} \tag{2.54}$$

In developing this model we will assume (in a sense to be made precise below) that there is no net torque being applied at the disc surface. We argued (in §2.2.2) that this implies that the vertical transport of angular momentum within the disc is to be neglected. An extension of this argument is that there is very little transport of angular momentum at the surface, both radially and vertically. Therefore we neglect the viscous terms in the boundary equations (2.52 - 2.54).

The zero order terms from (2.52) and (2.54) give the condition $\Delta P = 0$. This defines the disc surface: at $\zeta = \zeta_s$ the external pressure equals the internal pressure

$$P(\omega,\zeta_s) = P_{ext}(\omega). \tag{2.55}$$

Later we shall find small departures in the disc flux from the standard thin disc values. This can be traced back to our neglect of the discontinuity in the viscous stresses at the surface. If, for example, $\frac{d\zeta_s}{d\omega} > 0$, then material in the surface experiences a torque from fluid at larger radii, but zero torque from smaller radii, so giving rise to an inward surface current. (The surface layer contains no mass, but the radial velocity diverges because of the discontinuity in viscous stresses). We are therefore neglecting this surface current giving rise to a lower accretion rate than the corresponding thin disc. (Conversely, to maintain the accretion rate we require a higher surface density which, for $\frac{d\zeta_s}{d\omega} > 0$, gives rise to the greater dissipative flux). In the situation we are modelling, therefore, an element in the disc surface experiences zero net torque: the environment provides a stress that everywhere balances the stress exerted by the adjoining disc on the surface.

We turn now to the boundary condition for the energy equation. In using the radiative diffusion equation (2.38) the disc is assumed to be optically thick,

i.e.

$$\tau = \int_0^{\zeta} \rho\kappa d\zeta > 1. \tag{2.56}$$

Here the radiation field is locally very close to the blackbody form. When τ becomes < 1 the disc becomes optically thin and the radiation escapes directly. The total dissipation rate through one half of the vertical structure must give the dissipation rate per unit face area $D(r)$ (equation (1.16)). In our case, the disc has a surface, defined by a pressure balance between the disc and its external medium. We shall see that this affects the total dissipation rate by a surface term, depending on the external pressure and the disc slope. Equation (1.16) must be modified to take this into account:

$$D(r) = \frac{3GM\dot{M}}{8\pi r^3} - X. \tag{2.57}$$

The value of X is calculated along with the solutions of the disc equations (see §2.2.4) and can be positive or negative. For a significant external pressure, X can become quite large. This leads to a noteable, but probably not observable (see §2.5), change in the emitted flux. We also find a change in the internal disc structure depending on the external pressure.

To obtain a relation between the outgoing radiation flux F_0 and the temperature in the surface layers, the equations for radiative transfer must be solved. If the opacity in the disc is mainly absorption (Kramers' opacity) then the disc emits roughly as a blackbody and the spectrum of outgoing radiation is Planckian, i.e. the radiative flux is related to the disc temperature at the photosphere by

$$\sigma T^4 = D(r) \tag{2.58}$$

where the photosphere is defined as $\tau = 1$. However electron scattering alters the emitted flux and in this case the spectrum cannot be thought of as blackbody. A modified blackbody approximation must be used such as the one developed by Rybicki & Lightman (1979) shown in §1.7

$$\sigma\sqrt{\frac{\kappa_R}{\kappa_R + \kappa_{ES}}}T^4 = D(R) \tag{1.33}$$

This condition is applied at the adjusted photospheric surface defined as $\sqrt{\tau_R(\tau_R + \tau_{ES})} = 1$ and was used by Czerny & Elvis (1987). It also closely resembles the modified blackbody equations used by Laor & Netzer (1989) and Ross et al. (1992). It can be seen that when Kramers' opacity dominates, (1.33) reduces to the blackbody equation (2.58). In §2.2.4 we will explain that our method of solving the disc equations means that we must consider a disc that is wholly optically thick. A consequence of this is that the modified blackbody approximation reduces to the Planckian equation (2.58). This condition will be adopted in the following model.

We can define the boundary conditions that govern the flux and temperature, assuming a symmetric disc about $\zeta = 0$, as

- at $\zeta = 0$

$$F = 0. \tag{2.59}$$

- at $\zeta = \zeta_s$

$$F = D(r) = \frac{3GM\dot{M}}{8\pi r^3} - X \tag{2.60}$$

$$T = \left(\frac{D(r)}{\sigma}\right)^{1/4}. \tag{2.61}$$

To complete the boundary conditions we should specify an inner and an outer radial boundary condition. One of these is usually the mass flux in the

disc, the other is usually some condition at the inner edge. We therefore expect the disc equations above will yield a two parameter family of solutions.

2.2.4 Obtaining the disc structure

In the standard thin disc the vertical and radial structures are largely decoupled. If the local energy generation rate $D(r)$ is known for a given radius then the vertical disc structure can be calculated. It is only the radial dependence of $D(r)$ that ties the vertical and radial structures. Our method of solving the disc equations is similar.

To obtain the internal structure of the disc, the disc equations derived in §2.2.2 are developed analytically as far as possible, before a final system of first order differential equations is solved using a NAG library routine. The NAG library routine used is D02HBF which solves the two-point boundary value problem for a system of ordinary differential equations, using initial value techniques and Newton iteration. The parameters determined correspond to the unknown boundary conditions. The routine is used to calculate the vertical disc structure, integrating between the $z = 0$ centre line and the disc surface. A consequence of using this NAG routine is that all boundary conditions must be fulfilled at one of these limits. The boundary condition usually applied to the diffusion equation (2.11) governs the vertical region of the disc that is optically thick. As this must be applied at our disc surface it means that our disc must either be wholly optically thick or optically thin. The flux limited diffusion equation (2.12) cannot be used as a singularity occurs when its boundary condition (2.58) is satisfied. Hence, the diffusion equation we apply is the standard equation for a fully optically thick disc (2.39) radiating as a blackbody (2.58).

This is obviously quite restricting and any results obtained must be checked for consistency (§2.3.1). Future improvements to the model will include solving the ordinary differential equations with an alternative NAG

routine such as D02SAF. This solves the two-point boundary-value problem for a system of first order ordinary differential equations with boundary conditions combined with additional algebraic equations. It uses initial value techniques and a modified Newton iteration in a shooting and matching method. In this way the parameters determined need not be boundary values; they may be eigenvalues, parameters in the coefficients of the differential equations etc. Attempts were made to use this routine, but it has proved difficult to apply.

The equations that govern the vertical structure of the disc at each r, derived in §2.2.2, are the equations for hydrostatic equilibrium (2.32) and energy transport ((2.37) and (2.38)). These are solved using the NAG routine D02HBF subject to their appropriate boundary conditions at $\zeta = 0$ and $\zeta = \zeta_s$, where ζ_s, the disc surface, is calculated by solving a radial equation.

In §2.2.3 it was stated that this disc model requires two further boundary conditions. These will be equivalent to specifying a condition at r_{in} and another at r_{out}. One of them, as we have seen, is the disc surface ζ_s, and the second is the mass flux in the disc, the accretion rate $\dot{M}$. It will be shown later (§2.3.1) that the initial value chosen for ζ_s has little effect on the final disc structure as the solutions settle fairly rapidly with radius.

From (2.36) it is seen that the radial velocity depends on $P_{0,\omega}$, which in turn depends on $F_{0,\omega}$ and $T_{0,\omega}$ (2.32). If we are to gain a picture of the internal structure of the disc, we must construct a closed system of equations that can be solved to give $P_{0,\omega}$, $F_{0,\omega}$ and $T_{0,\omega}$ at all radii. Given the boundary conditions of §2.2.3, solutions for P_0, F_0, T_0, $P_{0,\omega}$, $F_{0,\omega}$ and $T_{0,\omega}$ can be obtained by using the NAG routine D02HBF to solve the first order differential equations (2.32), (2.38), (2.39) and their ω-derivatives as a function of ζ for a given disc height ζ_s. These solutions are then coupled together radially by determining the evolution of the disc surface. This is achieved by calculating $\zeta_{s,\omega}$ through the assumption of constant mass flow through the disc using (2.42).

To summarise, given the two starting conditions ζ_s and $\dot{M}$, the NAG routine D02HBF is used to calculate the vertical structure of the disc by solving the following eight first order differential equations

$$\frac{\partial P_0}{\partial \zeta} = -\frac{\beta_0 P_0 \zeta}{T_0 \omega^3} \tag{2.32}$$

$$\frac{\partial F_0}{\partial \zeta} = \frac{A_V P_0}{\omega^{3/2}} \tag{2.37}$$

$$\frac{\partial T_0}{\partial \zeta} = -\frac{\beta_0 P_0 \kappa_0 F_0}{T_0^4} \tag{2.38}$$

$$\frac{\partial \Xi_0}{\partial \zeta} = \frac{\beta_0 P_0 U_0 \omega}{T_0} \tag{2.42}$$

$$\frac{\partial \tau_0}{\partial \zeta} = \frac{\beta_0 P_0}{T_0} \kappa_0 \tag{2.62}$$

$$\frac{\partial P_{0,\omega}}{\partial \zeta} = -\left(\frac{\beta_0 P_0 \zeta}{T_0 \omega^3}\right)_{,\omega} \tag{2.63}$$

$$\frac{\partial F_{0,\omega}}{\partial \zeta} = \left(\frac{A_V P_0}{\omega^{3/2}}\right)_{,\omega} \tag{2.64}$$

$$\frac{\partial T_{0,\omega}}{\partial \zeta} = -\left(\frac{\beta_0 P_0 \kappa_0 F_0}{T_0^4}\right)_{,\omega} \tag{2.65}$$

subject to the sixteen boundary conditions at $\zeta = 0$ and $\zeta = \zeta_s$

- at $\zeta = 0$	- at $\zeta = \zeta_s$
$P_0 = S(1)$	$P_0 = P_{Ext}$
$F_0 = 0$	$F_0 = S(6)$
$T_0 = S(2)$	$T_0 = A_T [S(6)]^{1/4}$
$\Xi_0 = 0$	$\Xi_0 = \dot{M}$
$\tau_0 = S(3)$	$\tau_0 = 0$
$P_{0,\omega} = S(4)$	$P_{0,\omega} = P_{Ext,\omega} + \frac{\beta_0 P_{Ext} \zeta_s}{A_T [S(6)]^{1/4} \omega^3} S(7)$
$F_{0,\omega} = 0$	$F_{0,\omega} = S(8)$
$T_{0,\omega} = S(5)$	$T_{0,\omega} = A_T \left(\frac{1}{4} S(8)[S(6)^{-3/4}]\right) + \frac{\beta_0 P_{Ext} \kappa_0}{A_T^4} S(7).$

(2.66)

The parameter A_T is

$$A_T = (\frac{16\tilde{M}}{3\kappa\rho\bar{r}})^{1/4}$$

and S is an array that contains the eight unknown boundary conditions determined by the NAG routine.

We found that the strong dependence on temperature in equations (2.38) and (2.65) meant that any slight variation in the centre-line temperature would lead to a large alteration of the temperature at the surface. This was remedied by changing the direction of integration, i.e. by integrating down through the disc from $\zeta = \zeta_s$ to $\zeta = 0$.

The boundary condition (2.55) defines a disc surface at the height corresponding to a pressure balance between the disc and its external medium. We bypass the physics here and investigate the disc structure considering a range of power law external pressures

$$P_{Ext} \propto r^{-n}. \tag{2.67}$$

The unknown $S(7)$ corresponds to the disc surface gradient $\zeta_{s,\omega}$ and this is used to calculate the disc height ζ_s as a function of ω from the given starting radius. Written as a first order differential system, this is

$$\begin{aligned} y &= \zeta_s \\ y_{,\omega} &= S(7). \end{aligned} \tag{2.68}$$

Equation (2.68) is a radial equation that can be solved using various NAG routines. We use D02CAF which integrates a system of first-order ordinary differential equations over a range with suitable initial conditions, using a variable-order variable-step Adams method. The internal disc structure can now

be determined by integrating radially using (2.68). The vertical structure at each radius is calculated for the current disc height ζ_s and the result used as an input to the function $S(7)$ in (2.68) for the radial integration.

To understand the resulting disc flow it is useful to derive an analytic solution for $\zeta_{s,\omega}$. Substituting the expression derived for the radial velocity (2.36) into the equation of vertical mass flow (2.42) gives

$$-\dot{M} = -6\omega^{3/2}\int_0^{\zeta_s} P_0 d\zeta - 3\omega^{5/2}\int_0^{\zeta_s} P_{0,\omega}\, d\zeta \tag{2.69}$$

This equation can be solved explicitly because, by using the α-viscosity prescription, a relationship is developed between the pressure in the disc and the emitted flux: from (2.37) we get

$$\int_0^{\zeta_s} P_0 d\zeta = [\frac{\omega^{3/2}}{A_V} F_0]_s \tag{2.70}$$

$$\int_0^{\zeta_s} P_{0,\omega}\, d\zeta = [\frac{\omega^{1/2}}{2A_V}(2\omega F_{0,\omega} + 3F_0)]_s \tag{2.71}$$

and from the flux boundary condition (2.57)

$$[F_0]_s = \frac{A_F \dot{M}}{\omega^3} - X \tag{2.72}$$

$$[F_{0,\omega}]_s = -\frac{3A_F \dot{M}}{\omega^4} - X_{,\omega} - \frac{A_V P_{Ext}}{\omega^{3/2}}\zeta_{s,\omega} \tag{2.73}$$

$$A_F = \frac{9GM_{bh}\overline{\kappa\rho}}{128\pi\bar{r}^2\bar{T}^4\tilde{M}} = \frac{2}{3}A_V .$$

Substituting (2.70) and (2.71) into (2.69) and using (2.72) and (2.73) leads to the expression

$$0 = \frac{21\omega^3 X}{2A_V} + \frac{3\omega^4 X_{,\omega}}{A_V} + 3\omega^{5/2} P_{Ext}\zeta_{s,\omega} . \tag{2.74}$$

This can be rearranged to give an expression for the surface gradient

$$\zeta_{s,\omega} = -\frac{\frac{21\omega^3}{2A_V}X + \frac{3\omega^4}{A_V}X_{,\omega}}{3\omega^{5/2}P_{Ext}}. \qquad (2.75)$$

When the external pressure exerted by the surrounding environment of the disc is small, we have $X \sim X_{,\omega} \sim 0$. This is the thin disc approximation,

$$\zeta_{s,\omega} = 0. \qquad (2.74)$$

The standard thin disc central pressure in the gas pressure/Kramers' opacity dominated disc discussed in §1.3 was found to have an $r^{-21/8}$ radial dependence (1.22). Therefore it is probable that if the external pressure applied by the surrounding environment of the disc decreases more slowly than $r^{-21/8}$, the internal structure will be 'pushed down' as the external medium begins to dominate at larger distances. This is illustrated by considering the disc scale height H (1.7). This has a radial dependence of $r^{9/8}$. From (2.74) it is seen that if $n < 21/8$ in (2.67) then the surface of the disc will force the scale height to deviate from its thin disc value and a change in disc structure is likely. Therefore we can define a 'critical' external pressure with $n = n_c \sim 21/8$. For external pressures with $n > n_c$ we expect the thin disc to give a good approximation to a disc with vertical structure, whilst when $n < n_c$ changes in the internal structure may occur.

To complete the calculation of the disc internal structure and fluid velocity, the vertical velocity W_0 needs to be found. We obtain only an approximate evaluation here (see chapter 3 for a detailed treatment in a vertically isothermal disc). The continuity equation is satisfied to order of magnitude $W_0 = -\frac{\zeta}{\omega}U_0$ (assuming $\frac{\partial}{\partial\zeta} \sim \frac{\omega}{\zeta}\frac{\partial}{\partial\omega}$). We obtain an expression that

satisfies the condition on the boundaries at $\zeta = 0$ and $\zeta = \zeta_s$, if we write this in the form

$$W_0 = -\frac{\zeta\zeta_{s,\omega}}{\zeta_s} U_0 \tag{2.75}$$

since this automatically satisfies the boundary condition (2.47):

$$[W_0]_s = [U_0]_s \zeta_{s,\omega} \tag{2.76}$$

We therefore adopt (2.75) for W_0 with the provision that this is at best an order of magnitude approximation. (This does not effect the computation of any other quantities, especially the radial velocity.

2.3 Presentation and analysis of results

2.3.1 Testing the code and optically thick assumption

The code has been run for various values of accretion rate, external pressure, and disc radius. Recall that the disc solutions require the specification of two parameters. The first corresponds to the mass flux within the disc, the accretion rate $\dot{M}$, which is taken to be constant throughout. The second, which replaces an inner radial boundary condition (see Glatzel, 1992), we take as the height of the disc ζ_s at the starting radius for the radial integration. It is found that the choice of ζ_s has little influence on the disc solutions away from r_{in}. Figure 5 and 6 show the evolution of the disc quantities $T_0(\omega,\zeta_s)$ and $P_0(\omega,0)$ with radial distance ω for a choice of initial disc heights ($\zeta_s = 2, 3, 4, 5$, corresponding to $z_s \sim H, 2H, 3H, 4H$, where H is the disc scale height (1.7)). The solutions correspond to a disc dominated by Kramers' opacity, with $M = 10^8 M_0$, $\dot{M} = 0.1 M_0 yr^{-1}$, $\alpha = 0.1$, and putting $n = 3$ in the external pressure law (2.67). The two functions $T_0(\omega,\zeta_s)$ and $P_0(\omega,0)$ rapidly converge towards

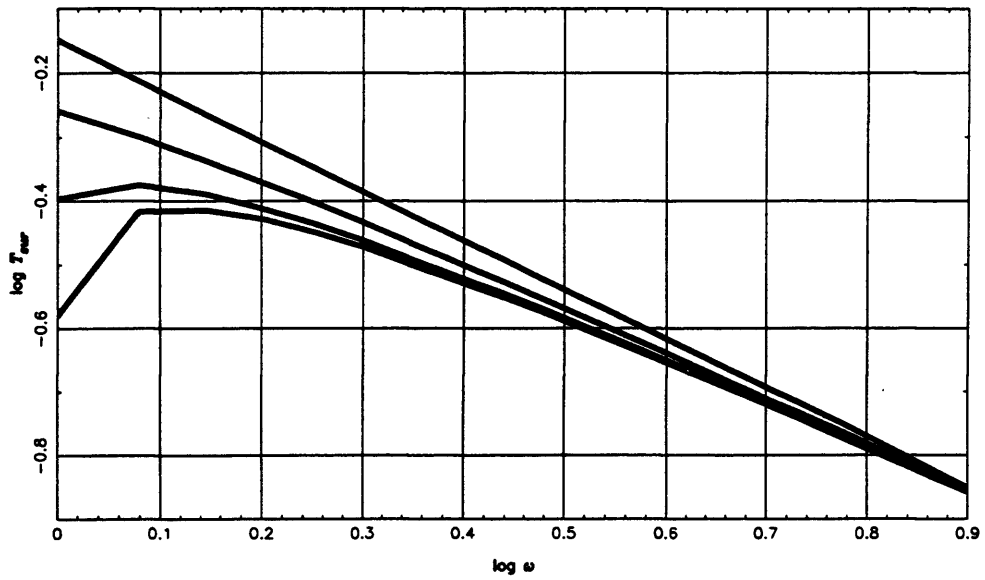

Figure 5

The evolution of the surface temperature $T_0(\omega,\zeta_s)$ *with respect to the dimensionless radial variable* ω *for a range of initial disc heights (with increasing* T_{sur}*:* ζ_s *=2, 3, 4, 5). Disc system:* $M = 10^8 M_0$, $\dot{M} = 0.1 M_0 yr^{-1}$, $\alpha = 0.1$.

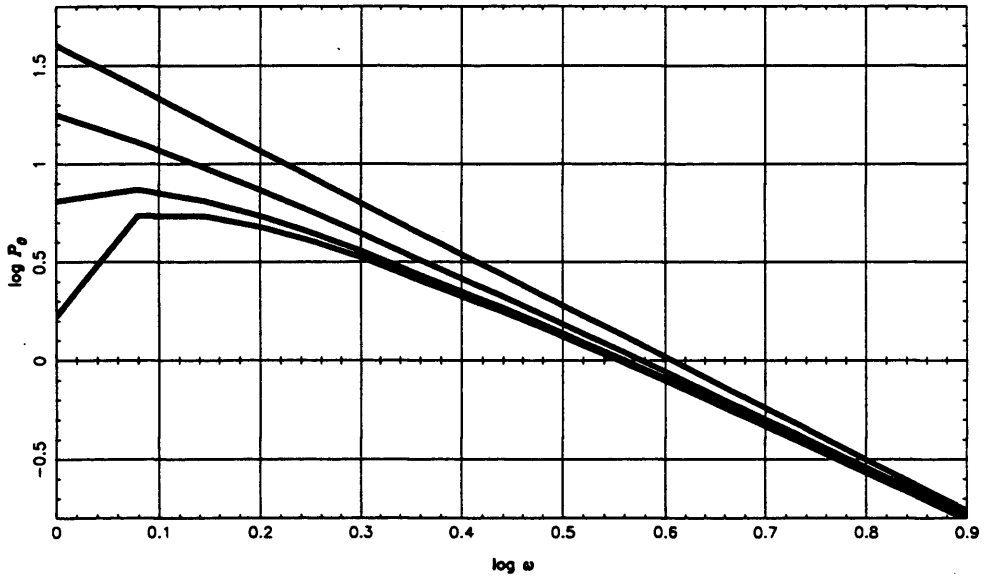

Figure 6

The evolution of the central pressure $P_0(\omega,0)$ *with respect to* ω *for a range of initial disc heights (with increasing* P_0*:* ζ_s *=2, 3, 4, 5). Identical disc to figure 6.*

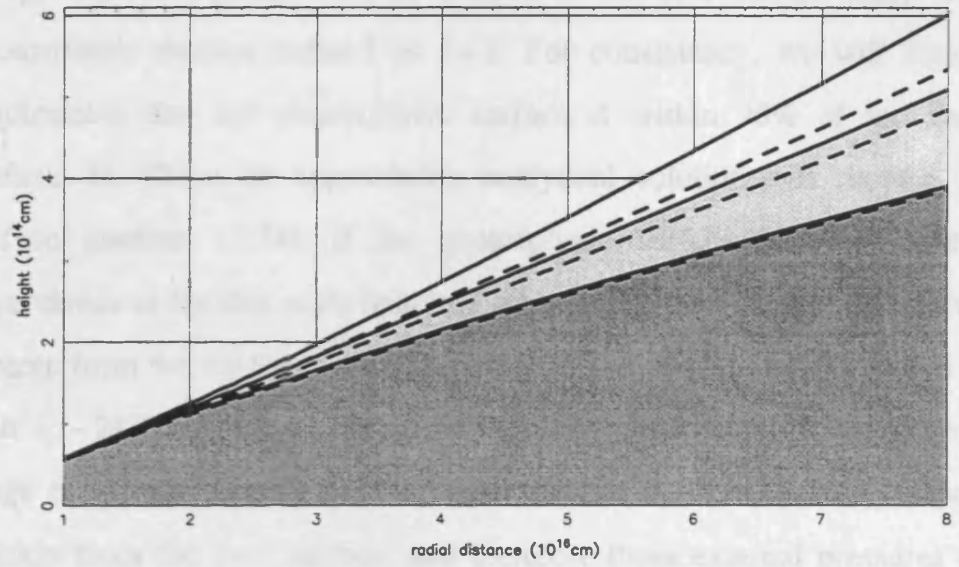

Figure 7

The effect of an external pressure on the disc (solid line) and photospheric (dashed line) surface. The external pressures applied correspond to $n = 1$ (dark shade), $n = 2$ (light shade) and $n = 3$ (clear).

equilibrium solutions. Indeed the two most extreme choices of ζ_s are within 95% of the 'average' solution by $\sim 1.3 r_{in}$.

This computation has been repeated assuming electron scattering, and using various permutations of accretion rate, alpha parameter and external pressure. All results that are obtained by running the code will be shown after sufficiently large radial distances from the inner edge so as to ensure that the solutions are independent of the initial choice of ζ_s.

In §2.2.4 we introduced an external pressure, in the form of a power law (2.67), which is applied at the disc surface. In all disc solutions to follow, this pressure will be assumed to be small, compared with the disc central pressure, at the starting radius (i.e. $P_{Ext} / P(\omega,0) << 1$ at r_{in}). This is so that any effects associated with the external pressure will be independent of the initial conditions.

A consequence of using the NAG routine D02HBF to solve the vertical structure of the accretion disc, is that the boundary condition applied to the

energy equation (2.65) must be utilised at the disc surface rather than the photospheric surface defined as $\tau = 1$. For consistency, we will impose the requirement that the photospheric surface is within 95% of the 'real' disc surface. In §2.2.4 an approximate analytical solution was derived for the surface gradient (2.74). If the photospheric surface has the same radial dependence as the disc scale height (Urpin, 1982), then the disc surface will diverge from the $\tau = 1$ surface when the external pressure falls off more rapidly than $n_c \sim 21/8$. In figure 7 the disc and photospheric surfaces are shown for a range of external pressures. It is found that for $n > 3$ in (2.67) ζ_s departs too quickly from the $\tau = 1$ surface, and therefore these external pressures will be considered only in special circumstances. Although there is a departure for external pressures with $n = 3$, the divergence is gradual and only becomes significant at large radial distances.

In the following sections, the disc model will be used to investigate the three separate zones apparent in a thin accretion disc. These zones were first defined by Shakura & Sunyaev (1973) and Novikov & Thorne (1973). Zone A where the radiation pressure P_r dominates (i.e. $\beta << 1$) and the opacity is determined by electron scattering, zone B where gas pressure P_g plays the main role (i.e. $\beta \sim 1$) and electron scattering is the major contributor to opacity, and finally zone C, where the disc solutions are controlled by the effects of gas pressure and free-free transitions.

2.3.2 Zone C

This section concerns the disc model in zone C, where the inequalities $P_g > P_r$ and $\kappa_R > \kappa_{ES}$ (c.f. (2.40)) hold. In §1.3 it was shown that these inequalities are generally fulfilled in the outer regions of the accretion disc (1.25) where the temperature is not too high. It should be noted that at such temperatures bound-free and bound-bound transitions can become relatively important along with free-free. Czerny & Elvis (1987) approximated their

effect by increasing the numerical coefficient in κ_{abs} (1.35) by a factor ~ 30. This raised the temperature within the disc to a value close to that found by Malkan & Sargent (1982). However, changing κ_{abs} is not expected to alter quantitatively the internal structure of the disc (Cannizzo, 1992) and therefore any corrections to the opacity by bound-free and bound-bound transitions are ignored.

Figure 8 shows $F_0(\omega,\zeta_s)$ scaled by the thin disc flux in the case $M = 10^8 M_0$, $\dot{M} = 0.04 M_0 yr^{-1}$, $\alpha = 0.5$ between $1\times10^{16} cm$ and $1.6\times10^{17} cm$ for three different laws. Note that the fluxes are above the thin disc values. Examples of the internal structure of the discs from figure 8 are shown in figures 10-12. The fluxes are decreasing with respect to the thin disc values where the disc has a positive slope. Where this disc flux ratio is decreasing and less than 1, the disc surface has turned over and the slope is negative (compare figure 12).

We now show that this behaviour is a general property of these discs. We have, from equations 2.69 and 2.70 that:

$$F_s = \frac{A_V}{\omega^{3/2}} \int_0^{\zeta_s} P_0 d\zeta$$

and

$$\begin{aligned}(-\dot{M}) &= 6\omega^{3/2} \int_0^{\zeta_s} P_0 d\zeta + 3\omega^{5/2} \int_0^{\zeta_s} \frac{\partial P_0}{\partial \omega} d\zeta \\ &= 6\omega^{3/2} \int_0^{\zeta_s} P_0 d\zeta + 3\omega^{5/2} \frac{\partial}{\partial \omega} \int_0^{\zeta_s} P_0 d\zeta - 3\omega^{5/2} \frac{d\zeta_s}{d\omega} P_0(\zeta_s)\end{aligned}$$

So

$$\frac{6\omega^3 F_s}{A_V} = (-\dot{M}) - 3\omega^{5/2} \frac{\partial}{\partial \omega} \int_0^{\zeta_s} P_0 d\zeta + 3\omega^{5/2} \frac{d\zeta_s}{d\omega} P_0(\zeta_s) \qquad (2.77)$$

Now, since the thin disc flux $F_d = a\omega^{-3}$, we have $F_s / F_d \propto \omega^{3/2}\int_0^{\zeta_s} P_0 d\zeta$, and if F_s / F_d is decreasing then

$$\frac{\partial}{\partial\omega}\left(\omega^{3/2}\int_0^{\zeta_s} P_0 d\zeta\right) = -k^2$$

say. We deduce that

$$\frac{3\omega^3 F_s}{2A_\nu} = (-\dot{M}) + 3\omega k^2 + 3\omega^{5/2}\frac{d\zeta_s}{d\omega}P_0(\zeta_s). \tag{2.78}$$

We now make the comparison with the thin disc by using these expressions to relate our constants to the value of *a*. For the thin disk flux we drop the final term in (2.77) to get

$$\frac{6\omega^3 F_d}{A_\nu} = (-\dot{M}) - 3\omega^{5/2}\frac{\partial}{\partial\omega}\left[\frac{\omega^{3/2}F_d}{A_\nu}\right], \tag{2.79}$$

from which, putting $F_d = a\omega^3$, we obtain

$$F_d = \frac{2A_\nu(-\dot{M})}{3\omega^3}. \tag{2.80}$$

Thus, finally, we obtain

$$F_s = F_d + \frac{2A_\nu}{\omega^3}K, \tag{2.81}$$

where $K = 3\omega k^2 + 3\omega^{5/2}(d\zeta_s / d\omega)P_0(\zeta_s)$. If the surface of the disc is rising with radius and equation (2.77) holds then we obtain the theorem (pointed out to us by C. Clarke) that the disc flux can only be above the thin disc value.

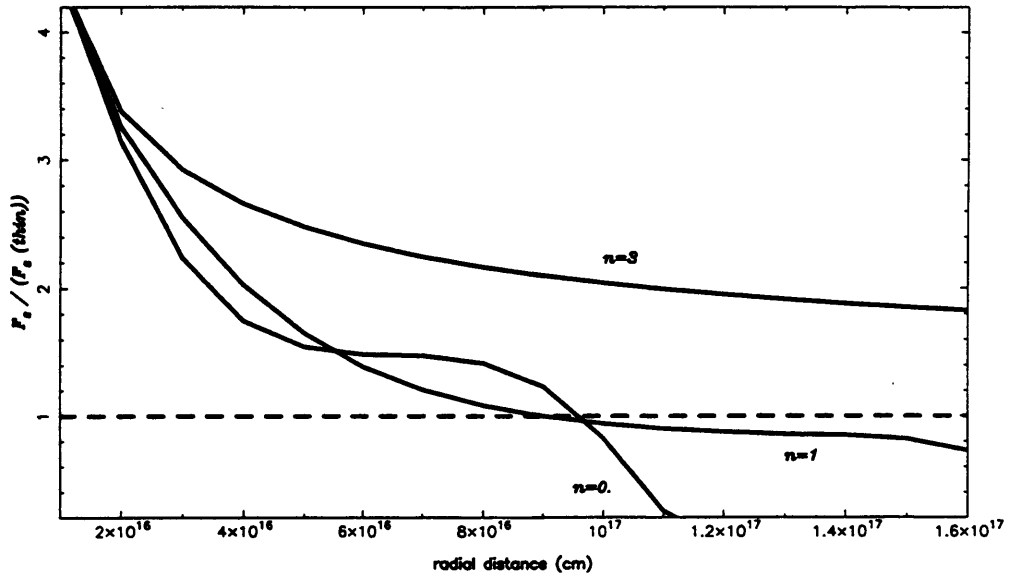

Figure 8

The ratio between the emitted flux and the predicted thin disc value as a function of radius for three external pressure power laws ($n=0$, 1, 3). The dashed line corresponds to $F_0(\omega,\zeta_s)=F(thin)$.

Disc system: $M=10^8 M_0$, $\dot{M}=0.4 M_0 yr^{-1}$, $\alpha=0.5$, *Kramers' opacity.*

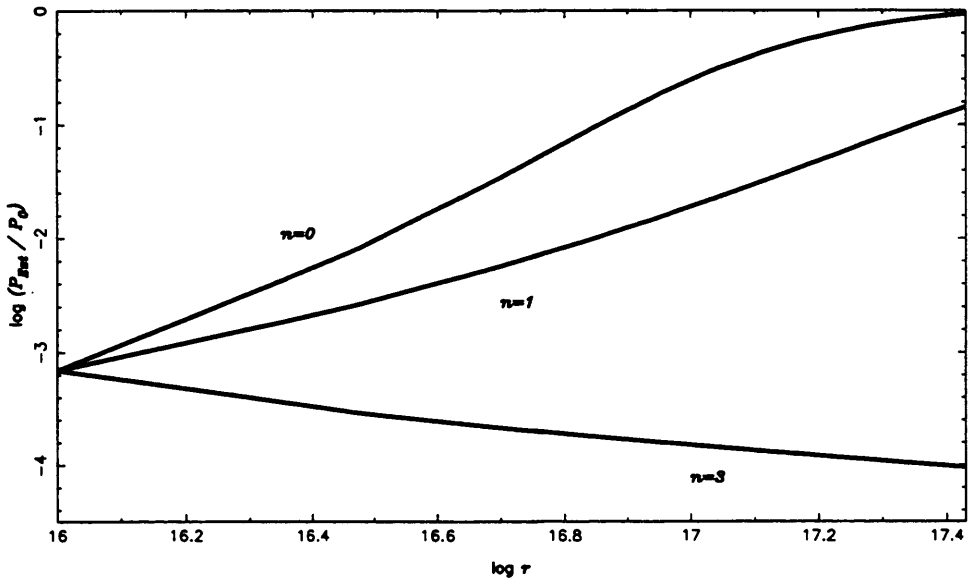

Figure 9

The ratio between the external pressure and the central pressure as a function of radius for the three values of n (=0, 1, 3).

Disc system: $M=10^8 M_0$, $\dot{M}=0.1 M_0 yr^{-1}$, $\alpha=0.5$, *Kramers' opacity*

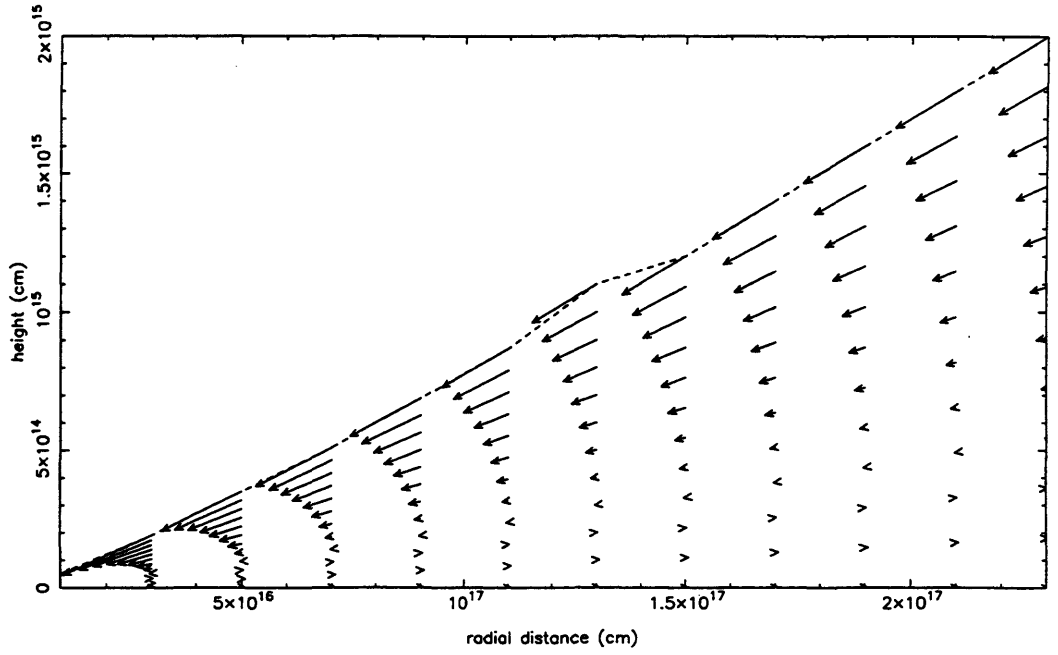

Figure 10

The r-z velocity field of the disc in figure 9 with $n = 3$. The dashed line shows the disc surface. The inflow velocities at the surface are $\sim 10^4 cm\ s^{-1}$, the outflow velocities at the equatorial plane $\sim 10^3 cm\ s^{-1}$.

Alternatively, if the disc slope is negative (height decreasing with radius) and F_s / F_d is increasing then the disc flux is below the thin disc value.

Figure 9 shows that at large distances the external pressure has become negligible and the disc solutions converge to those of the standard thin disc, i.e. $T_0(\omega,0) \propto r^{-3/4}$ and $F_0(\omega,\zeta_s) \propto r^{-3}$. This result is confirmed by Urpin (1983) whose accretion disc was not influenced by an external medium.

The velocity structure of the disc with $n = 3$ is shown in figure 10. An outflow of material is observed close to the $\zeta = 0$ centre line, as first predicted by Urpin (1983). This outflow has since been confirmed by Siemiginowska (1988) and Kley & Lin (1992), and we showed in §2.2.2 that it is due to the viscous transport of angular momentum in the radial direction, summarised by the ratio

$$\frac{P_{0,\omega}}{P_0} < -\frac{2}{\omega}. \qquad (2.37)$$

Siemiginowska (1988) also found small meridional circulations close to the equatorial plane. However this is probably due to the poor ordering of the disc equations which is illustrated by their inability to keep the accretion rate constant. Eggum et al. (1987) solved the time dependent hydrodynamic equations to obtain the internal structure for a two-dimensional accretion disc around a black hole. Their solutions show a small convective cell moving away from the central black hole, but there is no outflow of material along the centre line. This is probably due to the lack of resolution inherent in finite difference methods, whilst the appearance of the cell seems to be a consequence of the initial conditions.

When $n = 1$ the external pressure applied at the disc surface becomes significant away from the central black hole (figure 9). The surface contribution to the flux becomes quite significant causing notable departures from the thin disc solutions (figure 8). In reality, any observable changes would depend on the source of the external pressure, and where and for how long the external pressure would be a sizeable fraction of the disc central pressure. Sources of external pressure will be discussed in §2.4.

Figure 11 shows that for $n = 1$, the disc begins its departure from the thin disc as the external pressure reaches approximately 1% of the disc centre line pressure. The surrounding medium exerts such a force that the disc and photospheric surface are suppressed from their thin disc radial dependence of $\sim r^{9/8}$ (as can be seen in figure 7). This effects the other quantities in the disc (seen in figure 8). The compression, caused by the external medium, forces the centre line pressure to fall less rapidly. This gives rise to a change in the velocity flow and the equatorial outflow is replaced by inflow (2.37). Figure 12 shows the velocity change occurring on the centre line at $\sim 1.6\times10^{17} cm$. The

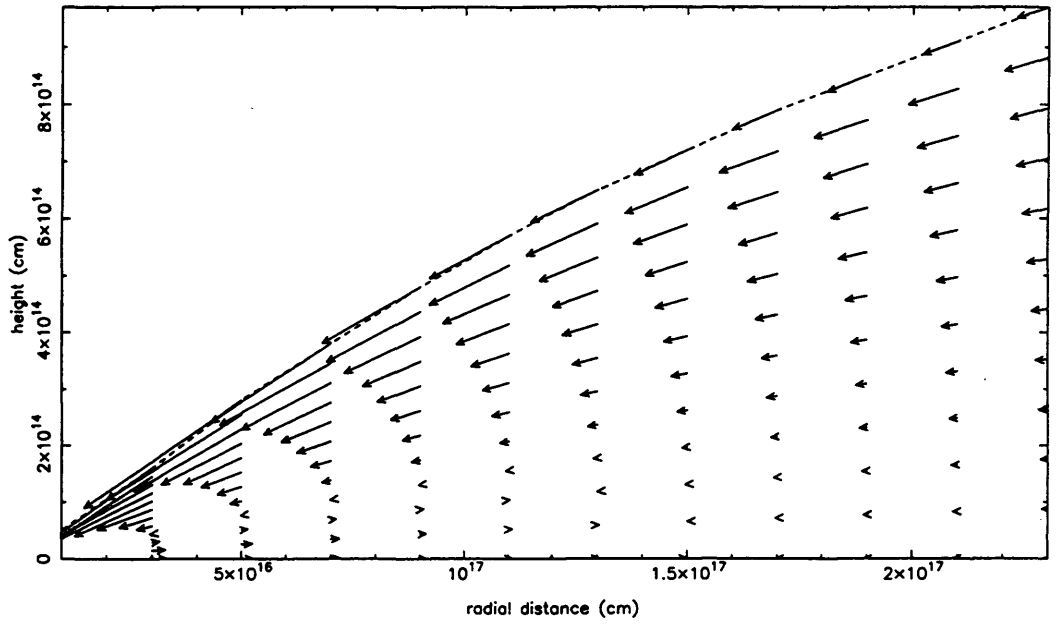

Figure 11

The r-z velocity field of the disc in figure 9 with $n = 1$. The effect of the external pressure becomes evident at large radii with a compression of the disc surface (dashed line).

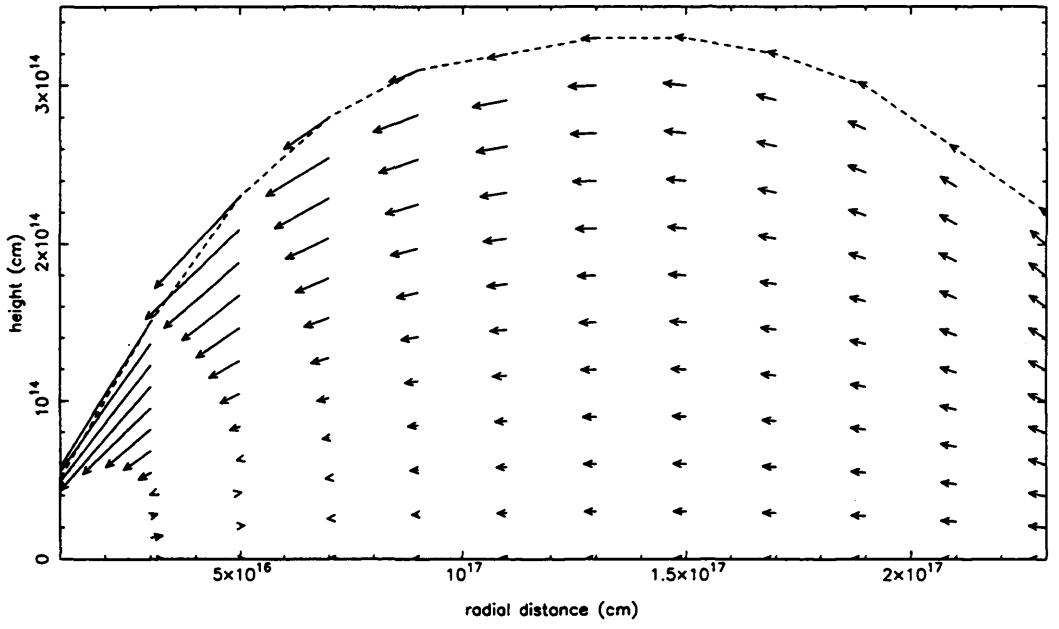

Figure 12

The r-z velocity flow of the disc in figure 9 with $n = 0$. At large radii $P_{Ext} \sim P_0(\omega,0)$ (figure 9) causing the disc surface (dashed line) to bend over. The flow on $z = 0$ changes direction at $\sim 6\times10^{16} cm$. Surface velocities range between $\sim 10^3 - 10^4 cm\ s^{-1}$, equatorial velocities $\sim 10^2 cm\ s^{-1}$.

values of the vertical velocity are approximate. A more accurate velocity field for a vertically isothermal disc showing the change from outflow to inflow will be shown in chapter 3, where a circulation of disc material will be shown to occur. Kley & Lin (1992) also predict a directional change in the centre line velocity. But this occurs at large values of α and is a consequence of assuming that the vertical transport of angular momentum is important within the disc. At this stage we neglect this vertical transport, although we will show that it is important when a external torque is applied to the disc (chapter 4).

The disc structure obtained for a disc under the influence of an extreme external pressure $n = 0$ is also shown in figure 12. Here the external pressure becomes of the same order of the disc centre line pressure (figure 9) at large radii. This is equivalent to calculating the $n = 1$ disc to greater radial distances, or considering an $n = 1$ disc with an increased α or decreased $\dot{M}$ over the same radial region. As seen in figure 12, the disc surface is 'pushed over', compacting the disc material into a very small region. The insistence on a fixed accretion rate means that the density and temperature within the disc decrease slowly with radius. An application of an external pressure 'pushing' the disc surface past the horizontal will be discussed in chapter 3.

The boundary condition for thermal equilibrium (2.58) implies that our disc remains optically thick. This has the result of 'warping' the standard $\dot{M}(\Sigma)$ curve (shown in the discussion of slim discs; figure 3). Figure 13 shows the equivalent of the lower branch of the $\log\dot{M}(\log\Sigma)$ curve (corresponding to a gas pressure dominated disc in figure 3) for the previous selection of discs at the selected radius $1\times10^{17} cm$. As can be seen for the $n = 3$ line, discs subjected to small external pressures ($n < n_c$) tend towards the thin disc value at large accretion rates. As the accretion rate gets smaller, the thin disc surface density declines and the disc becomes optically thin. Our insistence that the disc remain optically thick is shown by the disc tending towards a constant Σ at small $\dot{M}$.

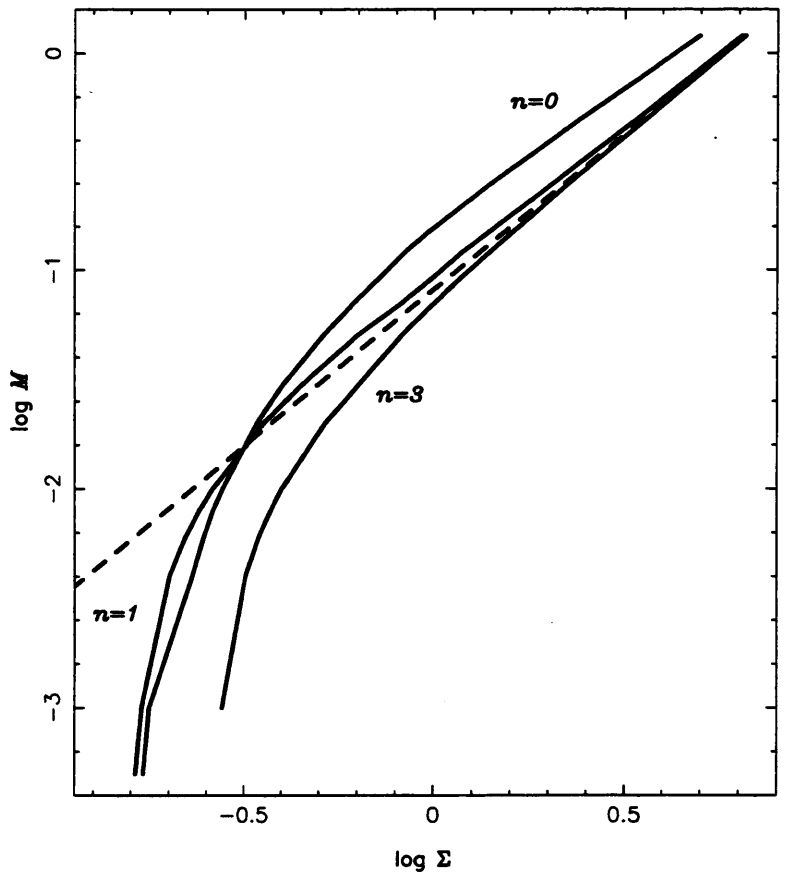

Figure 13

The $\dot{M}$ (Σ) relation for the disc in figure 9 taken at $r = 10^{17} cm$. The dashed line represents the thin disc value.

For the more significant external pressure $n = 1$ the velocity change near the equatorial plane, from outflowing to inflowing, is shown by the reduction in surface density. As mentioned previously, this is due to the fact that if the accretion rate is constant there is more material in a disc with both inflowing and outflowing matter. This is also shown when $n = 0$, although the large compression of the disc structure leads to a slight increase in the surface density. At large $\dot{M}$ the effects of the external pressures get smaller. This is seen by the convergence to the thin disc value for all n.

2.3.3 Zone B

We now consider zone B where the gas pressure is dominant and electron scattering gives the main contribution to opacity. As seen in §1.3 this region is situated closer to the central black hole than zone C. In §2.2.3 it was mentioned that when scattering becomes more important than absorption within the disc, the outgoing radiation can no longer be blackbody. Therefore, instead of trying to solve the full radiative transfer problem, a modified blackbody approximation is used (i.e. (1.33)). This has the effect of flattening the emitted spectrum (see §1.7). The form of (1.33) shows why the explicit calculation of the vertical structure is important for obtaining accurate emission spectras. It is not at all clear that the vertical averaging technique, as used by Czerny & Elvis (1987), Maraschi & Molendi (1990), Cannizzo & Wheeler (1984) etc., will produce the same solutions at a modified photospheric boundary. In principle, the emission spectrum will be affected by the vertical distribution of temperature and density (Shimura & Takahara, 1993).

As our method of solving the disc equations does not allow us to implement a modified blackbody assumption, our results must concentrate on the dynamical structure of the accretion disc.

Figure 14 and 15 show the radial variations of the scales flux $F_0(\omega,\zeta_s)$ with respect to the thin disc results, for three forms of the external pressure ($n = 3,\ 1,\ -1$). in the case of high and low accretion rate respectively. Figure 14 shows the case $M = 10^8 M_0$, $\dot{M} = 0.4 M_0 yr^{-1}$, $\alpha = 0.5$ between $5x10^{15} cm$ and $4x10^{16} cm$. This is analogous to figure 8. The flux ratio is greater than 1 and, where the disc surface has a positive gradient, is falling towards 1. Figure 15 shows $F_0\ (\omega,\zeta_s)$ in the case $M = 10^8 M_0$, $\dot{M} = 0.1 M_0 yr^{-1}$, $\alpha = 0.5$ between $5x10^{15} cm$ and $4x10^{16} cm$. For this relatively low value of accretion rate the flux is less than the thin disc value but is rising to meet it. In this case again, to within a small numerical error, the disc surface for both the cases $n = 1$ and $n = -1$ turn over at the point where the flux ratio starts to decrease. We have not

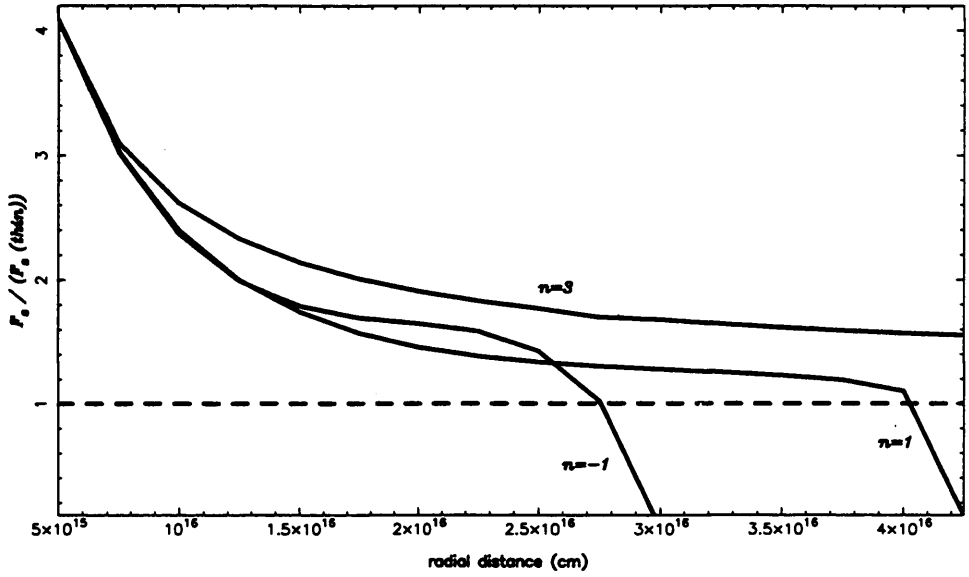

Figure 14

The ratio between the emitted flux and the predicted thin disc value as a function of radius for three external pressure power laws (n =-1, 1, 3). The dashed line corresponds to $F_0(\omega,\zeta_s) = F(thin)$.

Disc system: $M = 10^8 M_0$, $\dot{M} = 0.4 M_0 yr^{-1}$, $\alpha = 0.5$, *electron scattering.*

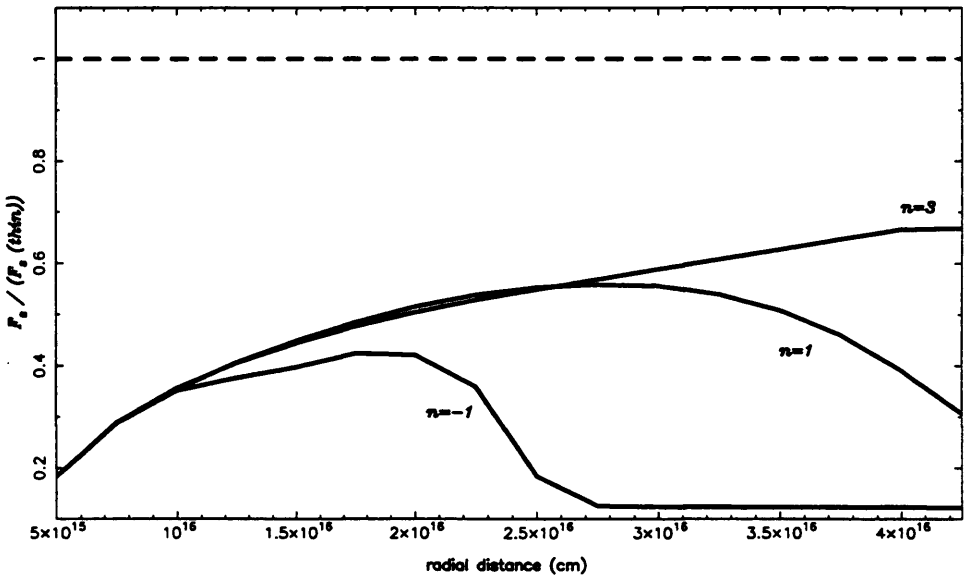

Figure 15

The same as figure 14 but with $\dot{M} = 0.1 M_0 yr^{-1}$

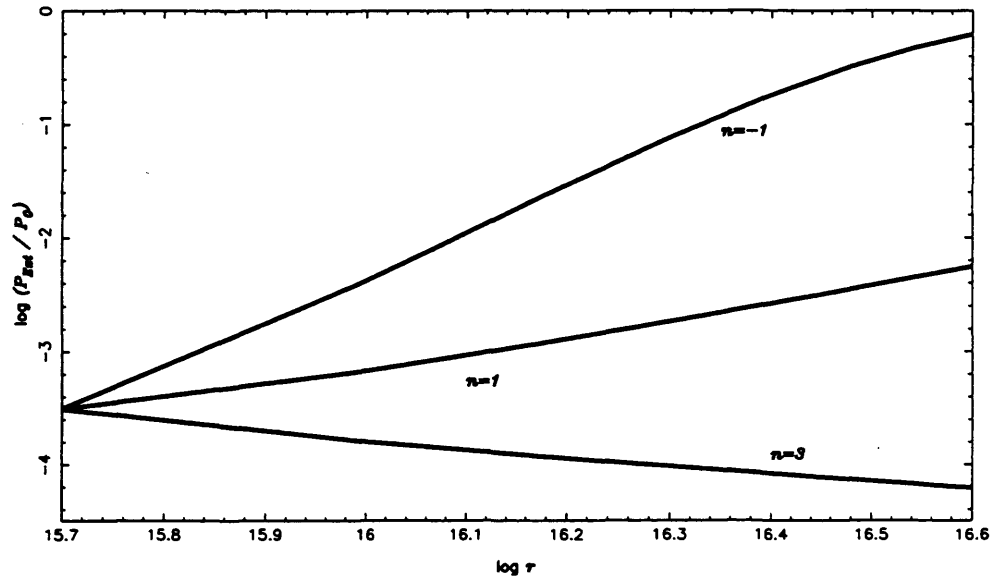

Figure 16

The same as figure 14 showing the ratio between the external pressure and the central pressure as a function of radius for the three values of n (= -1, 1, 3).

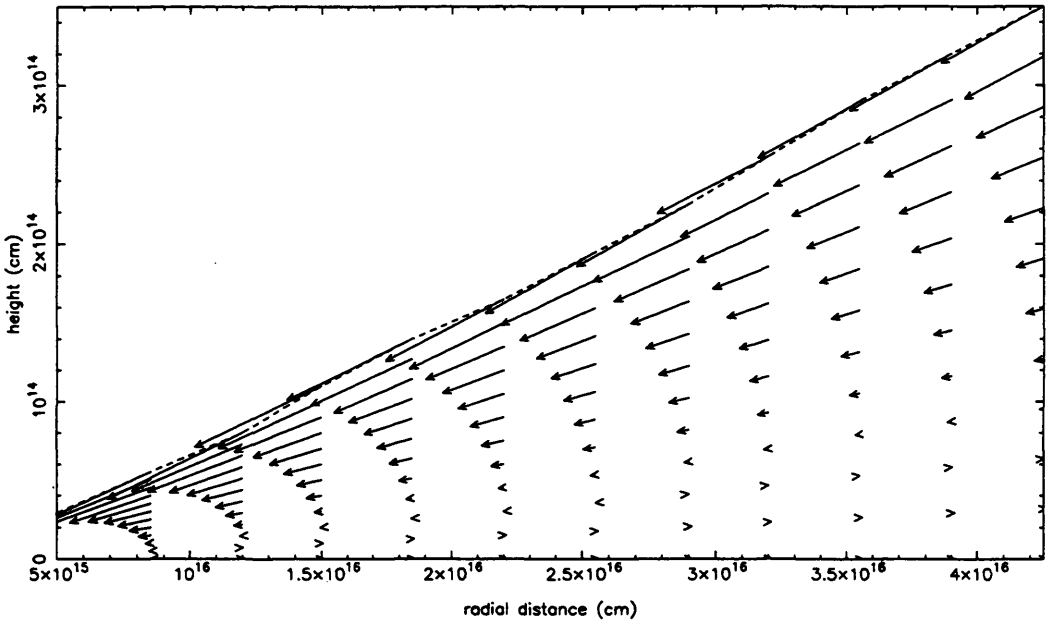

Figure 17

The r-z velocity field of the disc in figure 14 with $n = 3$. The dashed line shows the disc surface. The inflow velocities at the surface are $\sim 10^5 cm\ s^{-1}$, the outflow velocities at the equatorial plane $\sim 10^3 cm\ s^{-1}$.

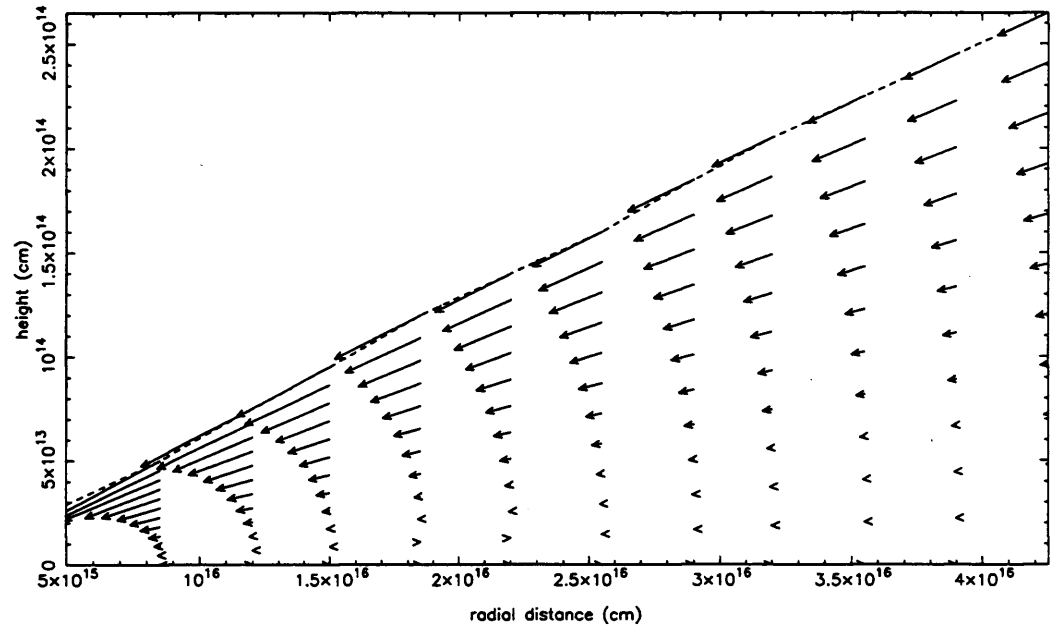

Figure 18

The r-z velocity field of the disc in figure 14 with $n=1$. The effect of the external pressure is evident at large radii with a compression of the disc surface (dashed line).

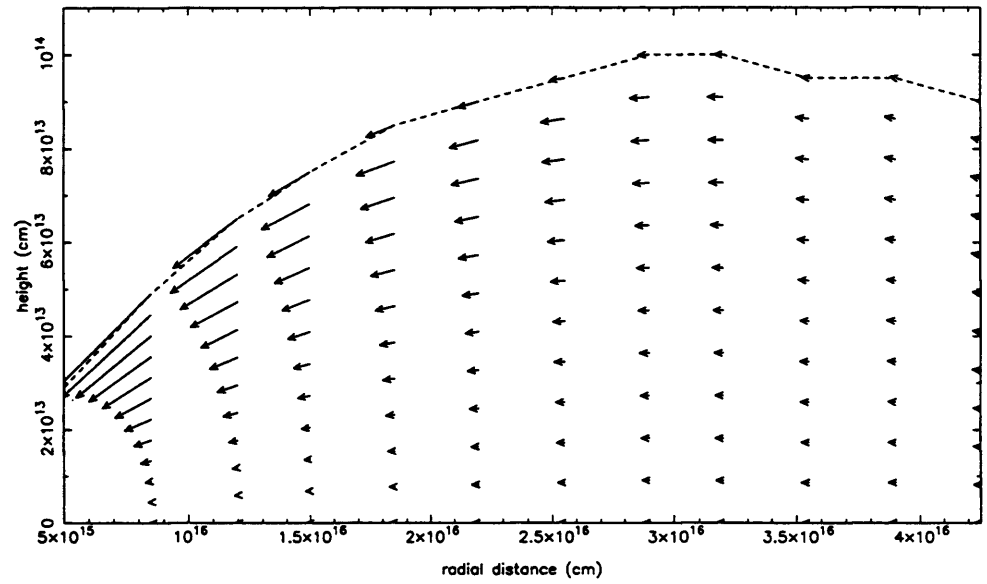

Figure 19

The r-z velocity flow of the disc in figure 14 with $n=-1$. At large radii $P_{Ext} \sim P_0(\omega,0)$ (figure 16) causing the disc surface (dashed line) to bend over. The flow on $z=0$ changes direction at $\sim 6\times10^{16} cm$. Surface velocities range between $\sim 10^4 - 10^5 cm\ s^{-1}$, equatorial velocities $\sim 10^3 cm\ s^{-1}$.

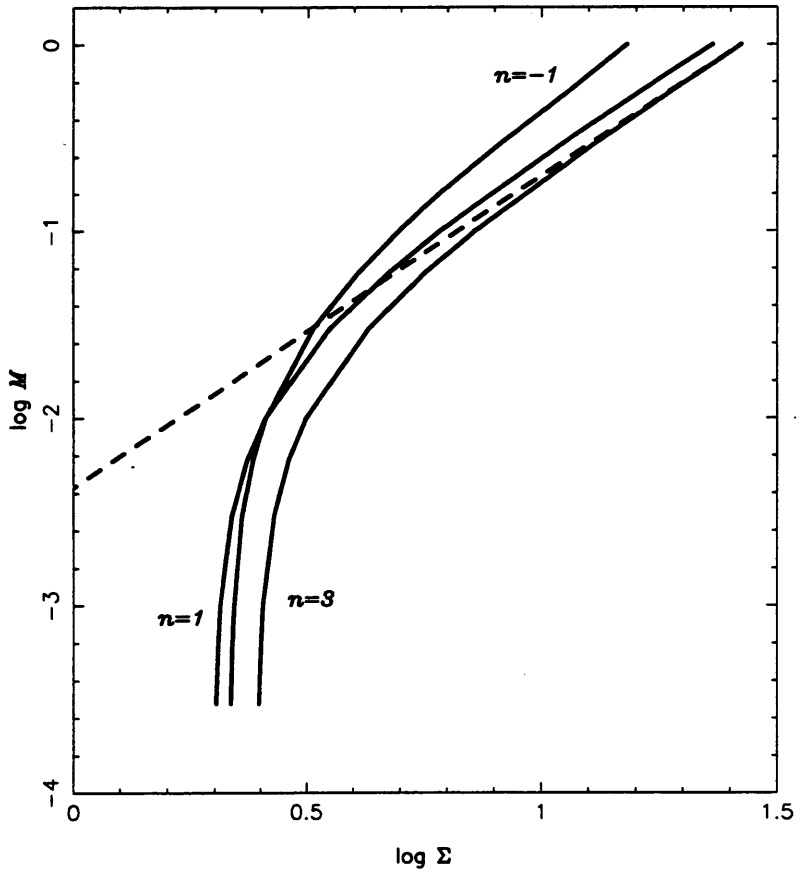

Figure 20

The $\dot{M}(\Sigma)$ relation for the disc in figure 14 taken at $r = 10^{16} cm$. The dashed line represents the thin disc value.

investigated the existence of this branch of solutions for Kramer's opacity in zone C, but it could be present for very low values of $\dot{M}$.

Returning to the thin disc equations (1.20), it is easy to see that if the opacity is given by electron scattering (1.24), then the central pressure has a radial dependence of $r^{-51/20}$. This translates to a critical external pressure (see §2.2.4) of $n_c \sim 5/2$. The $n = 3$ curve, as expected, converges towards thin disc values of $r^{-9/10}$ and $r^{-3/4}$ for the emitted flux and cental temperature respectively. The effect of the surface term on the flux becomes negligible at large radial distances ($X \rightarrow 0$ in (2.57)) due to the insubstantial external pressure (figure 16). For greater external pressures ($n < n_c$) we once again see

the effect of the surface term. The same effect occurs for all $n < n_c$, the radial range of these effects being controlled by the choice of α and $\dot{M}$.

Figures 17-19 show the velocity fields for the discs mentioned above. Once again, the outflow along the central line is observed for discs with $n > n_c$ as predicted by Urpin (1983) (c.f. his region B).

External pressures with $n < n_c$ 'warp' the internal structure of the disc to such an extent that the material flow changes direction near the equatorial plane and becomes inflow. The accompanying change in the surface density is shown in figure 20.

2.3.4 Zone A

In this section we investigate the disc in a region where radiation pressure dominates over gas pressure and electron scattering is the main source of opacity. This region corresponds to the inner regions of the accretion disc (see §1.3). The difficulty in obtaining smooth solutions for a disc moving between gas pressure and radiation pressure dominated regions has been highlighted by the fact that the internal structure of such a disc has not been investigated. Urpin (1983) considered disc regions comparable to zone C, zone B, and a disc zone corresponding to $P_g \sim P_r$. Similarly, both Siemiginowska (1988) and Kley & Lin (1992) concentrated on calculating the internal structure of the gas pressure dominated disc.

It has been found that when radiation pressure becomes more important than gas pressure the disc becomes thermally and viscously unstable. This is due to the fact that there is an insufficient dependence of the rate of radiative cooling Q^- on temperature, to counteract the rate of viscous heating Q^+. The disc suffers from overheating and thermal runaway occurs (Abramowicz, 1981). The general criterion for thermal stability of the standard thin disc model is

$$(\frac{\partial \ln Q^+}{\partial \ln H})_\Sigma < (\frac{\partial \ln Q^-}{\partial \ln H})_\Sigma . \qquad (2.82)$$

This inequality is usually represented as a limit on the ratio between gas pressure and total pressure β (2.30) (i.e. $\beta > 2/5$ (Abramowicz et al., 1988), $\beta > 2/9$ (Milsom et al., 1994)). If stable structures do not exist, then the disc is likely to become optically thin (Shapiro et al., 1976).

There have been various models proposed to quench the thermal runaway. Abramowicz (1981) suggested that advective cooling (heat transport by the bulk motion of the disc material) at the inner edge of an accretion disc could have a sufficiently high dependence on temperature to counterbalance the large rate of heating. This stabilization could only occur for large rates of accretion (close to the Eddington limit), where the standard, geometrically thin model was no longer applicable. Hence, a new thermally stable disc model was constructed, the 'slim' disc (Abramowicz et al., 1988), characterised by the S-shape $\dot{M}(\Sigma)$ curve (see §1.10 figure 3). The lower and upper branches correspond to disc solutions that are both thermally and viscously stable. The lower branch is the solution for a gas pressure disc, whilst the upper branch is the solution to a radiation pressure dominated disc cooled by vertical radiative flux and horizontal advection. The middle branch follows a radiation pressure disc with cooling due to the vertical radiative flux only. Accretion on this branch is both thermally and viscously unstable. Viscous instabilities arise because when $\partial \dot{M} / \partial \Sigma < 0$ more material is fed into those regions of the disc that are denser than their surroundings, and material is removed from those regions that are less dense, so the disc tends to break up into rings (Lightman, 1974; Lightman & Eardley, 1974).

Alternative models that predict a stable radiation pressure dominated disc, have been obtained by using different viscous prescriptions. In an attempt to understand dwarf novae outbursts it was necessary to have the viscous

parameter α vary from a low value in the quiescent state to a high value in the outburst state. A successful approximation was $\alpha = \alpha_0 (H/r)^n$ (Meyer & Meyer-Hofmeister, 1983; Mineshige & Shields, 1990). When this prescription is applied to radiation pressure dominated discs, limits are imposed upon the disc height and thermally stable discs are produced (Milsom et al., 1994). The disc solutions take the form of an $\dot{M}(\Sigma)$ S-shaped curve as mentioned in the discussion of slim discs. There are therefore two stable 'branches' corresponding to high and low accretion rates, and a thermally and viscously unstable middle branch for discs with intermediate $\dot{M}$.

As of yet, advection is not included in our model, so we do not expect our results to be relevant to those of the slim disc (Abramowicz et al., 1988). Similarly, our prescription for the viscous mechanism (1.43) assumes that α is constant. Therefore, we anticipate our solutions to suffer from the same viscous and thermal instabilities as the standard thin disc when radiation pressure dominates over gas pressure.

To find solutions when approaching the unstable region, the code is run 'backwards', the radial equation (2.68) being solved from an outer radius inwards towards the central gravitational source. When the code is reversed, external pressures become significant close to the central black hole when $n > n_c$.

Figure 21 shows the values of β at the surface and equator as a function of radius for the external pressure $n = 1$ and $M = 10^8 M_0$, $\dot{M} = 0.1 M_0 yr^{-1}$, $\alpha = 0.5$. This value of n means that the external pressure becomes negligible at inner radii and the disc solutions should approach those of the thin disc. However, as the vertical structure of the disc is calculated explicitly, we see that the upper regions of the disc rapidly become radiation pressure dominated. This can occur at fairly large distances from the central source ($\sim 1.5 \times 10^{15} cm$ in this example), significantly further than in the vertically averaged solutions of the thin disc (see equation (1.27)). As the surface value of $\beta \rightarrow 0$ the disc height

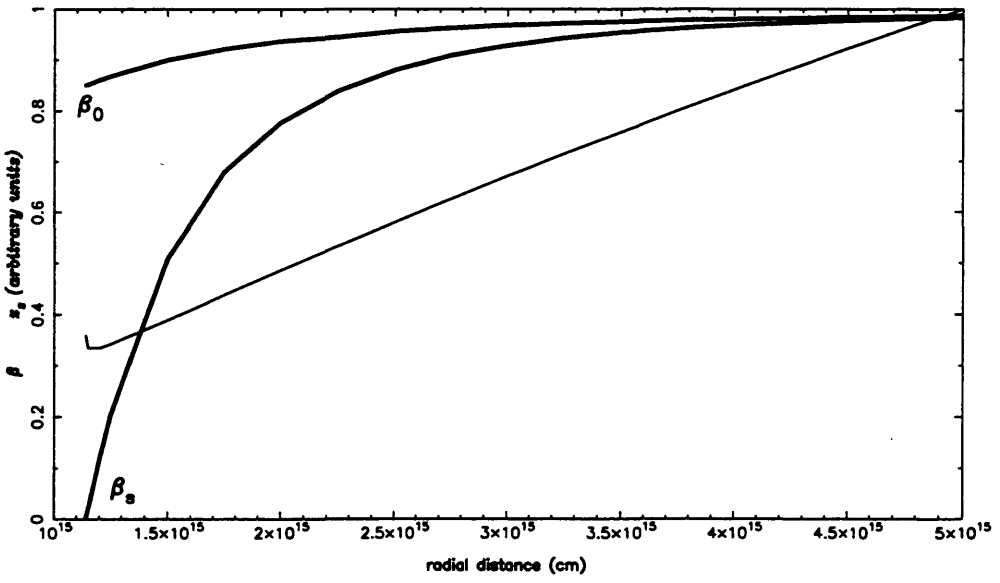

Figure 21

The gas pressure to total pressure ratio is plotted against radius at both the surface β_s and centre line β_0 (thick lines). The external pressure law (2.67) has $n = 1$. The disc surface (scaled) is also plotted (thin line).

Disc system: $M = 10^8 M_0$, $\dot{M} = 0.1 M_0 yr^{-1}$, $\alpha = 0.5$, electron scattering.

ζ_s begins to increase, signifying the onset of disc flaring. It should be noted that the equatorial zones of the disc, unaffected by the small external pressure, follow the standard thin disc solution and at this distance ($\sim 2\times10^{15} cm$) the equatorial region is dominated by gas pressure.

To understand what is happening within the disc, an approximate estimate of the solution of (2.39) can be investigated (where the subscript *s* denotes the value at the surface):

$$[T_0^5]_s = -[\beta P_0 F_0 \zeta]_s . \qquad (2.83)$$

Note that the model imposes the condition that the disc is in thermal and hydrostatic equilibrium. When the external pressure is insignificant at a given radius, accretion rate and black hole mass, the emitted flux $[F_0]_s$, and surface temperature $[T_0]_s$ are fixed quantities (2.57; 2.58). Therefore as radiation

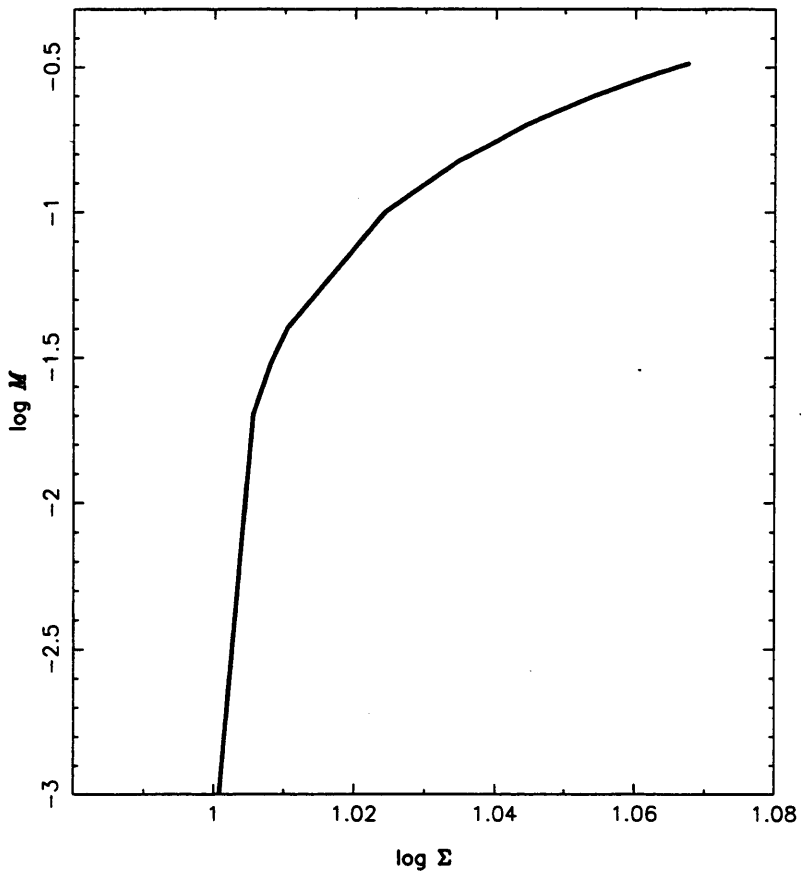

Figure 22

The $\dot{M}$ (Σ) curve for the disc in figure 21 taken at $1.5\times10^{15}cm$.

pressure begins to dominate ($\beta \to 0$), the disc surface flares up ($\zeta_s \to \infty$ in 2.83). It is due to this fact that past attempts to investigate the internal structure of geometrically thin, optically thick accretion discs (Urpin, 1982; Siemiginowska, 1988; Kley & Lin, 1992) have avoided the radiation pressure dominated region. In our example, at $\sim 10^{15}cm$ the upper regions of the disc effectively become optically thin and our model breaks down.

In figure 24 we show the $\log\dot{M}(\log\Sigma)$ relation for the disc at $1.5\times10^{15}cm$. The gradient is positive because the majority of the disc is still dominated by gas pressure which is viscously and thermally stable. When

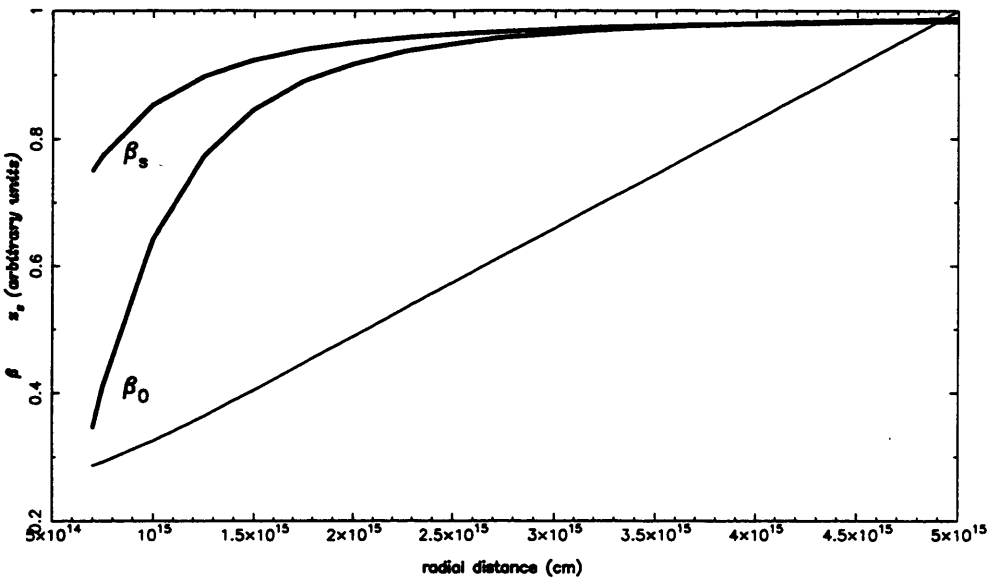

Figure 23

The gas pressure to total pressure ratio is plotted against radius for the disc in figure 21 with $n = 3$. Both the surface β_s and centre line β_0 (thick lines) values are shown. The disc surface (scaled) is also shown (thin line).

$\log \dot{M} \sim -0.5$ the disc surface begins to flare, the upper regions become optically thin and our results become unreliable.

In figure 25, a more significant external pressure is applied to the inner disc region ($n = 3$). In this case the material near the disc surface remains cooler than that of figure 23, thereby reducing the significance of radiation pressure. We find that in the inner regions of the accretion disc it is the material near the equator which is subjected to the greater proportion of radiation pressure. Another difference with the disc in figure 23 is that the disc surface does not flare up as the contribution from radiation pressure increases. As the only difference between figure 23 and 25 is the value of n, the change in the disc solutions must be a consequence of the effect of the surface pressure on the flux.

If we consider a radiation pressure dominated disc ($\beta \sim 0$) subjected to a large external pressure, we see that the disc cannot maintain hydrostatic equilibrium by raising the disc surface (as it did in the $n = 1$ case, see (2.83))

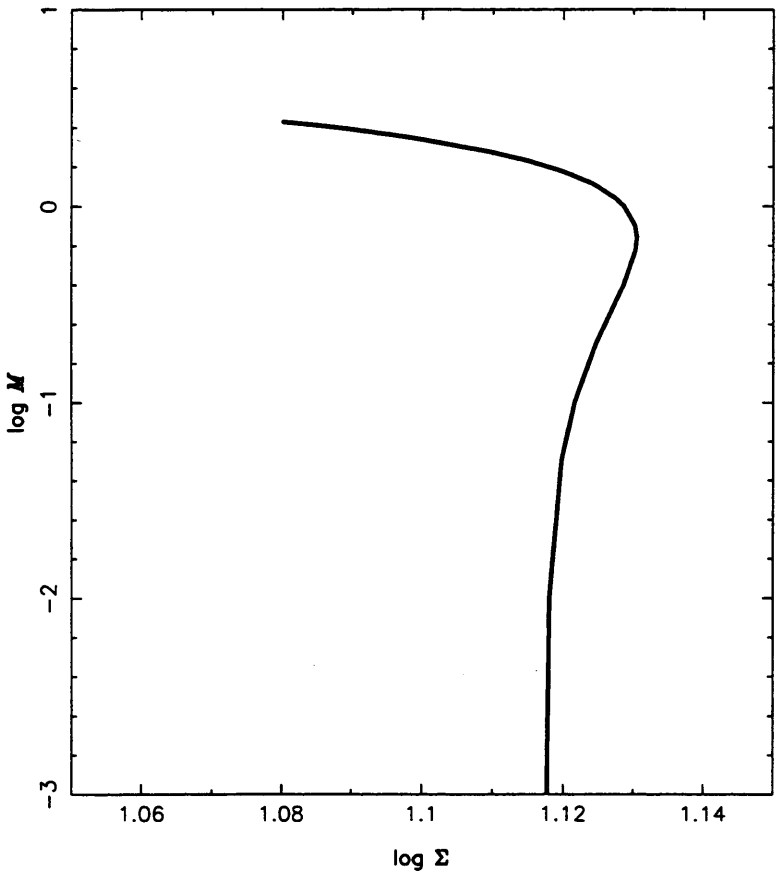

Figure 24

The $\dot{M}$ (Σ) *curve for the disc in figure 23 taken at* $8\times10^{14}cm$

because the surrounding medium 'pushes' the surface down. Therefore to keep (2..83) consistent, $[F_0]_s$ and $[T_0]_s$ are reduced by the surface terms (in a similar fashion to that seen in zones B and C).

Figure 24 shows a disc with the same configuration as that in figure 22, but in this case $n=3$ and the solutions are shown at $8\times10^{14}cm$. As in the standard thin disc our solutions become viscously unstable (at $\log\dot{M}$ ~ –0.1 in this example). As the accretion rate increases (figure 24) the effect of the external pressure lessens and the disc surface flares (as with the disc in figure 22). The upper regions of the disc become optically thin and our results unreliable.

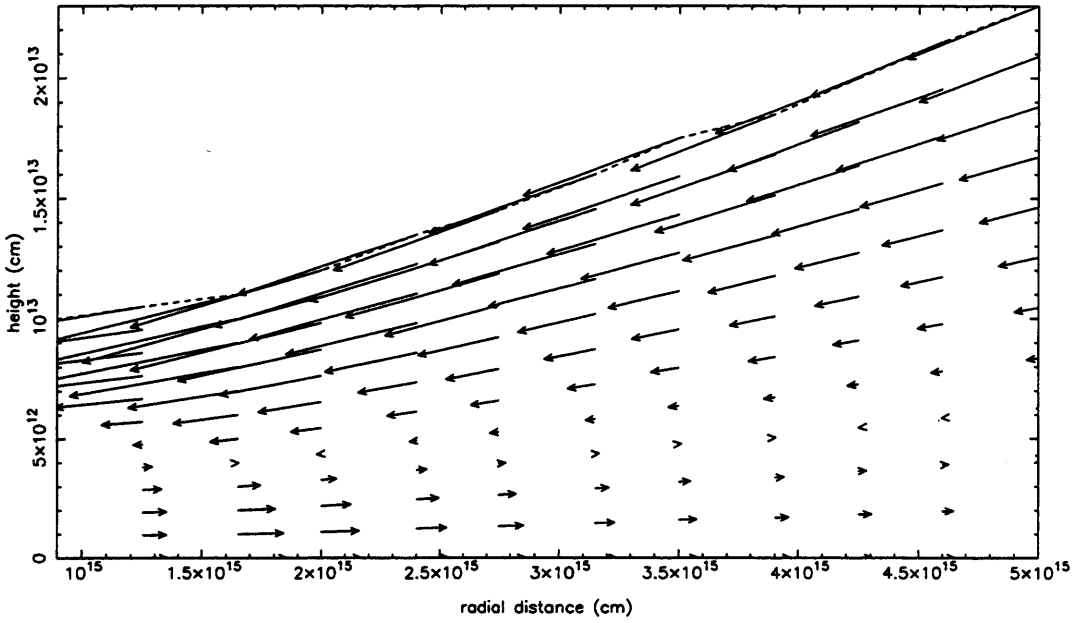

Figure 25

The r-z velocity field of the disc in figure 23. As radiation pressure begins to dominate the velocities become large (2.36; 2.80). The surface velocities $\sim 10^6 cm\ s^{-1}$ *and central velocities* $\sim 10^5 cm\ s^{-1}$.

The internal structure of the previously discussed disc ($n = 3$) is shown in figure 25. When radiation pressure dominates ($\beta \to 0$) the fluid velocities becomes large (c.f. (2.36) and (2.80)). This implies that advection (heat transport by the bulk motion of the disc material) could become important in this region. As discussed earlier in this section, this was proposed in the slim disc of Abramowicz et al. (1988), where the inflowing disc material carried a proportion of the locally generated energy before depositing it closer to the inner boundary. This was used as a cooling mechanism, to prevent the radiation disc thermal instability. However, figure 25 shows that the central regions of the disc are outflowing, and any advection would deposit energy at greater distances.

2.4 Sources of external pressure

In the previous section it was realised that when an external pressure is applied to an accretion disc in the form of a power law

$$P_{Ext} \propto r^{-n}, \tag{2.67}$$

then there is a critical value of $n = n_c$, where if $n < n_c$ the external pressure can become large enough (at large radii) to alter significantly the internal structure of the accretion disc.

Until now, the cause of the external pressure has been unspecified. In this section we will discuss a variety of pressure sources, and investigate if any of them can provide a significant 'push' that could influence the disc structure.

2.4.1 Disc coronae and winds

The scale height of a standard thin disc increases with radius as $r^{9/8}$ (1.22). X-rays emitted by the central component region near the black hole will either be intercepted directly by the 'flared' outer regions of the disc (Cunningham, 1976), or partly reflected towards the disc by a Compton thin medium (Jones & Raine, 1980; Begelman et al., 1983; Collin-Souffrin & Dumont, 1990). The radiation is sufficiently hard that material in the upper regions of the disc can be heated, by the Compton process, to temperatures exceeding $10^7 K$ (Begelman et al., 1983). As these temperatures are far greater than the internal temperatures associated with the outer regions of accretion discs, the heated gas forms a tenuous corona with a thickness exceeding that of the disc. If the sound speed in the heated gas also exceeds the escape speed of the system at that radius, then the gas steadily escapes as it is heated, forming a wind.

To summarize, we can define

$$\xi \equiv r / r_{IC} = T_{IC} / T_g \tag{2.84}$$

where r_{IC} is the radius at which the Compton temperature equals the escape temperature ($\sim 10^{18} cm$), T_{IC} is the 'inverse Compton temperature', at which Compton heating balances inverse Compton cooling ($\sim 10^8 K$), and T_g is the escape temperature. If $\xi < 1$, we expect a sharp transition from a disc photosphere to a static hot corona at $T = T_{IC}$. On the other hand, for $\xi > 1$, a vigorous wind may arise as the gas is heated to a temperature that exceeds the escape temperature.

The surrounding corona, or wind, will exert a pressure upon the disc. Begelman et al. (1983) found that in the inner regions of the disc ($\xi < 1$) the ratio of the external pressure to that of the internal disc pressure yielded

$$\frac{P_{Ext}}{P_0} = \frac{1}{22.0} \frac{\alpha \varepsilon_{-1} f T_4^{1/2}}{T_{IC8} \Xi_0'} \left(\frac{\xi}{0.1}\right) \tag{2.85}$$

where Ξ_0' is the ionization parameter at the base of the wind/corona, ε is the efficiency of mass-to-energy conversion in the accretion flow, and f is an attenuation factor. All these terms are of order unity. α is the usual α-viscosity parameter. At a distance of $\sim 10^{16} cm$, this ratio is $\sim 10^{-3} \alpha r_{16}^{5/8}$. This value is probably too small to effect the structure of an accretion disc.

For discs with $\xi > 0.1$, Begelman et al. (1983) found the ratio

$$\frac{P_{Ext}}{P_0} \geq \frac{\alpha}{28} \left(\frac{T_4}{T_{IC8}}\right)^{1/2} \frac{\ln(12.5\xi)}{\xi}. \tag{2.86}$$

At a distance of $\sim 10^{17} cm$, (2.86) corresponds to a ratio of about $\sim 10^{-2} \alpha r_{17}^{5/8}$. This magnitude of external pressure could be significant enough to cause structural changes within the disc, especially for discs with high α or low $\dot{M}$. In principle, this could be observed by a reduction in the predicted blackbody

emission spectrum. However, at such large distances from the central black hole ($\sim 10^{17} cm$) it is debatable whether any departures from a thin disc spectrum could be observed. Changes would occur in the optical/infrared end of the spectrum and most likely would be swamped by the reprocessed emissions associated with the infrared bump (Collin-Souffrin, 1994).

2.4.2 Jets

In the previous section (§2.4.1) X-rays emitted by the central region near the black hole were discussed as the energy sources that produced disc coronae and winds in the outer radii of accretion discs. However, it has also been suggested that there is a hard X-ray component associated with radio jets (Canizares & White, 1989). This component has a Compton temperature of order $10^8 K$ and illuminates both faces of the disc directly.

Irradiation of the disc by the jet will contribute to the pressure on the surface of the disc by heating the disc material. The external pressure on the disc from this source will take the form $P \propto 1/(r^2+h^2)$, where h is the height of the jet source above the disc. From Begelman et al., (1983), a more complete expression can be derived. Assuming that the incident X-rays are unattenuated while passing through the disc flow, the external gas pressure applied to the disc surface will be strictly proportional to the mean radiation intensity encountered there: i.e.

$$P_{Ext} = \frac{lL_{Edd}}{4\pi(r^2+h^2)c\Xi_0'}. \qquad (2.87)$$

Here lL_{Edd} is the luminosity of the jet. For Ξ_0', the ionization parameter at the disc surface, we put $\Xi_0' = 3$ (Begelman & McKee, 1983). The height of the jet source is of order $5\times10^{16} - 5\times10^{18} cm$, which means an almost constant external pressure applied to an accretion disc for $r < h$. When $r > h$ the external

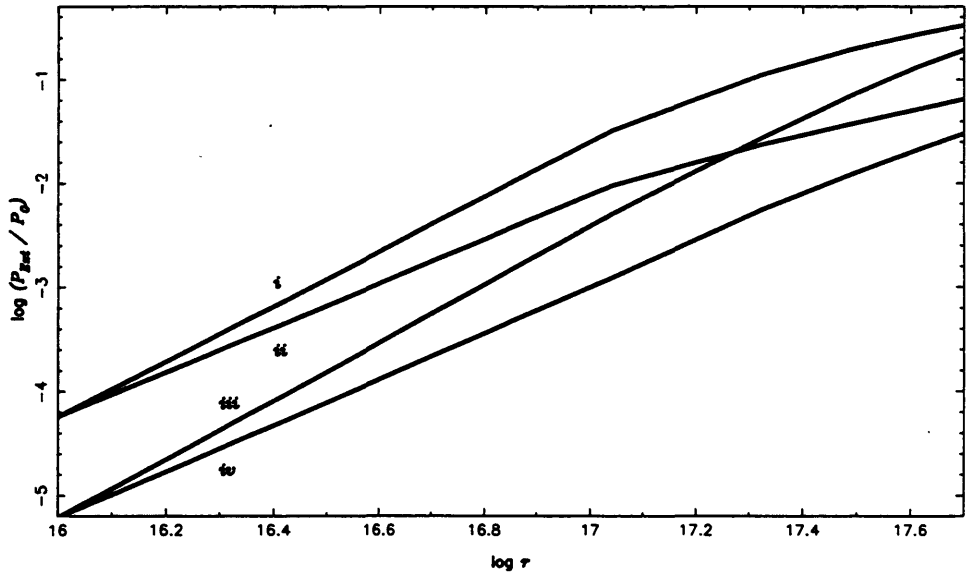

Figure 26

The ratio of external pressure to central pressure as a function of radius. The external pressure is provided by radiative heating of the disc atmosphere by the hard X-rays from radio jets with (i) $h = 5\times10^{16} cm$, $\dot{M} = 0.01 M_0 yr^{-1}$; *(ii)* $h = 5\times10^{16} cm$, $\dot{M} = 0.1 M_0 yr^{-1}$; *(iii)* $h = 5\times10^{17} cm$, $\dot{M} = 0.01 M_0 yr^{-1}$; *(iv)* $h = 5\times10^{17} cm$, $\dot{M} = 0.1 M_0 yr^{-1}$ *in (2.87).*
Disc system: $M = 10^8 M_0$, $\alpha = 0.5$, $lL_{Edd} = 0.1$, *Kramers' opacity.*

pressure falls off as $\sim r^{-2}$, which is still more slowly than the disc central pressure. Figure 26 shows how the $P_{Ext} / P_0(\omega,0)$ ratio changes with radius for a variety of disc configurations and disc heights. The more dominant external pressures are related to the discs with low accretion rates. In reality the luminosity of the jet is related to the accretion rate and so a reduction in $\dot{M}$ will be met by a similar reduction in lL_{Edd}, thereby changing $P_{Ext} / P_0(\omega,0)$. Even with this taken into account, it is clear that the external pressure will become significant enough to alter the internal structure ($P_{Ext} / P_0(\omega,0) > 0.01$) in the outer regions of the disc.

An alternative approach to calculating the external pressure provided by radio jets is outlined by Krautter et al. (1983). Their work involves calculating the external equilibrium pressure needed to collimate a jet. If it can be assumed

that the collimating pressure follows approximately spherical isocontours then a similar external pressure will be applied to the disc surface at equivalent distances. This would certainly mean that there are large external pressures in the inner regions of accretion discs.

2.4.3 An optically thin accretion disc

The discovery of new classes of galactic X-ray sources in the 1970's (the 'bursters', and the globular cluster sources; see Grindlay, 1976, for review) brought about the need for a new type of disc model. These new X-ray sources had an average X-ray luminosity $L_X \sim 10^{36-37} erg/s$, and peak luminosities exceeding $10^{38} erg/s$, at energies $E \geq 1keV$, along with remarkable time-variations. Black hole masses of $M \sim 10^3 M_0$ were postulated by Silk & Arons (1975).

The standard thin disc model (Shakura & Sunyaev, 1973) predicts a very soft X-ray spectrum under the relevant conditions $L \sim 10^{37} erg/s$, $M \sim 10^3 M_0$, with an observed emission temperature $kT_X << 1keV$. Therefore this model does not apply directly (Liang, 1977). However, Pringle et al. (1973) noted that 'non-standard' optically thin accretion discs around massive black holes could be constructed. These would predict a strong emission in the X-ray band.

Since the possibility of optically thin discs was first postulated, a great deal of work has been done in this area to provide a model of the hard X-ray and gamma-ray emission of AGN. This has taken the form of wholly optically thin discs (i.e. Payne & Eardley, 1977; Kusonose & Takahara, 1988) or 'sandwich discs', where a fraction of the accretion flow forms an optically thick disc, geometrically thin disc, while the rest of the material is in a hot, optically thin disk, extending as a corona above and below the optically thick region (e.g. Wandel & Liang, 1991).

In the case of a sandwich disc the optically thick disc and optically thin corona will be in pressure balance at the optically thick surface (Kusonose &

Mineshige, 1994). In this section we will derive a 'simple' optically thin disc in order to discover the magnitude of the external pressure it would provide to a geometrically thin slab of optically thick material in the equatorial plane.

In an optically thin disc ($\tau < 1$) radiation escapes freely once produced and the material itself reabsorbs very little. The diffusion equation (1.13) can no longer be used to describe the flux of radiant energy and instead the volume loss of energy is

$$-\underline{\nabla}.\underline{F} = -4\pi \int j_\nu d\nu \qquad (2.88)$$

where j_ν is the emission coefficient. A variety of optically thin disc models have been developed using different cooling mechanisms; the pure bremsstrahlung disc, the Comptonised bremsstrahlung disc and the Comptonised soft photon disc, all in both the one-temperature and two temperature (different temperatures for the electrons and protons) version and including the effects of electron-positron pairs (see Kusonose & Takahara, 1988 for pairs in the two temperature pure bremsstrahlung disc and Tritz & Tsuruta, 1988 for pairs in the two temperature Comptonised soft photon disc).

In developing a basic model for an optically thin disc we will not take into account soft photon sources (produced by blackbody emission or synchrotron radiation for example). Therefore we neglect the effects of Compton scattering. Comptonization of bremsstrahlung photons may play a role in creating a Wien bump if τ_{ES} (the optical depth if electron scattering is the dominant opacity mechanism) is large enough. However, as we will show, the effects are not significant for the obtained values of τ_{ES}.

In all disc models, energy is initially deposited into the protons. In the one-temperature disc, energy exchange between protons and electrons is rapid and the proton and electron temperatures are simply set equal, whilst in the two-temperature disc, protons cannot cool down to the temperature of the

electrons. The internal structure of the disc is unlikely to be strongly coupled to the electron temperature (Chen, 1995), and so we shall set the disc temperature equal to the proton temperature $T \approx T_p$. The electron temperature is approximately one order of magnitude smaller than the proton temperature (Guilbert & Stepney, 1985). Thus, our model is to be a simple one-temperature optically thin disc cooled by pure bremsstrahlung.

The model will take the same form as that derived for the optically thick disc in §2.2. Assuming that the local radiative cooling is provided by optically thin thermal bremsstrahlung, (2.88) becomes

$$-\underline{\nabla}.\underline{F} = c_{ff}\rho^2 T^{1/2} A \tag{2.89}$$

where $c_{ff} = 5.6\times10^{20} erg\, s^{-1} K^{-1/2} g^{-2} cm^3$ is the bremsstrahlung emissivity coefficient, and the Compton luminosity enhancement factor $A \sim 1$ (Wandel & Liang, 1991). For optically thin discs the pressure is given by the gas pressure ($P = P_g$ in (2.13), or $\beta = 1$ in (2.30); Eardley et al., 1978). This and equation (2.89) dramatically simplify the energy equation (2.8). Using the thin disc expansions derived in §2.2.2, (2.8) becomes

$$\frac{3}{2}[U(\sigma c^2)_{,\omega} + W(\sigma c^2)_{,\zeta}] + \frac{5}{2}\sigma c^2 (U_{,\omega} + W_{,\zeta} + \frac{U}{\omega}) - \frac{\nu\sigma\tilde{M}^3}{\alpha\bar{c}\bar{r}\omega^2}(\omega^2 (V_{,\omega})^2 - 2\omega V V_{,\omega} + V^2)$$
$$- \frac{\bar{c}\nu\sigma\tilde{M}^4}{\alpha\bar{z}} V_{,\zeta}^2 + \frac{c_{ff}\bar{\rho}\bar{T}^{1/2}\tilde{M}\bar{r}}{\alpha\bar{c}^3}\sigma^2 T^{1/2} = 0. \tag{2.90}$$

The zero order terms correspond to an energy balance between cooling by bremsstrahlung and the energy generated locally by viscous dissipation: using (2.28) and (2.33)

$$\frac{9\sigma_0 c_0^2}{4\omega^{3/2}} = \sigma_0^2 T_0^{1/2} A_{brem} \tag{2.91}$$

where

$$A_{brem} = \frac{c_{ff}\bar{\rho}\bar{T}^{1/2}\tilde{M}\bar{r}}{\alpha\bar{c}^3}. \tag{2.92}$$

As the disc is dominated by gas pressure, this zero order can be rearranged to give an explicit expression for the disc temperature in terms of pressure

$$T_0^{3/2} = \frac{4}{9}A_{brem}P_0\omega^{3/2}. \tag{2.93}$$

This indicates that a knowledge of the emitted flux from the disc is not needed in determining the internal disc dynamics, in contrast to the optically thick case. Therefore the final system of disc equations is greatly simplified, along with the applied boundary conditions. The radial derivative of temperature can be found explicitly from (2.93), and so the system of eight first order differential equations in §2.2.4 needed to obtain the vertical structure of an optically thick disc is reduced to a system of four first order differential equations for the optically thin disc:

$$\frac{\partial P_0}{\partial\zeta} = -\left(\frac{9}{4A_{brem}}\right)^{2/3}\frac{P_0^{1/3}\zeta}{\omega^4} \tag{2.94}$$

$$\frac{\partial P_{0,\omega}}{\partial\zeta} = -\left(\left(\frac{9}{4A_{brem}}\right)^{2/3}\frac{P_0^{1/3}\zeta}{\omega^4}\right)_{,\omega} \tag{2.95}$$

$$\frac{\partial\Xi_0}{\partial\zeta} = \left(\frac{9}{4A_{brem}}\right)^{2/3}P_0^{1/3}U_0 \tag{2.96}$$

$$\frac{\partial\tau_0}{\partial\zeta} = \left(\frac{9}{4A_{brem}}\right)^{2/3}\frac{P_0^{1/3}}{\omega} \tag{2.97}$$

where from (2.36) and (2.93) we see that

$$U_0 = (\frac{4A_{brem}P_0}{9})^{2/3}(-6\omega^{3/2} - 3\omega^{5/2}\frac{P_{0,\omega}}{P_0}). \qquad (2.98)$$

The equation for optical depth (2.97) is calculated using electron scattering to describe the opacity. It is included in order to check for consistency. The optical depth must remain low ($\tau_{ES} < 2.5$) for our disc to remain optically thin, and Comptonization of bremsstrahlung photons negligible (Kusonose & Takahara, 1988). Without the need to calculate the flux at the surface of the disc, the boundary conditions are simply a condition of pressure balance at the disc surface between the disc and its surrounding medium, and the condition of constant mass flux:

- at $\zeta = 0$	- at $\zeta = \zeta_s$
$P_0 = S(1)$	$P_0 = P_{Ext}$
$P_{0,\omega} = S(2)$	$P_{0,\omega} = P_{Ext,\omega} + (\frac{9}{4A_{brem}})^{2/3}\frac{P_{Ext}^{1/3}\zeta_s}{\omega^4}S(3)$
$\Xi_0 = 0$	$\Xi_0 = \dot{M}$
$\tau_0 = S(4)$	$\tau_0 = 0$

(2.99)

where similarly to §2.2.4 the array S contains the unknown parameters to be calculated by the NAG library routine.

To obtain the radial structure we need to prescribe two boundary conditions at r_{in} and r_{out}. As with the optically thick disc, these correspond to the accretion rate and disc surface height at the starting radius. The radial structure of the disc is obtained by solving the first order differential equations

$$\begin{aligned} y &= \zeta_s \\ y_{,\omega} &= S(3) \end{aligned} \qquad (2.100)$$

where $S(3)$ is the disc surface gradient $\zeta_{s,\omega}$.

The surface is defined by a condition of pressure balance with the external medium. Once again, we shall express the external pressure in the form of a power law

$$P_{Ext} \propto r^{-n}. \tag{2.101}$$

Its source maybe a static corona or disc wind that originates from disc irradiation by either the central continuum near the black hole or a jet.

To obtain an order of magnitude value for the central pressure of our optically thin disc, (2.94) can be solved explicitly with the appropriate boundary condition to give

$$P_0 = (P_{Ext}^{2/3} + (\frac{9}{4A_{brem}})^{2/3}(\frac{\zeta_s^2 - \zeta^2}{3\omega^4}))^{3/2}. \tag{2.102}$$

Therefore the central pressure is obtained as

$$P_c = (P_{Ext}^{2/3} + (\frac{9}{4A_{brem}})^{2/3}\frac{\zeta_s^2}{3\omega^4})^{3/2} \tag{2.103}$$

and from (2.97) the central temperature is

$$T_c = (\frac{4A_{brem}}{9})^{2/3}(P_{Ext}^{2/3} + \frac{9}{4A_{brem}}\frac{\zeta_s^2}{3\omega^4})\omega. \tag{2.104}$$

At a radial distance of $10^{16}cm$ this corresponds to a temperature of $\sim 10^8 K$. As the disc is in hydrostatic and thermal equilibrium, a disc temperature such as this translates to a relatively geometrically thick disc of height $\sim 8\times 10^{14}cm$. Therefore, we can consider a 'sandwich' disc system (Wandel & Liang, 1991) where a geometrically thick, optically thin disc 'sits' upon a geometrically thin, cold slab of material. In this case the optically thin

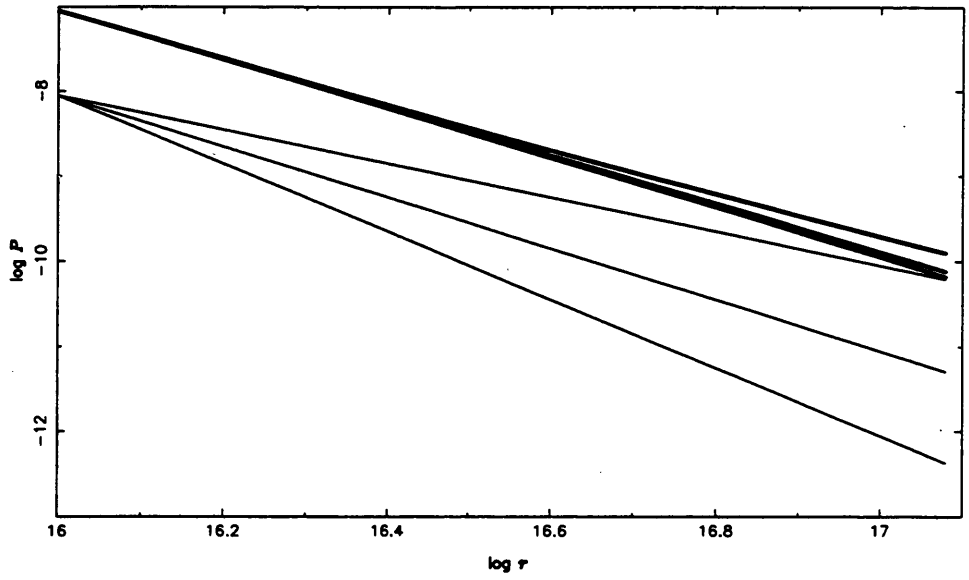

Figure 27

A plot showing the evolution of the central pressure (thick lines) and external pressure (thin lines) with radius for a three values of n *in (2.105). For both central and external pressure (in increasing* $\log P$ *)* $n = 1, 2, 3$.

Disc system: $M = 10^8 M_0$, $\dot{M} = 10^{-4} M_0 yr^{-1}$, $\alpha = 0.05$, *optically thin disc.*

disc will be in pressure balance with the optically thick slab; equation (2.103) gives the external pressure being applied to the lower material.

We have run the code described above for an optically thin disc under a variety of different accretion rates and external pressures (2.101). Figure 27 shows how the central pressure of the disc varies with radius under the influence of a variety of external pressures. We see that for low values of n (external pressures becoming significant at large radii) the central pressure converges towards its surface value. This is because the external pressure compresses the surface, keeping the value of ζ_s low in (2.103), and therefore $P \to P_{Ext}$. For higher values of n the central pressure departs from its surface value as the external pressure becomes negligible at large radii, and ζ_s large. The overall result is that the central pressure of an optically thin disc is unlikely to be many orders of magnitude greater than the pressures provided by coronae or winds (calculated in §2.4.1 and §2.4.2).

We have established the fact that real sources of external pressures can become large enough to alter the disc structure. We now discuss whether any of these changes will be significant enough to manifest themselves as observable phenomena.

2.5 Discussion

2.5.1 Vertically isothermal approximation

The internal structure of a geometrically thin, optically thick accretion disc has been investigated when an external pressure is applied at the disc surface. In §2.4 we showed that this external pressure could be provided by a hot corona or wind that surrounds the disc. When the applied pressure is small ($< 0.1\%$ of the disc central pressure) we find that the disc quantities can be approximated by the classical solutions of the standard thin disc (Shakura & Sunyaev, 1973; Lynden-Bell & Pringle, 1974). However, the vertically averaged solutions of the thin disc cannot resolve the internal structure of an accretion disc and the fluid flow is assumed to be wholly inflowing. In self-consistently solving the internal structure of the disc we find an outflow of material near the equatorial plane and inflow near the surface of the disc. This is a similar result to that found by Urpin (1983) (and after him Siemiginowska (1988) and Kley & Lin (1992)). However, in solving the vertical structure of the disc Urpin approximated the hydrostatic equation (2.32) with the vertically isothermal solution $\sigma_0 \propto \exp(-\zeta^2/2H^2)$, and therefore his solutions must be thought of as pseudo-isothermal. The similarity between our disc solutions for $n > n_c$ and those of Urpin means that discs subjected to small external pressures can probably be represented by vertically isothermal models. Although this cannot be used if the emitted spectrum is required, it will make the calculation of the disc structure easier. This is because the energy equation (2.8) can be

replaced by a known radial dependence for the temperature. This is adopted when applications of this disc model are developed in §3 and §4.

2.5.2 Absence of meridional circulations

Kippenhahn & Thomas (1982) proposed that a disc cannot simultaneously be in hydrostatic and thermal equilibrium if the azimuthal velocity is just a function of radius. If the disc is in hydrostatic equilibrium, then circulatory motions are induced to carry away the energy which cannot be transported by radiation. This introduces a non-zero vertical gradient to the azimuthal velocity. This is similar to that which is expected in the case of rotating stars (Eddington, 1925; Vogt, 1925; Roxburgh, 1966). The relevant timescales within an accretion disc can be estimated as follows:

The Kepler time τ_k

$$\tau_k = \frac{1}{\Omega_\phi} = \frac{r}{\upsilon_\phi} = \frac{r^{3/2}}{\sqrt{GM_{bh}}}. \tag{2.105}$$

The dynamical timescale $\tau_{dyn\,z}$, $\tau_{dyn\,r}$

These are the characteristic timescales for hydrostatic equilibrium in the vertical direction, which is of order of the timescale for free fall in the z-component of the gravitational force, and pressure equilibrium in the radial direction, which is the timescale for a sound wave travelling through the disc in the radial direction, respectively. Hence,

$$\tau_{dyn\,r} \approx \frac{r}{H}\tau_{dyn\,z} \approx \frac{r}{H}\tau_k. \tag{2.106}$$

The thermal adjustment time τ_{th}

Using the α-paramaterisation for the viscosity $\nu = \alpha H \upsilon_s$, where υ_s is the sound speed, gives

$$\tau_{th} \approx \frac{1}{\alpha}\tau_k . \tag{2.107}$$

The viscous timescale $\tau_{visc\,z}$, $\tau_{visc\,r}$

The time necessary for viscosity to smooth out vertical gradients of the angular velocity

$$\tau_{visc\,z} \approx \frac{H^2}{\nu} \approx \tau_{th} \approx \frac{1}{\alpha}\tau_k , \tag{2.108}$$

while the characteristic scale for viscosity to exchange information in the radial direction is

$$\tau_{visc\,r} \approx \frac{r^2}{\nu} \approx \frac{r^2}{H^2}\tau_{th} \approx \frac{r^2}{\alpha H^2}\tau_k . \tag{2.109}$$

If $\alpha < H / r$, then from (2.106) and (2.107) the thermal timescale is longer than the dynamical timescale in the radial direction and the solution will close to hydrostatic equilibrium and violate thermal equilibrium, thereby causing meridional circulations. In the other case $\alpha > H / r$ the thermal adjustment is a stronger condition than the hydrostatic adjustment in the radial direction. Here, the energy released by viscous dissipation is expected to be radiated vertically while there is no radial pressure equilibrium. Therefore motions will occur which, via their initial pressure, will take care of the horizontal balance.

Siemiginowska (1988) claim to show these meridional circulations but, as mentioned earlier, their inability to keep the accretion rate constant throws their results into some doubt. Similarly, the vertically isothermal approximation of the hydrostatic equation by Urpin (1983) (see §2.5.1) could be an explanation for the lack of small scale circulations in that model.

As can be seen in figures 10-12, 17-19 and 25, we obtain no such meridional circulations. This is a consequence of our boundary conditions and the insistence on obtaining the structure of a disc in both hydrostatic (2.55) and thermal (2.58) equilibrium. The effect of the surface pressure allows the disc to adopt the correct surface height so that hydrostatic and thermal equilibrium are not violated.

2.5.3 The nature and stability of the disc equilibrium solutions

Applying a large external pressure to the surface of the disc also alters the internal velocity field. Compression of the surface leads to a flattening of the radial pressure distribution within the disc. As a result (c.f. 2.37), the usual outflow of material near the equatorial plane changes direction, and the whole disc is inflowing towards the central black hole. The change in flow direction causes a displacement in the $\dot{M}(\Sigma)$ curve (figure 13 and 21). This is due to the fact that if the accretion rate is fixed, then there is more material in the disc with both inflow and outflow than in the disc with just inflow. Therefore, in a vertically averaged model, where the material in the disc is assumed to be wholly inflowing, the value of Σ is always too low unless a large external pressure is applied to the disc surface. This could have a significant effect on the stability of an accretion rate.

There has been much work in calculating the nature of the equilibrium solutions of the α-accretion disc. This includes inputting the correct opacity mechanisms in a given temperature regime, but this has generally been done using vertically averaged solutions (e.g. Clarke, 1988). Equilibrium solutions are shown on an $\dot{M}(\Sigma)$ curve where, as we have seen in §2.3.4, $\partial\dot{M}/\partial\Sigma > 0$ implies a viscously and thermally stable solution, whilst a disc with $\partial\dot{M}/\partial\Sigma < 0$ is prone to these instabilities. It has been predicted that $\partial\dot{M}/\partial\Sigma < 0$ for discs that are partially ionized and discs that are radiation pressure dominated (Lin & Shields, 1986; Clarke, 1988).

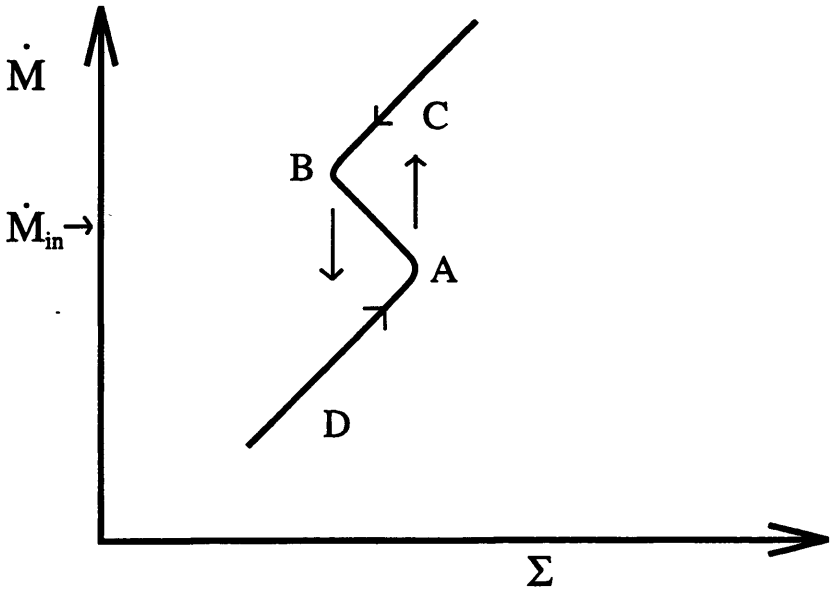

Figure 28

A schematic evolutionary path in the local ($\dot{M}$,Σ) plane showing limit cycle behaviour, where $\dot{M}_{in}$ corresponds to an unstable equilibrium solution (Clarke, 1988).

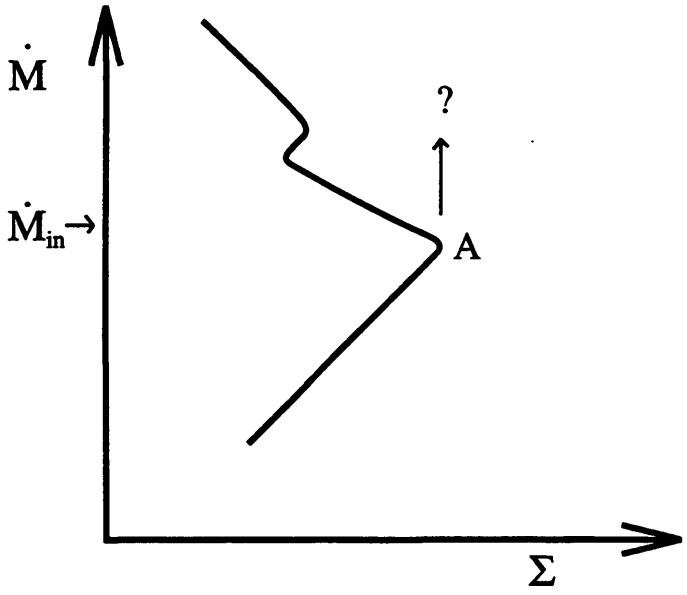

Figure 29

As in figure 28 but showing an example of runaway behaviour (Clarke, 1988).

Suppose the steady state accretion rate into an annulus, at radius R, is fixed at $\dot{M}_{in}$. If this accretion rate corresponds to an unstable equilibrium solution, then its evolution is determined by the shape of the equilibrium $\dot{M}(\Sigma)$

curve in the vicinity of the unstable regime. If the unstable sequence connects to stable sequences at higher or lower Σ (figure 28), the solution will undergo a vertical transition in the $(\dot{M},\Sigma)$ plane, (AC or BD) corresponding respectively to runaway heating and cooling at a give surface density. In this case the annulus is forced to perform the limit cycle ACBD in a search for a stable equilibrium corresponding to $\dot{M}_{in}$. If, however, there exists only one stable solution at the instability threshold (figure 29), then the outcome is more problematic. Here the onset of runaway heating could lead to the disc breaking down and becoming optically thin (Lin & Shields, 1986).

For a given set of disc parameters (including $\dot{M}$), the value of Σ depends on the amount of outflow within the disc and therefore the magnitude of the external pressure applied by the surrounding medium. This means that the external environment of the disc can play a crucial role in determining the outcome of an instability.

We have only applied our model to the regions where the disc is gas or radiation pressure dominated, with the opacity given by electron scattering or Kramers' formulae. These radial zones do not give the S -shaped $\dot{M}(\Sigma)$ curve needed to investigate the effects of the external pressure on the stability of the disc. In future work, different opacity mechanisms could be studied, where an S -shaped $\dot{M}(\Sigma)$ curve is believed to exist (i.e. partially ionized discs).

2.5.4 A thermally stable radiation pressure dominated disc?

In §2.3.4 it was said that the standard thin disc is thermally and viscously unstable when radiation pressure dominates. Stabilizing mechanisms have been suggested (advection, Abramowicz et al., 1988; and a z-dependent viscosity parameter, Milsom et al., 1992), but these are only effective at high accretion rates.

When our disc model was used in the radiation pressure dominated inner region of the accretion disc, we noted that disc flaring, caused by a low value

of β in (2.88), could be suppressed when a large external pressure was added (> 1% of the central pressure). The surface terms had a cooling effect on the disc and hydrostatic and thermal equilibrium could be achieved at a small disc height.

This implies that the disc could be thermally stable. If the temperature within the disc is increased by a small perturbation then the disc surface will rise to maintain thermal and hydrostatic equilibrium. However, as the surface gradient changes, the surface terms will have a cooling effect on the disc causing the disc surface to fall back down to a stable height. Similarly if the temperature is decreased by a small amount we expect that the change in surface gradient will introduce a heating effect and a stable solution will be found. The observed collimation of radio jets (§2.4.2) would suggest that large external pressures are apparent in the inner regions of disc - black hole systems. Since we have only treated a special case (zero net torque boundary condition) a more formal investigation into the stability of radiation pressure dominated discs subjected to large external pressures would be needed to establish these results.

2.5.5 UV variability of AGN

In the previous section §2.5.4 we proposed that the radiation pressure dominated inner regions of an accretion disc could be thermally stabilized when subjected to a large external pressure (< 1% of the central pressure). This result could help explain the observed UV variability in AGN spectra which is thought to be caused by accretion disc instabilities.

Siemiginowska & Czerny (1989) have suggested that the instabilities apparent in the radiation pressure dominated disc may develop over a limited time-scale, before the disc is stabilized by irradiation of the disc by the non-thermal component of the spectrum (Czerny et al., 1986) or the advective term (Abramowicz et al., 1988). The instability should then manifest itself as an

observed variability in the AGN spectrum. The UV band would be the most interesting to study because, as we have seen, it is this region where the domination by the disc is most profound (Malkan, 1983). Siemiginowska & Czerny then used the observed UV variability to determine the viscosity parameter α using the thermal timescale (2.107). The observed UV variability in AGN ranges from ~5-5000 days which corresponds to a range of α between 0.1 and 0.001.

This predicted range of α is rather large. In other astrophysical systems where accretion discs are believed to exist, a much smaller range of α is predicted (i.e. α ~ 0.7 - 1.0 in C.V.'s, see Frank et al., 1992). If in some of the AGN, the inner disc is subjected to a large external pressure, then the disc would be thermally stable. Any variability could then be interpreted as due to viscous instabilities within the disc. For a disc of $M = 10^8 M_0$ and $\alpha = 0.1$, then from (2.109) we get $\tau_{visc\,r} \sim 3000$ days at $50r_s$ (the largest value used by Siemiginowska & Czerny). Therefore this could imply that all AGN have a similar value of α. The observed short timescale variability in the UV spectra could be due to thermal instabilities in disc systems experiencing little external pressure, whilst the large variability timescales would be due to viscous instabilities in systems with significant external pressures.

In this chapter we have developed a model that shows the internal structure of an α-accretion disc. However, our model can only accurately describe a disc in which the velocities are small. As we have seen with the 'slim' disc (Abramowicz et al., 1988), in a radiation pressure dominated region, the velocities can become large enough that advection of heat could become important (figure 27). This implies that the next order $1/\tilde{M}^2$ terms, in the disc equations §2.2.1, should be considered in this region. Similarly, we have not investigated the effects of the radial transport of flux in the energy equation, and the $1/\tilde{M}^2$ gravity term in the z-component of conservation of momentum

equation. These terms, although small, could change the internal structure of the disc over a large radius. We hope to expand the disc model to include the next order terms in our expansion of the disc equations in order to investigate their effects on the disc solutions in the future.

Chapter Three

A model for asymmetric radio sources

3.1 Asymmetries in jets and double radio sources

High-resolution observations of extended double sources over the last few decades have shown that many of them contain jets or beams, which are intimately related to the transport of energy from the nuclei of active galaxies to the outer lobes. A crucial morphological feature of these extended sources is that there are actually two fundamentally distinct classes of object: FR I and FR II (Fanaroff & Riley, 1974).

Sources of low luminosity (power at $14GHz$, $P_{14} < 5\times10^{25}W\,Hz^{-1}$) are known as FR I type objects. These tend to have prominent, smooth, continuous two-sided jets running into large scale lobe structures (plumes) which are limb darkened, i.e. their brightness fades gradually with increasing distance away from the central object. Most straight jets are one-sided (by > 4:1 intensity ratio) close to the core but become two-sided after a few kpc. The one-sided region lasts typically <10% of the total length of the jet. Although large-scale two-sided symmetry is a general feature of FR I type structures it should be noted that some sources show significant side to side asymmetry (i.e. NGC 315 and NGC 6251; Perley, Bridle & Willis, 1984), where the brighter jet tends to be the one with the one-sided base.

Radio galaxies with $P_{14} > 5 \times 10^{25} W\,Hz^{-1}$ tend to have large-scale structures which are limb brightened, with bright outer hotspots and are referred to as FR II sources or 'classical doubles'. Although the absolute luminosities of the jets and cores in FR II objects are in general higher than in FR I galaxies, the proportionately greater increase in lobe and hotspot luminosities results in the jets and cores being far less prominent in the radio structures than for FR I type objects. Therefore, the cores and extended jets are difficult to detect. When detected, the jets in FR II sources differ significantly from those in FR I structures. They are usually one-sided with a jet / counterjet ratio > 4:1 (Bridle & Perley, 1984). The situation is further complicated since the jets are in general not smooth but dominated by 'knots', whilst the opening angles of jets in FR II structures are lower than those for FR I sources.

One of the intriguing aspect in jet research is the paradox that the majority of FR II jets are very asymmetric, often only one-sided, although the outer extended lobes are roughly symmetric. Several possible solutions to the problem have been suggested. The usual explanation is in terms of Doppler boosting of emission from relativistic plasma moving at small inclinations to the line of sight (Shklovsky, 1977; Begelman, Blandford & Rees, 1984). The apparent one-sidedness reflects the Doppler boosting of radiation from the approaching jet over that from the receding counterjet. However, the relativistic interpretation leads to some complications:

1. If large jets are beamed towards us, then their true lengths greatly exceed their projected lengths, making the extended sources, which are believed to be unbeamed, unusually large (Schilizzi & de Bruyn, 1983). Observations of the jet - counterjet system in the nucleus of NGC 6251 (Jones, 1986) have shown that they are consistent with a simple two-sided relativistic beaming model only if the radio axis is aligned within 10° of our line of sight, and the flow velocity in the two jets is greater than $0.7c$. This implies

an unreasonably large physical size for the extended radio emission associated with this galaxy.

2. Cygnus A possesses a one-sided jet structure which would require an angle of 60° or less between the jet and the line of sight, while the structure of the extended radio lobes suggests that the jet axis lies close to the plane of the sky (Hargrave & Ryle, 1976). Also, the straight forward beaming picture does not seem to allow for the apparently observed differences between the flux densities and spectra of the jet / counterjet system (Saikia & Wiita, 1982).
3. Garrington & Conway (1991) (and Garrington, Conway & Leahy, 1991) found that some one-sided sources had additional asymmetries in spectral brightness and hotspot brightness. These asymmetries are surprising because if the source is intrinsically symmetric then no such differences between the two sides of the source are expected (Tribble, 1992).
4. In about half the FR II sources with weak radio cores and lopsided hot spot brightnesses, the brighter jet points to the dimmer hot spot (Bridle & Perley, 1984). This observation is not consistent with the beaming of symmetric jets.
5. In an investigation into a geometrical and kinematical description of the curved jets associated with the S5-quasar 1928+738 in terms of a precessing beam model (Hummel et al., 1992), a moderate intrinsic brightness asymmetry of the jets has to be invoked to account for the apparent brightness ratio of jet to counterjet. Hummel et al. found that this comparatively low ratio seems to contradict the Doppler interpretation of the one-sidedness.
6. Observations of the radio emission from GRO J1655-40, a recently discovered black-hole candidate, show two highly collimated relativistic jets, one on each side of the source, which expand and decay over a few

days (Hjellming & Rupen, 1995). The alternate brightening and fading of the jets cannot be explained by relativistic beaming.

This leads to the possibility that some core-dominated sources with one-sided jets and symmetric extended structure may be intrinsically asymmetric. Saikia et al. (1989) have reported observations which suggest a new class of intrinsically one-sided lobe-dominated radio sources. Similarly, observations of an FR I type radio galaxy, 3C 338, could imply a jet that is intrinsically one-sided and alternately feeds energy into opposite directions (Feretti et al., 1993). Increasingly high resolution studies of radio galaxies and QSOs have also shown substantial differences in component size, shape and strength between the two 'symmetric' lobes (Neff & Rudnick, 1980; Macklin, 1981).

These observations have led to various proposals for intrinsically one-sided jet mechanisms. Ryle & Longair (1967) suggested time delay effects could account for the asymmetries observed. The high ejection velocities from the parent galaxy would mean that the two components would be seen at significantly different ages, unless the axis of the system is perpendicular to the line of sight. Other ideas include the possibility that the beam shines through clumpy material and that these clumps occasionally block the beam (Miley, 1980), anisotropic electron pitch-angle distributions (van Groningen et al., 1980), and transient phenomena (Christiansen et al., 1982).

Wiita (1978a, b) produced a twin beam model where a continuous source of energy and relativistic plasma lies within a cloud of confining gas in an active galactic nucleus. Wiita & Siah (1981) showed that in this model, if the source of plasma is even slightly displaced with respect to the centre of the confining gas cloud, a strongly asymmetric cavity is formed, leading towards single jet formation. However, the model is somewhat simplified; plasma processes are ignored and relativistic motions are not included properly.

The asymmetry problem of Cygnus A (see 2. above) was addressed by Saikia & Wiita (1982). They showed that the observations could be accounted

for using a flip-flop model, where the jet flips, alternately supplying energy and plasma to the two outer lobes. However, they admitted that knowledge of the actual turnover frequencies and the fact that their model is highly simplified may rule this out. They concluded that the most likely explanation is that intrinsic asymmetries between the jets exist (although Doppler effects would clearly play a role).

Rudnick (1982) and Rudnick & Edgar (1984) presented the case for a specific pattern to the asymmetries between sides of an individual source, namely that where an emission peak occurs on one side of a source, no peak will be found at the corresponding distance on the other side of the nucleus. After analysing the asymmetries in various samples of radio galaxies and QSOs Rudnick & Edgar arrived at the conclusion that the distribution of arm length ratios indicated a preferential difference between the two arms of each source which cannot be explained in terms of random fluctuations, projection or time delay effects. The distributions could possibly be explained by differential drag due to galaxy motion, or separate ejection times for each arm in a flip-flop model. However, observations that one-sided sources have preferentially stronger central components (Kapahi, 1981) does not fit naturally into Rudnick & Edgar's flip-flop picture, whilst their model cannot also explain the observations of twin jets or symmetric structures around a central component (e.g. B2 1323+31, Ekers, 1982).

Lovelace et al. (1987) and Wang et al. (1990) obtained the axisymmetric field structure for the inside of an accretion disc. They found jet solutions in which the power flow was carried mainly by the Poynting flux of the electromagnetic field and the angular momentum outflow from the disc was carried by the magnetic field. This work was extended by Wang et al. (1992) to include magnetic fields which have no reflection symmetry about the equatorial plane. The power flow was found to be different above and below the disc, and the ratio of the jet luminosities (top/bottom) depended directly on the degree of

asymmetry of the field and was shown to be much greater than unity. Therefore, this is a disc/jet model that produces intrinsically asymmetric jets. However, the authors do not investigate the time dependency of the model, and the degree of asymmetry in the jet depends on the asymmetry of the weak galactic field fed into the disc at large distances over long periods of time. Hence, it is difficult to see how the model can predict the distribution of arm length ratios seen by Rudnick & Edgar (1984) and produce two-sided lobes.

It is our aim to provide a self-consistent intrinsically asymmetric model to explain the above anomalies. We will show that by investigating the internal structure of an accretion disc we can provide a mechanism for the large scale jet changes.

3.2 The asymmetric disc model

By investigating disc asymmetry we will show that the radio jets can be maintained in an intrinsically asymmetric state through a combination of the effect of the jet luminosity on the mass loss from the surface of the accretion disc and the effect of this mass loss on the jet luminosity (figure 30). In order to obtain the latter we assume that the jet collimation and dissipation depends on the pressure in the surrounding medium near the base of the jet. This medium is supplied by the mass evaporated off of the disc.

The dependence of the mass loss from the disc on the jet luminosity which gives rise to the disc asymmetry arises by assuming that there is a hard X-ray component associated with the radio jet (Canizares & White, 1989). This component has a Compton temperature of order 10^8K. In addition, there is a soft X-ray component associated with the base of the jet or with the inner accretion disc. The Compton temperature of this emission may be as low as 10^6K (Fabian et al., 1986). We do not know the spectrum as seen by the disc, so we assume that the disc is exposed to a mean active galactic spectrum

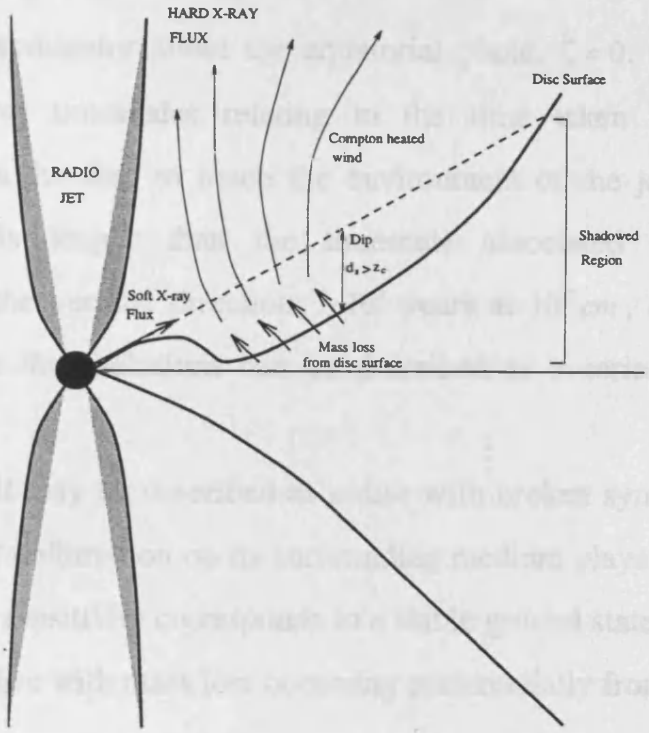

Figure 30
The asymmetric disc model.

(Mathews & Ferland, 1987). The inverse Compton temperature of the combined radiation field is of order 10^7K, which is significantly less than the inverse Compton temperature of the hard component.

This assumption leads to asymmetry in the following way. The shape of the surface of the disc is responsive to the external pressure produced by the ambient radiation. Under certain circumstances, regions of the disc, at radii where the atmosphere is otherwise too cool for mass loss to occur, can become shielded from the central soft X-ray source. In these regions the temperature of the disc is raised and mass loss occurs. Even a small change in the radius of the mass losing region can raise the dissipation in the jet by a large amount.

Our accretion disc model solves the zero order disc equations of §2, assuming the disc is vertically isothermal. This assumption is justified using the results of §2 and §2.5.1 as we are only interested in studying the velocity structure of the disc and not in predicting a disc spectrum. We also relax the

assumption of symmetry about the equatorial plane, $\zeta = 0$. The disc will be investigated over timescales relating to the time taken for the material evaporated from the disc to reach the environment of the jet, $\sim 10^4$ years at $10^{17} cm$. This is longer than the timescale associated with hydrostatic equilibrium in the vertical direction, $\sim 10^3$ years at $10^{17} cm$, and therefore we assume that the disc solutions can be described as a series of steady state systems.

The result may be described as a disc with broken symmetry where the sensitivity of jet collimation on its surrounding medium plays the role of order parameter: high sensitivity corresponds to a stable ground state configuration of an asymmetric disc with mass loss occurring preferentially from one surface.

3.3 A vertically isothermal disc model

3.3.1 The disc equations

In the application we wish to make, mass loss from the disc surface, by which we mean the base of the externally heated atmosphere of the disc, will turn out to depend on the shape of the disc surface. We saw in §2 that to compute this shape the internal structure of the disc must be considered. Therefore our model will be similar to that used in §2, solving the zero order disc equations and including the effects of an external pressure applied at the surface of the disc. Where this model will differ is that for computational ease we will replace the energy equation (2.8) with a prescribed vertically isothermal temperature distribution $T = T(r)$. The function $T(r)$ will be specialised for specific numerical computations.

The energy equation was solved consistently for an accretion disc in §2, and in §2.5.1 we showed that the disc solutions and internal structure were similar to those of the pseudo-vertically isothermal solutions of Urpin (1983). Also, the temperature at the base of the externally heated atmosphere will be of

order $10^4 K$; the temperature in the mid-plane of an optically thick, geometrically thin disc at the radii we shall be interested in ($10^{16} - 10^{17} cm$) will lie typically between $4\times10^4 K$ and $10^4 K$ (1.22). The presence of the heated atmosphere may, of course, alter his somewhat, but it seems reasonable as a first approximation to take the disc to be isothermal in the z-direction. This will allow us to obtain results with only a limited amount of numerical computation.

As mentioned in §3.2, when applying our asymmetric disc model to the case of one-sided jets, the shortest timescale we will consider is the time taken for mass evaporated from the disc surface to reach the jet environment, $\sim r_d / c_s \sim 10^4$ years at $10^{17} cm$, where r_d is the radius of the mass losing region. This compares to the timescale for hydrostatic equilibrium in the vertical direction (2.106), $\sim 10^3$ years at $10^{17} cm$. Therefore, we assume that the evolution of the disc can be described as a series of steady-state solutions.

From §2.2.2 we can identify the zero order disc equations for a vertically isothermal disc. The radial region we shall be interested in $\sim 10^{16} - 10^{17} cm$ corresponds to a disc dominated by gas pressure, $\beta_0 = 1$ (2.30), with Kramers opacity κ_R (2.40). The radial component of the momentum equation (2.22) gives a lowest order equal to the Kepler approximation to the azimuthal velocity,

$$V_0 = \frac{1}{\omega^{1/2}}. \tag{3.1}$$

The zero order terms in the vertical component (2.24) leads to the hydrostatic equation

$$(\sigma_0 c_0^2)_{,\zeta} = -\frac{\sigma_0 \zeta}{\omega^3}. \tag{3.2}$$

Remember that we are using a vertically isothermal approximation. Therefore (3.2) integrates to

$$\sigma_0 = \sigma_{00} \exp(-\frac{\zeta^2}{2c_0^2\omega^3}). \tag{3.3}$$

Here $\sigma_{00} = \sigma_0(\omega,0)$, and comparison with (1.6) gives us a pressure scale height $H = c_0\omega^{3/2}$.

For a disc described with α-viscosity (§1.3) we have that the total pressure P is proportional to the component of viscous stress $\overline{T}_{r\phi}$ which drives the accretion, where

$$\alpha = \frac{\overline{T}_{r\phi}}{P} \tag{3.4}$$

is taken to be a constant. Under our assumption of isothermality in the vertical direction, the kinematic viscosity coefficient ν is a function of radius only (c.f. 1.3)

$$\nu = \alpha c_s H . \tag{3.5}$$

The radial velocity is obtained from the conservation of angular momentum (2.23). As with the models developed in §2 and §3 we ignore terms associated with the vertical transport of angular momentum (see §2.2.2). Hence, zero order terms in (2.23) give

$$\sigma_0 U_0 = -\frac{3}{\omega^{1/2}}(\sigma_0 c_0^2 \omega^2)_{,\omega}. \tag{3.6}$$

Using the equation for the dimensionless density (3.3), we can obtain an expression for U_0:

$$U_0 = B + C\zeta^2 \tag{3.7}$$

where

$$B = -(3\omega^{3/2}c_{0,\omega}^2 + 6\omega^{1/2}c_0^2 + 3\omega^{3/2}c_0^2\frac{\sigma_{\infty,\omega}}{\sigma_\infty})$$

$$C = -(\frac{3c_{0,\omega}^2}{2c_0^2\omega^{3/2}} + \frac{9}{2\omega^{5/2}}).$$

In a similar fashion to §2 we can derive an expression for the condition of outflow ($U_0 > 0$) along the mid-plane ($\zeta = 0$) of the disc: outflow occurs if

$$\frac{\sigma_{\infty,\omega}}{\sigma_\infty} < -(\frac{c_{0,\omega}^2}{c_0^2} + \frac{2}{\omega}). \tag{3.8}$$

To determine the zero order term for the sound speed c_0^2, we would normally be required to solve the energy equation (2.26). However, in our vertically isothermal approximation, c_0^2 becomes a specified function of radius. The results of §2 show that for a gas pressure dominated disc with Kramers' opacity, being subject to a small external pressure, the disc quantities follow their thin disc radial dependencies. Hence, $c_0^2 \propto \omega^{-3/4}$ (1.22). In the case of larger external pressures being applied to the disc surface, this radial dependence alters. However, in §3.6.4 we show that altering the radial dependence of c_0^2 has little effect on the internal structure of the accretion disc. Therefore for simplicity, we restrict our computations to the thin disc temperature law

$$c_0^2 = \frac{1}{\omega^{3/4}}. \tag{3.9}$$

This allows us to give an explicit expression for the condition of outflow on the equatorial plane (3.8), namely,

$$\frac{\sigma_{00,\omega}}{\sigma_{00}} < -\frac{5}{4\omega}. \tag{3.10}$$

With reference to the thin disc solutions (1.22) we see that a gas pressure dominated disc with Kramers' opacity has a radial density dependence of $r^{-15/8}$ at the mid-plane. Therefore the disc consists of outflowing material on the $\zeta = 0$ centre line as predicted in §2 and by Urpin (1983), Siemiginowska (1988) and Kley & Lin (1992).

Finally, the continuity equation (1.25) has as its lowest order:

$$(\sigma_0 U_0 \omega)_{,\omega} + \omega(\sigma_0 W_0)_{,\zeta} = 0. \tag{3.11}$$

This completes the set of zero order equations needed to obtain the disc structure of a vertically isothermal accretion disc.

3.3.2 Boundary conditions

In §2.2.3 we described the boundary conditions for a zero order accretion disc which is subject to an external pressure. These were a definition of the disc surface, as the condition of pressure balance between the disc and external medium (the external pressure could be provided by a corona or disc wind; see §2.4), a boundary condition for the energy equation which we can ignore as the temperature in the disc is prescribed, and a condition that describes the velocities at the disc surface. For the model derived in §2 the latter was a no mass-loss condition (c.f. 2.46)

$$\left.\frac{\partial \zeta}{\partial \omega}\right|_s = \left.\frac{W_0}{U_0}\right|_s \tag{3.12}$$

which shows that the material follows a mathematical 'streamline' along the surface (as expected for no mass loss).

For the model we are developing in this chapter, we lose the assumption of symmetry about the equatorial plane ($\zeta = 0$). Therefore we must consider both the upper and lower disc surfaces; the surface definition (2.55) is adapted to

$$P(\omega, \zeta_{s\pm}) = P_{Ext\pm}(\omega). \tag{3.13}$$

In §2.4.1 we discussed the effect of illuminating the disc by X-rays emitted by the central region near the black hole or radio jet. The radiation is sufficiently hard to heat the material in the upper regions of the disc, by the Compton process, to high temperatures ($T_c > 10^7 K$). The heated gas forms a tenuous corona above the disc. If the sound speed in the heated gas also exceeds the escape speed of the system at that radius, then the gas steadily escapes as it is heated, forming a wind. In §3.5 we will show that this mass loss occurs when the disc surface is depressed by a sufficient distance d_s (by the external pressure provided by the corona or wind upon illumination by a radio jet, say; see figure 30). We use the result of Begelman et al. (1983) for their 'case A' outflows

$$\frac{1}{2\pi r}\frac{d\dot{M}_{loss}}{dr} = \frac{P_{Ext\pm}}{c_{ic}}, \qquad r > 0.1 r_{ic}. \tag{3.14}$$

Here c_{ic} $(= (kT_{ic}/\mu m_H)^{1/2})$ is the isothermal sound speed at the Compton temperature of the radiation falling on the disc and r_{ic} $(= 10^{18}(\frac{10^8 K}{T_{ic}})(\frac{M}{10^8 M_0})\ cm)$ is the radius at which the Compton temperature equals the escape temperature. To incorporate this induced mass loss into our model, we recall equation (2.45):

$$\frac{d\dot{M}_{loss}}{dr} = 2\pi r\rho\upsilon_{n\pm}\left(1+\left(\frac{dz}{dr}\right)_{s\pm}^{2}\right)^{1/2} \tag{2.45}$$

where $\upsilon_{n\pm}$ is the velocity (at the upper and lower surfaces respectively) normal to the surfaces of the disc

$$\upsilon_{n\pm} = [\frac{\upsilon_z dr - \upsilon_r dz}{(dr^2+dz^2)^{1/2}}]_{s\pm}.$$

Equating (3.14) and (2.45) and using the expansions introduced in §2.2.2, we find

$$\left.\frac{\partial\zeta}{\partial\omega}\right|_{s\pm} = [\frac{\sigma_0 W_0 - P_{Ext}A_{loss}}{\sigma_0 U_0}]_{s\pm} \tag{3.15}$$

where

$$A_{loss} = \frac{\tilde{M}^2}{\alpha\bar{c}\bar{\rho}c_{ic}}.$$

Therefore we have two conditions that relate the radial and vertical velocity at the disc surface: the no mass loss condition (3.12) if the surface depression $< d_s$, and the mass loss condition (3.15) if the surface dip $> d_s$.

As in §2 and §3, to complete the boundary conditions we should specify an inner and an outer radial boundary condition. One of these is usually the mass flux in the disc, the other is usually some condition at the inner edge. We therefore expect the disc equations above will yield a two parameter family of solutions.

3.3.3 Calculating the disc structure

The equation that governs the vertical structure of the disc at each r was derived in §3.3.1, namely the hydrostatic equation (3.3), as the temperature within the disc is specified. To obtain a global solution the continuity equation (3.11) must also be solved.

We shall now show that the continuity equation is a second order differential equation for $\sigma_{00}(\omega)$. In §3.3.2 it was stated that this disc model requires two further boundary conditions. These will be equivalent to specifying σ_{00} and $\sigma_{00,\omega}$ at r_{in} (equivalent to the accretion rate and an inner boundary condition) in order to obtain $\sigma_{00,\omega\omega}$. Radial integration then provides σ_{00} and $\sigma_{00,\omega}$ for the next radius. To see this we take the continuity equation (3.11) in the form

$$(W_0\sigma_0)_{,\zeta} = -U_0\sigma_{0,\omega} - \sigma_0 U_{0,\omega} - U_0\sigma_0/\omega. \tag{3.16}$$

This equation can now be integrated vertically between the lower and upper disc surfaces, where ζ_{s-} and ζ_{s+} are obtained using (3.3)

$$\bar{\rho}\bar{c}^{-2}c_0^2\sigma_{00}\exp\left(-\frac{\zeta_{s\pm}^2}{2c_0^2\omega^3}\right) = P_{Ext\pm}.$$

The external pressure P_{Ext} is defined in §3.4. Integrating (3.16) from $\zeta = \zeta_{s-}$ to $\zeta = \zeta_{s+}$, and using the expression we derived in §3.3.1 for U_0 (3.7), we get

$$[W_0\sigma_0]_{s-}^{s+} = -\sigma_{00}(B_{,\omega}J_1 + C_{,\omega}J_2) - Z_2 - Z_3 \tag{3.17}$$

where

$$Z_2 = \left(\frac{\sigma_{00}}{\omega} + \sigma_{00,\omega}\right)(BJ_1 + CJ_2)$$
$$Z_3 = \sigma_{00}\left(\frac{c_{0,\omega}^2}{2c_0^4\omega^3} + \frac{3}{2c_0^2\omega^4}\right)(BJ_2 + CJ_4) \tag{3.18}$$

and

$$J_1 = \int_{\zeta_{s-}}^{\zeta_{s+}} e^{-\zeta^2} d\zeta$$
$$J_2 = \int_{\zeta_{s-}}^{\zeta_{s+}} \zeta^2 e^{-\zeta^2} d\zeta \tag{3.19}$$
$$J_4 = \int_{\zeta_{s-}}^{\zeta_{s+}} \zeta^4 e^{-\zeta^2} d\zeta.$$

and B and C are defined in (3.7). The term $B_{,\omega}$ on the right side of (3.17) contains $\sigma_{00,\omega\omega}$ so equation (3.17) is a second order equation for σ_{00}. Thus, we solve (3.17) for $\sigma_{00,\omega\omega}$, and write the resulting equation in the equivalent first order form

$$y = \sigma_{00}$$
$$y' = Y \tag{3.20}$$
$$Y' = \bar{F}(y, Y, \omega)$$

where the form of $\bar{F}$, obtained from (3.17), is

$$\bar{F} = (3c_0^2\omega^{3/2}J_1)^{-1}\{Z_1 + Z_2 + Z_3 + Z_4$$
$$-[(3c_{0,\omega}^2\omega^{3/2} + 6c_0^2\omega^{1/2})_{,\omega} \tag{3.21}$$
$$+\left(\frac{3c_0^2\omega^{3/2}}{\sigma_{00}}\right)_{,\omega}\sigma_{00,\omega}]\sigma_{00}J_1\}$$

and using (3.15)

$$Z_1 = [\sigma_0 W]_{s-}^{s+}$$
$$Z_4 = \sigma_{00}C_{,\omega}J_2$$

$$[W_0]_{s\pm} = [U_0]_{s\pm}\zeta_{s\pm,\omega} + \frac{P_{Ext}A_{loss}}{\sigma_{\infty}}\exp(\frac{\zeta_{s\pm}^2}{2c_0^2\omega^3}).$$

Note that the term that includes A_{loss} is neglected if there is no mass loss (i.e. the surface depression $< d_s$; c.f. §3.5). The radial system (3.20) is solved by a NAG library routine given the starting conditions σ_{∞} and $\sigma_{\infty,\omega}$ at r_{in}. We use D02CAF which integrates a system of first-order ordinary differential equations over a range with suitable initial conditions, using a variable-order variable-step Adams method. The NAG library routine D02CAF is also used to calculate the three vertical equations in (3.19) to yield $\bar{F}$ at each radial integration point. We check the accuracy of the integration by computing the accretion rate at each radius. This should be constant when there is no mass loss.

3.4 The disc structure in the presence of external illumination

Having described our method of obtaining the internal structure of a vertically isothermal accretion disc, we now outline the features of the proposed asymmetric disc model. We assume a soft X-ray excess emission ("big bump") from close to the central black hole, either from the inner accretion disc (Pounds et al., 1984) or from the base of the jet (George et al., 1988). It is important for what follows that this radiation comes from close to the equatorial plane. In addition to this we assume a hard X-ray component associated with the radio jet as suggested by the observations of Canizares & White (1989). The hard X-ray component is taken to illuminate both faces of the disc directly. It contributes to the pressure on the surface of the disc by heating the disc material. Thus, the external pressure on the disc from this source is $P_{Ext} \propto 1/(r^2+h^2)$, where h is the height of the jet source above the

disc. Begelman et al. (1983) showed that the external pressure applied to the disc surface is proportional to the mean radiation intensity encountered there:

$$P_{Ext\pm} = \frac{l_{\pm} L_{Edd}}{4\pi(r^2+h^2)c\Xi_0'}. \qquad (3.22)$$

Here $l_{\pm}L_{Edd}$ is the X-ray luminosity of the upper and lower jet respectively, and for Ξ_0', the ionization parameter at the disc surface, we put $\Xi_0' = 3$ (Begelman & McKee, 1983). If the luminosity of the top jet is equal to the luminosity of the lower jet then the disc will be symmetric. The soft X-ray excess will also contribute to the heating of the disc surfaces, where these are exposed to it; but its effect on the external pressure is small and will be neglected.

In §3.3.1 the hydrostatic equation (3.3) was solved explicitly. This allows us to obtain an expression for the disc surface as defined by the condition of pressure balance between the disc and the surrounding corona/wind. Using equation (3.3) with the boundary condition (3.13) gives

$$\zeta_{s\pm} = \sqrt{2c_0^2\omega^3 \log\left(\frac{\overline{\rho}\overline{c}^2\sigma_{00}c_0^2}{P_{Ext\pm}}\right)}. \qquad (3.23)$$

At small radii ($< 10^{16} cm$) along the disc, the external pressure is negligible compared with the pressure in the disc, so has little effect on the shape of the surface. At intermediate radii ($\sim 10^{17} cm$) the pressure from the jet becomes significant compared with that of the central disc and, because it falls less rapidly than the internal disc pressure, can now be sufficient to alter the curvature of the disc surface in such a way that the surface becomes hidden from the central source (as seen in figures 11 and 12 in §2.3.2).

The shadowing of a region of the disc from the soft X-ray source implies a raised Compton temperature on the disc surface. Beyond a radius $\sim 0.1 r_{ic} = 10^{17} cm$, for a black hole of mass $10^8 M_0$ and a hard X-ray source with

Compton temperature $10^8 K$, material will be evaporated from the disc surface (Begelman et al., 1983). This material constitutes the environment of the jet. At a distance r the jet is therefore subject to an external pressure $P_{jet\pm}(r)$ of order $P_{Ext\pm}(r)$ (Smith & Raine, 1985). The dissipation in the jet is proportional to a high power of P_{jet} (e.g. Begelman et al., 1984); thus, a bending of the disc surface can result in positive feedback, increasing the pressure on the disc and giving rise to further changes in surface shape until the whole of the potential mass losing region beyond r_{ic} is shielded, and the jet reaches its maximum luminosity. Whether this can occur in practice depends on the effect of the external pressure on the disc central pressure. We are, however, able to find asymmetric solutions in which the disc pressure is raised on one side only, hence with a self-consistent asymmetric jet structure. We will investigate the evolution of the model in §3.7.

3.5 An optically thin Compton heated wind

In §3.4 we discussed the possibility that mass can be evaporated off of an asymmetric disc in the region of a surface depression caused by hard X-rays from the jet. Once it has risen above the surface dip, the material is exposed to the central soft X-ray flux which has a lower Compton temperature. Nevertheless, we show in this section that, for dips of the order of magnitude predicted here, a strong disc wind can still form. The argument follows essentially from that of Begelman et al. (1983) who show in their 'case A' solutions, appropriate to disc radii $R > 0.1R_{ic}$, that material reaches the isothermal sound speed close to the disc surface. We show that this occurs in fact at a Compton heating length scale above the disc surface. Since subsequent cooling then leads to a further increase in the Mach number of the flow (Begelman et al., equations (3.17)), we do not require a non-zero transverse expansion of the streamlines to force the material through the critical point at

the adiabatic sound speed, in contrast to Begelman et al. Thus, in their notation, we put $\beta = 0$ and consider a one-dimensional flow. As a consequence the critical point here also lies close to the disc surface and not at $z \sim R$.

The basic equations of continuity, momentum and energy for flow in the z-direction at radius R_0 in the disc are

$$\rho \upsilon = \dot{m} = const. \tag{3.24}$$

$$\rho \upsilon \frac{d\upsilon}{dz} = -\frac{dP}{dz} - \frac{GM\rho}{R_0^3} \frac{z}{(1+z^2/R_0^2)^{3/2}} \tag{3.25}$$

$$\frac{3}{2} P \upsilon \log \frac{d}{dz}\left[\frac{P}{\rho^{5/3}}\right] = \frac{n_e \Gamma_0 (1 - T/T_{ic})}{(1+z^2/R_0^2)}. \tag{3.26}$$

We assume a fully ionised hydrogen plasma:

$$P = \frac{2\rho}{m_H} kT \,. \tag{3.27}$$

Near the disc and for $R_0 > 0.1 R_{ic}$ the gravity term in (3.25) makes a negligible difference, so for simplicity we neglect it. Then, in terms of the Mach number, $M = \upsilon / c_s$, (3.25) can be written

$$(M^2 - 1)\frac{d \log M^2}{dz} + (1 + M^2)\frac{d \log c_s^2}{dz} = 0 \tag{3.28}$$

and (3.26) can be manipulated to give

$$(3M^2 - 5)\frac{d \log c_s^2}{dz} \propto [M^2 - 1][1 - c_s^2 / c_{ic}^2] \tag{3.29}$$

where $c_{ic} = c_s(T_{ic})$ is the sound speed at the Compton temperature.

From (3.28) we see that for $d\log c_s^2/dz > 0$ we have $M^2 < 1$, since the gas starts from rest, and $d\log M^2/dz > 0$; thus M increases as the gas is heated. Then from (3.29) we see that if $M^2 < 1$ and $c_s < c_{ic}$ we have $d\log c_s^2/dz > 0$; hence the gas continues to be heated until $M^2 \to 1$ and $c_s \to c_{ic}$. It follows that the gas is accelerated to speed $v = c_{ic}$ at a height z_1 which must be of order z_c, the Compton heating length scale. We can confirm this by an approximate integration of the equations of motion.

From (3.25), for $z << R_0$, $P + \rho v^2 = P_0$, so at $M = 1$ we have $P_1 = P_0/2$. Equation (3.26) may be written alternatively as

$$(3M^2 - 5)\frac{d\rho}{dz} = \frac{4\rho^2\Gamma_0(1 - T/T_{ic})}{\dot{m}\, c_s^2 m_H (1 + z^2/R_0^2)}.$$

So for $M^2 << 5/3$, $c_s^2 \sim P_0/\rho$ and we get

$$-\frac{5}{\rho^3}\frac{d\rho}{dz} \sim \frac{4\Gamma_0}{\dot{m}\, m_H P_0}$$

and hence

$$z_1 \sim \frac{5}{16}\frac{kT_1}{\Gamma_0}c_1 = \frac{5}{16}\frac{kT_{ic}}{\Gamma_0}c_{ic} \sim z_c.$$

This result is sufficient for our purposes; provided $z_1 < d_s$, the depth of the depression in the disc, we can appeal to Begelman et al. to see that subsequent cooling will assist expansion in driving a wind through the critical point at $M^2 = 5/3$. If expansion is unimportant, we can investigate the fate of the gas as follows. Manipulating (3.28) and (3.29) we get

$$(5 - 3M^2)\frac{d\log M^2}{dz} \propto [1 + M^2][1 - c_s^2/c_{ic}^2]. \qquad (3.30)$$

Hence at $c_s = c_{ic}$ we have $d\log M^2/dz = 0$ and also, from (3.29), $d\log c_s^2/dz = 0$. Beyond z_1, therefore, the velocity of the gas is constant. The wind enters a coasting phase until either radial expansion or cooling can force it through the critical point at $M^2 = 5/3$. If the coasting phase is ended by a reduction in the inverse Compton temperature of the ambient radiation field, to T_{ic}', say, so c_{ic} is reduced to $c_{ic}' = c_s(T_{ic}')$, then from (3.30) we see that the critical point occurs on a Compton cooling length scale. If $T_{ic}' \sim \frac{1}{10}T_{ic}$ then $c_{ic}' \sim \frac{1}{3}c_{ic}$; since $M^2 > \frac{5}{3}$ the velocity υ becomes $\upsilon' > \frac{1}{3}\sqrt{\frac{5}{3}}\upsilon$, i.e. $\upsilon' \sim \upsilon \sim c_{ic}$. We summarise this by saying that if the initial heating phase provides sufficient *bulk* energy to escape, then a modest amount of subsequent cooling cannot extract this bulk energy to prevent the wind escaping.

Thus to determine the consistency of our model we compute the Compton heating length scale z_c. The Compton heating rate is

$$\Gamma_0 = \frac{kT_{ic}}{m_e c^2}\frac{\sigma_T L}{\pi R^2} \tag{3.31}$$

which can be rewritten as

$$\Gamma_0 = 4.6\times 10^{-17}\left(\frac{T_{ic}}{10^8 K}\right)^3\left(\frac{10^8 M_0}{M_{bh}}\right)\left(\frac{L}{L_{Edd}}\right)\left(\frac{r_{ic}}{r}\right)^2 erg\, s^{-1}. \tag{3.32}$$

The Compton heating timescale at $r = 0.1r_{ic}$, $T_{ic} = 10^8 K$ and $M_{bh} = 10^8 M_0$ is therefore

$$t_n = 2.2\times 10^6\left(\frac{L_{Edd}}{L}\right)\, s. \tag{3.33}$$

Hence the height above the base of the outflow at which the wind reaches a temperature $T_{ic} = 10^8 K$ and a Mach number of order unity is

$$z_c \sim c_s t_n \sim 2\times 10^{14}(\frac{L_{Edd}}{L})\ cm\,. \qquad (3.34)$$

Material rising from the disc in a surface depression $d_s > z_c$ cannot be cooled sufficiently by the central soft X-ray flux, once it rises above the dip, to prevent a strong wind.

3.6 Asymmetric disc solutions

3.6.1 Testing the code

The code has been run for various values of accretion rate, external pressure, and disc radius. In §3.3.2 we showed that the disc solutions require the specification of two starting parameters. These are $\sigma_{\infty}(\omega)$ and $\sigma_{\infty,\omega}(\omega)$ (3.20), which as in §2 and §3 correspond to the mass flux within the disc, the accretion rate $\dot{M}$, and the height of the disc, ζ_s, which replaces the inner radial boundary condition. It turns out that the choice of ζ_s (or $\sigma_{\infty}(\omega)$; 3.23) has little influence on the disc solutions away from r_{in} (for a given $\dot{M}$). Figure 31 shows the evolution of the disc quantity $\sigma_{\infty}(\omega)$ with radial distance ω for a choice of initial disc heights ($\zeta_s = 1.5$, 2.3, 2.8, 3.0, corresponding to $z_s \sim 1.5H$, $2.3H$, $2.8H$, $3H$, where H is the disc scale height (1.7) at the starting radius). The solutions correspond to a symmetric disc (i.e. equal jet luminosities in 3.22) with $M = 10^8 M_0$, $\dot{M} = 0.1 M_0 yr^{-1}$ and $\alpha = 0.1$. The function $\sigma_{\infty}(\omega)$ rapidly converge towards equilibrium solutions. The two most extreme choices of ζ_s are within 95% of the 'average' solution by $\sim 1.3 r_{in}$. This computation has been repeated using various permutations of accretion rate, alpha parameter and jet luminosity in (3.22) with similar results.

3.6.2 The vertical velocity component

The model developed in §2 gave the vertical velocity term W_0 by using the fact that the continuity equation (3.11) decouples the r and z components

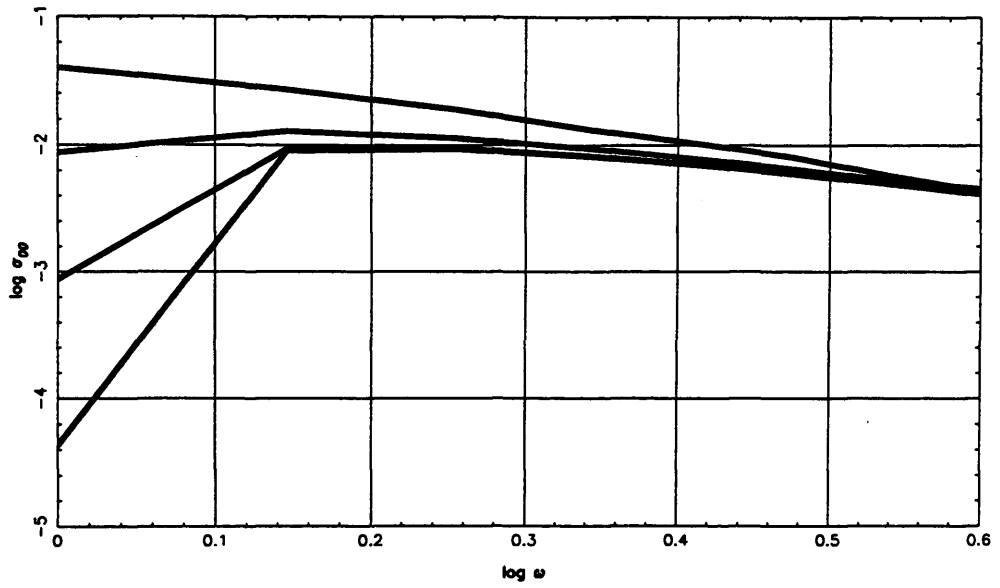

Figure 31

The evolution of the central density $\sigma_{00}(\omega)$ with respect to the dimensionless radial variable ω for a range of initial disc heights (with increasing $\sigma_{00}(\omega)$: $\zeta_s = 1.5,\ 2.3,\ 2.8,\ 3.0$).

Disc system: $M = 10^8 M_0$, $\dot{M} = 0.1 M_0 yr^{-1}$, $\alpha = 0.1$.

from the ϕ direction. This allowed us to use mathematical 'streamlines' in the r-z plane on the disc surface and equatorial plane to determine W_0 (see §2.2.4). However, this method fails if the external pressure becomes significant enough, with respect to the disc central pressure, to change the outflow of material along the equatorial plane into inflow (see §2.3.2 and 2.37). In this instance, the $\zeta = 0$ centre line ceases to be a 'streamline' and the calculated values for W_0 become unreliable.

This chapter solves the simpler vertically isothermal disc equations and, as a result, the vertical velocity term W_0 can be computed easily (by integrating equation 3.16 vertically from $\zeta = 0$ to $\zeta = \zeta_s$) without the need to invoke mathematical 'streamlines'. Therefore we can investigate the internal structure of the disc at the radii where outflowing material becomes inflowing. Figure 32 shows the r-z velocity flow for the 'top half' of a disc, symmetric about its $\zeta = 0$

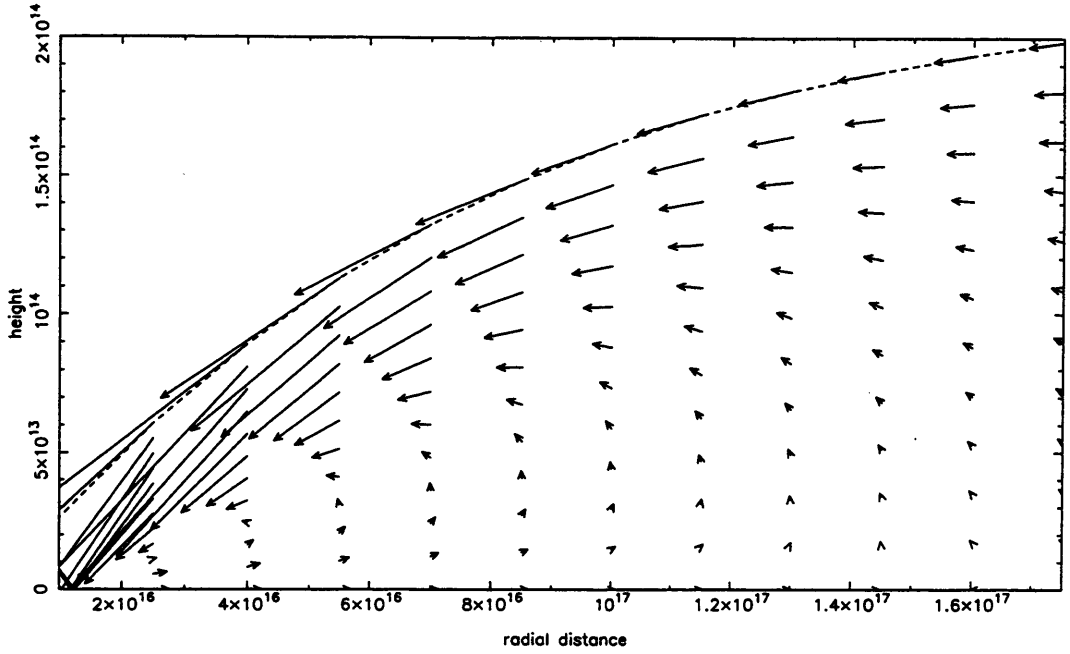

Figure 32

The r-z velocity field for a symmetric disc about the equatorial plane showing the velocity direction change on the $\zeta = 0$ centre line (axis units are in cm).

Disc system: $M = 10^8 M_0$, $\dot{M} = 0.01 M_0 yr^{-1}$, $\alpha = 0.1$, $L_{\pm} = 0.8 L_{Edd}$, $h = 2 \times 10^{17} cm$.

midplane. The disc system is $M = 10^8 M_0$, $\dot{M} = 0.01 M_0 yr^{-1}$ and $\alpha = 0.1$, with the external pressure to both surfaces being provided by points at heights of $2 \times 10^{17} cm$ on the axis of the disc emitting at 0.8 Eddington luminosities.

Remember that there is an associated reduction in surface density as the disc becomes wholly inflowing due to the fact that the accretion rate is fixed and there is more material in a disc with both inflow and outflow. This is evident by the 'turning back' of material between ~ $4 \times 10^{16} cm$ and $1.5 \times 10^{17} cm$. This could not be seen with the 'streamline' calculation of §2.

3.6.3 An asymmetric disc

In this section an asymmetric disc structure is investigated in order to illustrate the theory of §3.4 and §3.5. We present the results for a disc with $\alpha = 0.1$, around a black hole of mass $10^8 M_0$. We also take $T_{ic} = 10^8 K$ as the

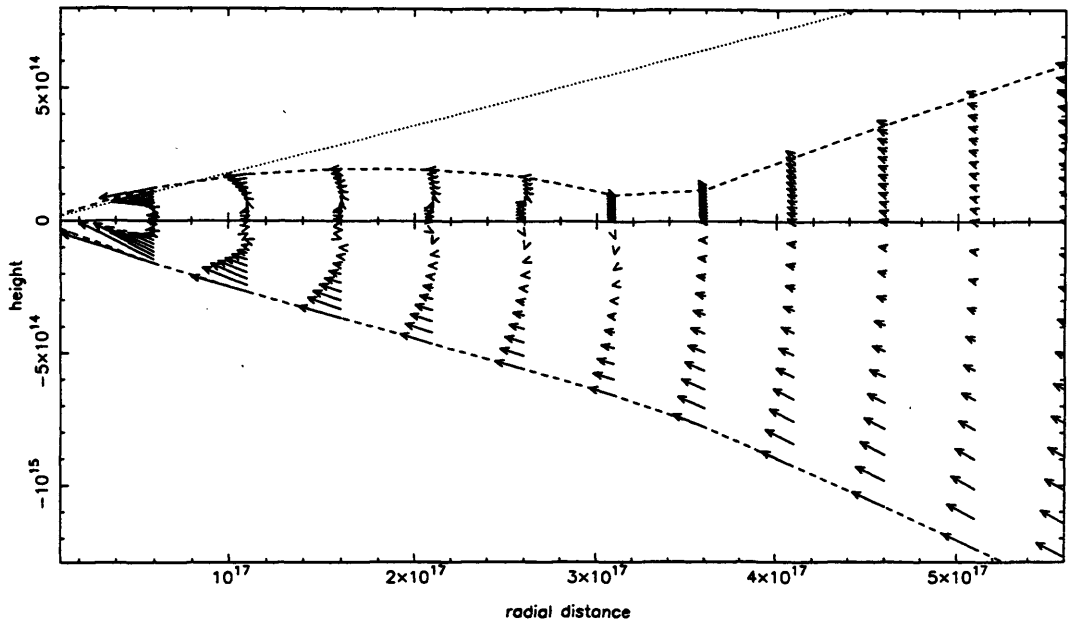

Figure 33

The r-z velocity field for an asymmetric disc (axis units are cm). The dotted line shows the approximate line-of-sight for the central soft X-ray flux.

Disc system: $M = 10^8 M_0$, $\dot{M} = 0.01 M_0 yr^{-1}$, $\alpha = 0.1$, $L_+ = 0.6 L_{Edd}$, $L_- = 0.1 L_{Edd}$, $h = 2 \times 10^{17} cm$.

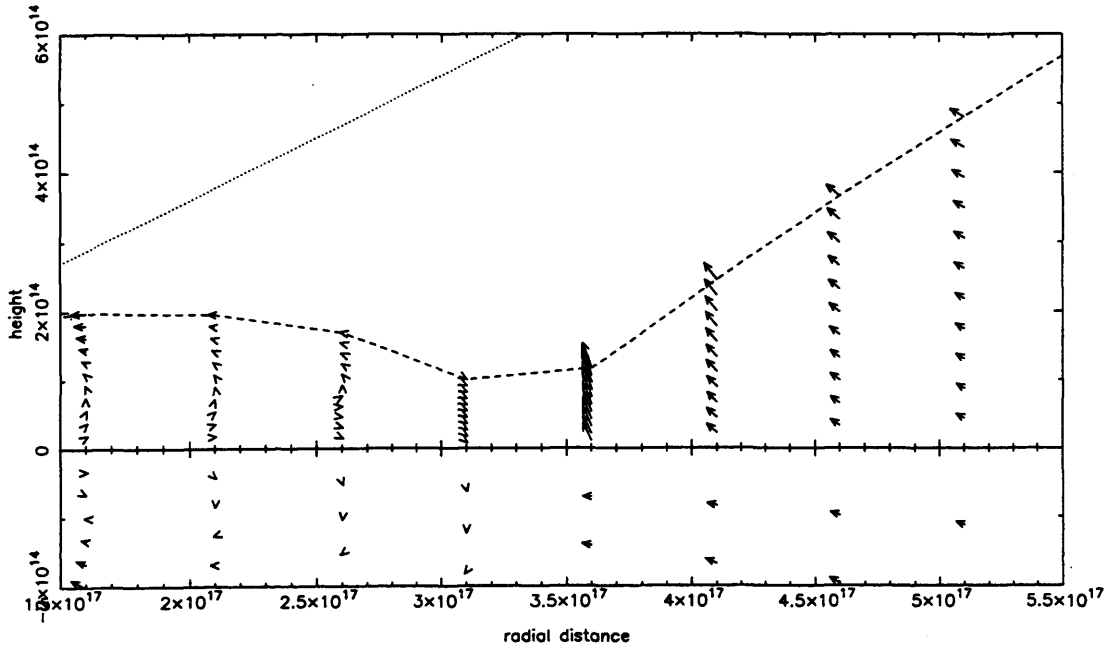

Figure 34

A close up of figure 33 focusing on the dipped top surface region.

Compton temperature appropriate to the region of the disc shielded from the central source. The disc solution is shown between the radii $1\times10^{16}cm$ and $5.5\times10^{17}cm$. Mass loss from even larger radii is not relevant to dissipation in the jet at $10^{17}cm$. We have approximated the effect of the soft X-ray central source in reducing the Compton temperature, by allowing mass loss only from areas of the disc surface shielded from direct radiation from the central source by a depth $d_s > z_c$ (see §3.5 and 3.34).

Figure 33 shows the *r*-*z* velocity field for a disc where the luminosity of the jet on the top side of the disc is $0.6L_{Edd}$. The luminosity from the bottom side is $0.1L_{Edd}$. Both luminosities are provided by points at heights of $2\times10^{17}cm$ on the axis of the disc, and the accretion rate at the disc's inner edge is $0.01M_0yr^{-1}$. The effect of the larger external pressure (top jet) is to push the top surface down at a radial distance close to the jet height $\sim 3\times10^{17}cm$. Figure 32 shows a close up of the dipped region of the disc and we see that the depression in the surface is caused by material being forced over the $\zeta = 0$ central plane into the lower half. When the depth of the depression is sufficiently large ($d_s > z_c$), the evaporated material forms a wind that reaches the (isothermal) sound speed before being exposed to Compton cooling. From (3.34) we see that for a top surface luminosity of $0.6L_{Edd}$, this occurs when the dip is $\sim 3-4\times10^{14}cm$. Figure 34 shows us that this occurs at $\sim 3.5\times10^{17}cm$. At this point the mass loss boundary condition (3.15) is introduced. Material from both sides of the disc move towards the mass loss region. The effect of this transfer of mass is that the dipped surface is 'pushed' back up. The surface continues to rise with increasing *r* until eventually the disc region will no longer be shielded from the soft X-ray flux and mass loss will cease.

Note that the lower surface, being subjected to a smaller external pressure, is not forced over in the same manner as the top surface. We find that, except for discs with very low accretion rates, $\dot{M} < 10^{-4}M_0yr^{-1}$, with both sides

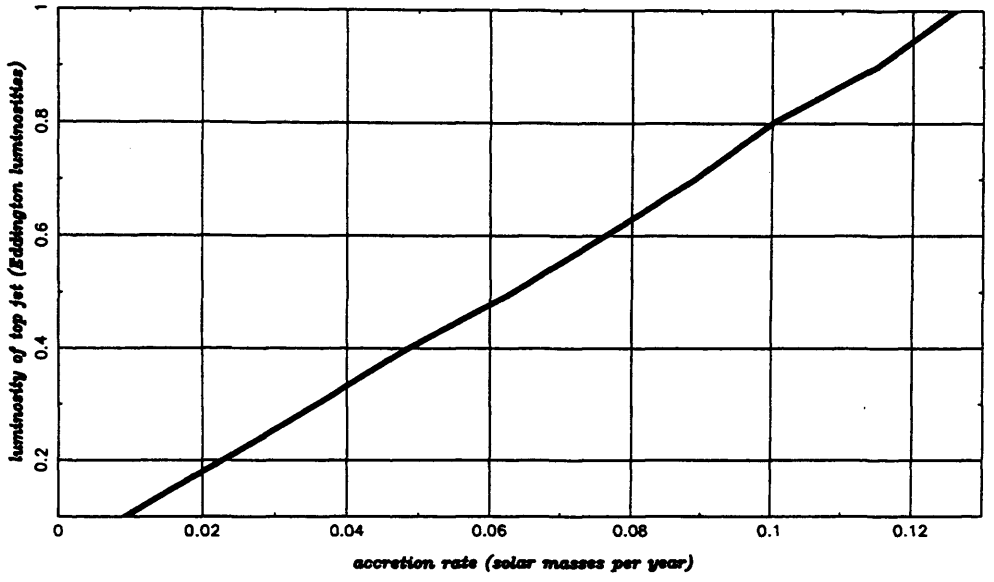

Figure 35

A plot of L_+ vs. $\dot{M}$ showing the minimum luminosity required to produce a dip of $d_s > z_c$ by a radii $5\times10^{17}cm$. L_- is fixed at $0.01L_{Edd}$.
Disc system: $M = 10^8 M_0$, $\alpha = 0.1$, $h = 2\times10^{17}cm$.

being subjected to high pressures, $L/L_{Edd} > 1.0$, discs will experience a dip on one side only.

It is clear from the velocity field of figures 33 and 34, that to achieve an asymmetric disc shape the internal structure of the disc must be calculated. With vertically averaged models, material cannot cross the equatorial plane, and therefore a significant surface dip does not appear (Raine & Thomas, unpublished).

In order to maintain a typical power of $10^{46} erg\, s^{-1}$, the Eddington limit for a $10^8 M_0$ black hole, the rate of gas supply must be approximately $1M_0 yr^{-1}$, assuming a high total efficiency (about 10%) of conversion of rest mass into radiant energy. However, we find that the one-sided dipped solutions occur only when the approximate inequality $(\dot{M}/1M_0 yr^{-1}) < 0.1(L/L_{Edd})$ holds, where L represents the luminosity of the jet shining on to the shadowed region. This is highlighted in figure 35. Here we see luminosity plotted against accretion

rate. The accretion rate is that at the inner edge, whilst the luminosity is the lowest luminosity required to produce an external pressure (using equation 3.22) capable of causing a dip with $d_s > z_c$ by an outer radius of $5\times10^{17} cm$. The luminosity of the opposite jet is fixed at $0.01L_{Edd}$. It should be noted that asymmetric disc shapes are possible for higher accretion rates (or alternatively for smaller ratios of top to bottom jet luminosities), but these will occur at larger radii (i.e. $10^{18}-10^{19} cm$) because the external pressure takes a larger distance to become significant. However, we shall only concern ourselves with systems where surface shadowing occurs by $10^{18} cm$.

To obtain a consistent model, where a dominant high luminosity jet can be supported by a low inner edge accretion rate, we must investigate the energetic feasibility of such a system. This is studied in §3.7.

3.6.4 The radial structure of the sound speed

Having obtained an asymmetric disc structure, we can use this to check that our specification of the disc sound speed to its thin disc dependence of $r^{-3/4}$ is valid. In §3.3.1 we noted that when a large external pressure is applied to a disc, the work done in moving the disc surface can cool the disc, and the disc temperature may diverge from its thin disc dependence. Figures 36 and 37how the *r-z* velocity fields for discs systems identical to that in figure 33except the sound speed radial dependence has been altered to $r^{-7/10}$ and $r^{-4/5}$ respectively. It is clear that the internal structure of the disc has not altered significantly, and we surmise that different specifications for the sound speed will not alter the results in this chapter.

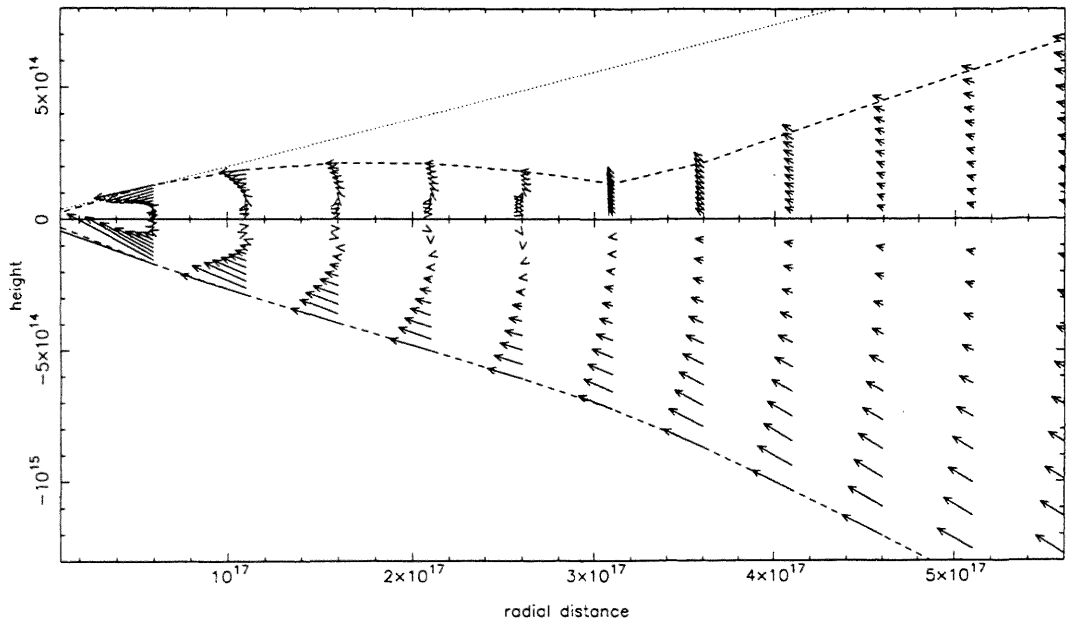

Figure 36
The r-z velocity field for the disc in figure 33ith $c_0^2 = \omega^{-7/10}$ *(axis units in cm).*

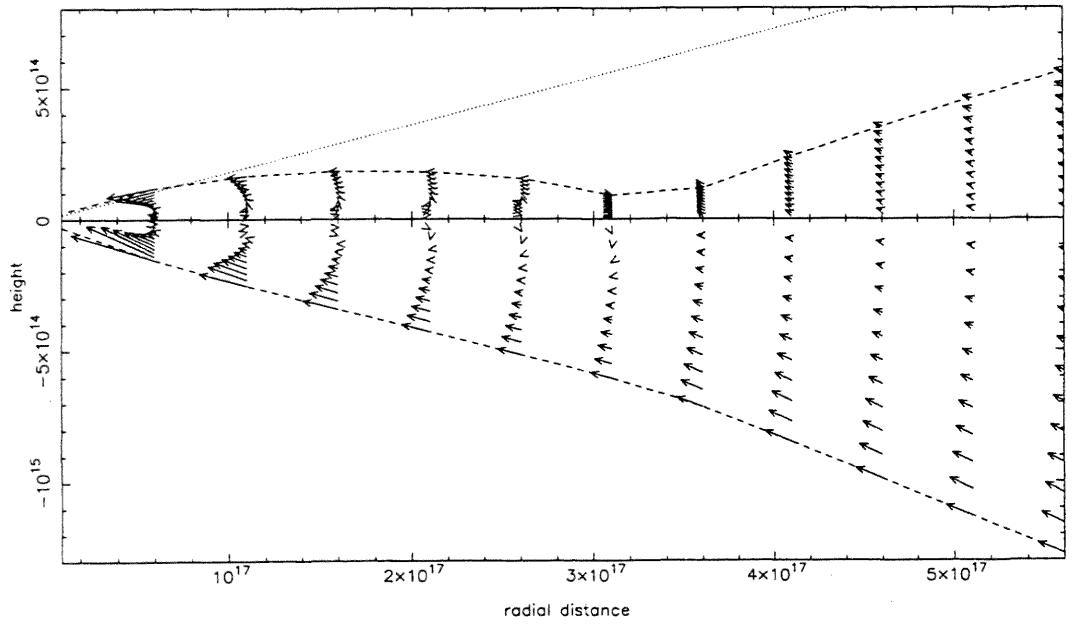

Figure 37
As in figure 36ut with $c_0^2 = \omega^{-8/10}$.

3.7 Dynamical evolution

In §3.6.3 we showed that our vertically isothermal disc model could be used to obtain asymmetric solutions which would excite mass-loss from shielded surface regions. However, to do this, a low accretion rate at the inner edge is needed. This must be able to support the dominant, high luminosity jet. Therefore in this section we investigate the energetic feasibility of our model.

The central powerhouse of a radio galaxy is widely acknowledged to be a supermassive black hole ($\sim 10^8 M_0$; see §1). The reservoir of extractable energy coming from the orbital energy of the gas near the black hole horizon, and the spin energy of the hole itself. Energy and angular momentum can be extracted from a black hole by the magnetic torques believed to be associated with radio jets (Blandford, 1979).

We assume that the energy from the accreting disc material (accretion rate $\dot{M}_{acc}$) is coupled to the spin of the central black hole. Therefore the rate of spin of the black hole is equal to the energy received from the disc minus the power, P, extracted to fuel the jet, i.e.

$$M_{bh}c^2 \frac{d}{dt}\left(\frac{a}{m}\right) \sim (1-\varepsilon)\dot{M}_{acc}c^2 - P \qquad (3.35)$$

where $a = m$ for a maximally rotating black hole. For the efficiency of the black hole, we take $\varepsilon = 0.1$. From (3.35) we see that for a disc system with a low accretion rate, the energy required to power a radio jet can be obtained directly from the spin energy of the black hole itself. This will cause the black hole to spin down, as it loses angular momentum, until all its energy has been extracted and the radio jet ceases.

An estimate for the power extracted from the hole can be taken from Blandford & Znajek (1977)

$$P \sim \left(\frac{a}{m}\right)^2 P_0 \tag{3.36}$$

where

$$P_0 \sim 1\times 10^{46}\left(\frac{M_{bh}}{10^8 M_0}\right) erg\, s^{-1} \tag{3.37}$$

is the maximum extractable power from the hole, i.e. when $a = m$.

A disc wind can be created by the illumination of an accretion disc by the X-rays emitted from a radio jet (see §2.4.1). Begelman et al. (1983) showed that such a wind will occur at distances of $\sim 10^{18} cm$. The wind material goes to constitute the environment of the jet and the extracted black hole energy is converted to radiative energy

$$L \sim k' \mathcal{P} \tag{3.38}$$

where the conversion efficiency $k' < 1$.

In §3.4 we discussed the idea that if a region of the disc surface can become hidden from the cooling central soft X-ray flux associated with the inner regions of the disc, then the subsequent rise in temperature could induce mass loss from the shadowed region. The lost material would add to the environment of the jet. This introduces a time scale into the dynamics, corresponding to the time taken for the material that is lost from the shielded region of the disc surface (travelling at the isothermal sound speed from a radial distance r_d) to reach the jet: $t_1 \sim r_d / c_s \sim 10^4 yr$ for $r_d \sim 10^{17} cm$. We adapt (3.38) by assuming that the self-consistent jet luminosity is increased by the external pressure provided by the mass lost from the disc surface, $\dot{M}_{loss}$, as a power law

$$L \sim P\left(\frac{1+k\left[\frac{\dot{M}_{loss}(t-t_1)}{1M_0yr^{-1}}\right]^n}{1+k\left[\frac{\dot{M}_{loss(\max)}}{1M_0yr^{-1}}\right]^n}\right). \qquad (3.39)$$

Here both k and n are constants. If k is large, then when the disc is symmetric and there is no additional mass loss, the luminosity of the jet will only be a small fraction of its maximum. If the disc becomes one-sided and mass loss is induced then, depending on the value of n, the luminosity of the jet could increase to a maximum brightness as $\dot{M}_{loss}$ approaches its largest value (presumably related to the accretion rate at an outer radial boundary in the disc).

At the shadowed disc region, we have seen in §3.3.2, the rate of mass loss is proportional to the luminosity, using the expression given by Begelman et al. (1983) (c.f. 3.14). Remember, that mass loss only occurs if the surface dip satisfies $d_s > z_c$, where z_c is the Compton heating length scale above the disc surface (3.34). If $d_s < z_c$ then no mass loss occurs. This is summarised as

$$\left(\frac{\dot{M}_{loss}}{1M_0yr^{-1}}\right) \sim \begin{cases} j\left[\frac{L}{L_{Edd}}\right] & \text{if } d_s > z_c. \\ 0 & \text{if } d_s < z_c. \end{cases} \qquad (3.40)$$

Here j is a constant. Assuming that only mass loss between $10^{17}cm$ and $10^{18}cm$ is considered, equation (3.14) can be used to give a value $j \sim 1.0$. In calculating the dynamical evolution of the disc-jet system the asymmetric disc model derived in §3.3 must be used to discover if $d_s > z_c$.

To complete this set of equations we insist on a constant accretion rate at some outer boundary. This introduces another time scale $t_2 \sim r_d / v_r \sim 10^6 yr$

which is the inflow time of material left in the disc after mass-loss has occurred. Therefore, we have

$$\dot{M}_{acc}+\dot{M}_{loss}(t-t_2)=\dot{M}_{total}. \tag{3.41}$$

We can now solve equations (3.35)-(3.41) for different values of k and n.

We have identified two types of solutions to the dynamical flow equations. The dominant factor is the parameter k in (3.39). As we have mentioned, k is a measure of the jet efficiency in converting jet energy into radiation. It determines the sensitivity of the dissipation in the jet to its environment, which consists of material brought by a disc wind from large radii.

In the two examples to follow, the disc is assumed initially symmetric with a fixed accretion rate at the outer boundary of $\dot{M}_{total}=1.0M_0yr^{-1}$. The accretion rate at the inner edge is temporarily reduced to $\dot{M}_{acc}=0.1M_0yr^{-1}$ for $\sim 10^4 yr$ and a large perturbation is given to the disc system in which the top jet has a higher luminosity than the lower jet: $L_+=0.8L_{Edd}$ and $L_-=0.2L_{Edd}$ (the jet height is $2\times10^{17}cm$). This creates an asymmetric disc shape and a region of the top disc surface is shadowed from the central soft X-ray flux by a distance $d_s>z_c$ at $\sim 5\times10^{17}cm$. The requirement of a large perturbation to produce an asymmetric system is discussed in §3.8.

Figure 38hows the dynamical evolution of the system with $k=10$ and $n=0.1$. The thick lines represent the two jet luminosities, the crosses correspond to the accretion rate at the inner edge, and the triangles show the spin of the black hole as the ratio a/m. The high value of k means that the dissipation in the jet is highly sensitive to its environment. When the material from the shadowed region reaches the jet, it improves the jet's efficiency. The resultant increase in luminosity raises the mass loss from the shadowed region (3.40) which in turn feeds back to the jet until its luminosity reaches a

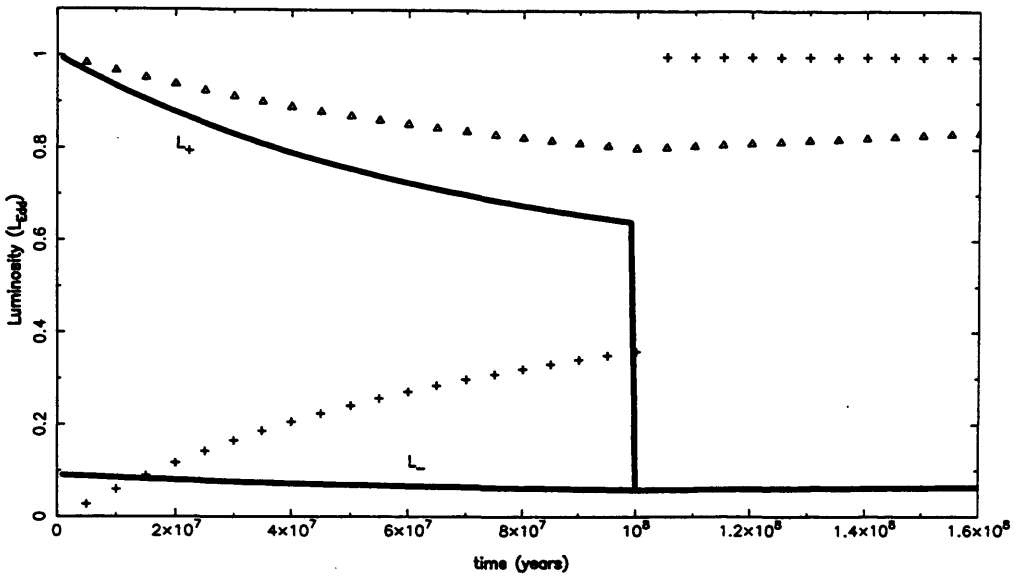

Figure 38

The evolution of the upper and lower jet luminosities with time for a disc system with $k = 10$ and $n = 0.1$. The crosses show the accretion rate at the inner edge, $\dot{M}_{acc}$, in units of solar masses per year. The triangles show the ratio a/m, representing the spin of the black hole.

maximum, i.e. $L \sim P$ (3.39). After a time scale $t_2 \sim 10^6 yr$ the accretion rate at the inner edge becomes very small due to the large loss of disc material. The power extracted from the black hole by the jet is greater than the power the hole receives from the accreting material and the black hole starts to lose angular momentum (3.35). As the black hole spins down it reduces the maximum power available to the two jets. This in turn reduces the rate of mass loss from the shadowed region of the top disc surface, and again this affects the accretion rate at the inner edge after $t_2 \sim 10^6 yr$ as $\dot{M}_{acc}$ begins to rise.

With the chosen parameters in figure 38 the reduction in both upper and lower jet luminosities continues for $\sim 10^8 yr$, as the black hole spins down. Eventually, the upper jet drops to a luminosity of $\sim 0.6 L_{Edd}$. This induces mass loss at the rate of $\sim 0.6 M_0 yr^{-1}$ from the shadowed surface area (from 3.40). The corresponding disc accretion rate is $\dot{M}_{acc} \sim 0.4 M_0 yr^{-1}$. Now $\dot{M}_{acc}$ is too large to

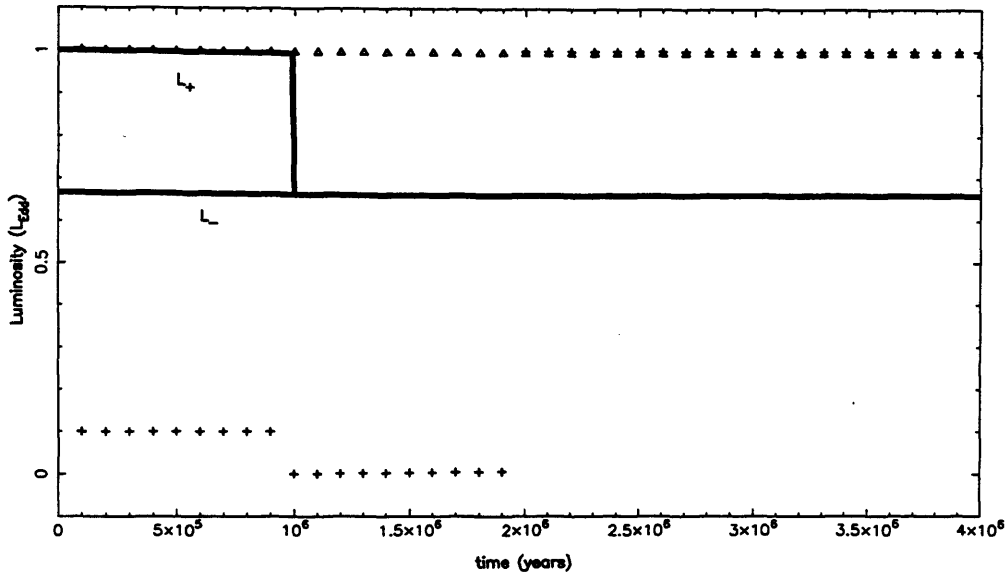

Figure 39
The same as figure 38 but with $k = 1$.

support an asymmetric disc shape. The disc is forced to become symmetric and mass loss from the disc surface ceases.

With no additional material in the jet environment, the efficiency in converting jet energy into radiation declines and the luminosity of the top jet falls off dramatically becoming equal to that of the bottom jet. After a disc inflow time of $10^6 yr$, the accretion rate at the inner edge reaches $1.0 M_0 yr^{-1}$ and the black hole, having a surplus of energy from the accreting disc material, starts to spin back up.

Figure 39 shows the same initial disc configuration, but k has been lowered to $k = 1$. This smaller value of k means that the dissipation in the jet is less sensitive to its environment. Therefore, when the additional material from the shadowed region of the top surface reaches the jet, the subsequent rise in luminosity is not as significant. The lower jet, without this extra material, has a jet luminosity which is comparable with that of the upper jet. The disc cannot maintain the asymmetric shape and the mass loss ceases. Note that the

accretion rate at the inner edge takes $\sim 10^6 yr$ to adapt to the changes in mass loss.

3.8 Comparison with observations

We have seen in the previous section that the dynamical evolution of a one-sided jet can be described by one of two categories. These categories relate to the magnitude of the effect the surrounding medium of the jet has in converting the jet energy into radiant energy. We found that if the jet environment raises dissipation within the jet, then a stable one-sided jet / asymmetric disc system is likely to remain for large timescales. However, if the jet environment has little effect in enhancing the efficiency of dissipation, then a one-sided jet / asymmetric disc system is unstable and will only last for a short time.

As we mentioned in §3.7, the two examples (figures 38 and 39) only consider disc solutions that contained shadowed surface regions within $10^{18} cm$. In reality, shadowing can occur at much larger radii. This would change the examples in two ways. We would not need such a large initial perturbation to create the initially asymmetric disc. The jet luminosities were originally perturbed to $L_+ = 0.8 L_{Edd}$ and $L_- = 0.2 L_{Edd}$. A smaller perturbation would create the initial shadowed region at a larger radii, but the subsequent increase in jet luminosity would move the dip inwards. Conversely, we would not expect the disc to suddenly 'snap' back into a symmetric shape when an asymmetric solution became unviable, as in the examples, but rather the dip would begin to move outwards.

As small perturbations in jet luminosities are likely, this leaves us with a picture where a disc is always in an asymmetric shape, the region of the surface dip moving between inner ($\sim 10^{17} cm$) and outer ($\sim 10^{19} cm$) radii, and possibly

moving from top to bottom surfaces in a random fashion. The one-sidedness of the jet depends on how sensitive the jet dissipation is to its surrounding's.

Our model is unrealistic in at least one respect: systems in which jet energy is converted efficiently into radiation should correspond to the bright jets. However, putting the efficiency factor $k = 0$ in (3.39) leads to the jet having its maximum luminosity. We should introduce a factor k / k_{max} into (3.39) to account for the efficiency of dissipation in the jet even in the absence of mass loss:

$$L \sim \frac{k}{k_{max}} P\left(\frac{1 + k\left[\frac{\dot{M}_{loss}(t - t_1)}{1 M_0 yr^{-1}}\right]^n}{1 + k\left[\left(\frac{\dot{M}_{loss(max)}}{1 M_0 yr^{-1}}\right)\right]^n}\right). \qquad (3.42)$$

This then means that the brightest jets are those most sensitive to their surrounding environment, and as we have seen in §3.7, are likely to be in a stable one-sided system. This is consistent with the observations of Perley, Dreher & Cowan (1984); Bridle et al. (1986) etc. who have found that the vast majority of FR II radio galaxies and quasars appear to be completely one-sided.

Fluctuations in jet luminosities due to, for example, differential efficiencies of dissipations in bulk-energy flows for the two jets, could lead to disc systems where the surface dip would occasionally flip sides. This would occur when a one-sided jet was coming to the end of its 'lifetime', as the surface dip moved to larger radii. In this fashion the more luminous jet would randomly flip-flop from one side to the other. For stable one-sided jets (high k) this random direction change would occur on timescales of $10^7 - 10^8 yr$ (see figure 38).

This could explain the 'specific avoidance' effect observed in the extended lobes of radio sources (see §3.1 and Rudnick & Edgar, 1984). A large

number of high-resolution maps have been rotated 180° around their cores or reflected about their symmetry axis and then overlaid on their respective originals. The high surface brightness regions from one-side is seen to 'avoid' those from the other plate, for most sources. Rudnick & Edgar discussed the possibility that this avoidance behaviour could be due to ejections from the nuclear source alternating sides. This idea has also been mentioned by Saikia & Wiita (1982), Macklin (1981) and Robson (1981). However, one problem with these models is in finding a mechanism to switch the jet from one side to the other. Another problem is that they do not explain the existence of symmetric lobes. The model derived in this chapter has a mechanism for switching sides on the timescales associated with avoidance behaviour ($\sim 10^7 - 10^8 yr$). Also, the lobes are always symmetric because they are fed by the same bulk jet kinetic energy, even though one jet is more luminous.

Our model for one-sided radio jets illustrates an important point. The picture of lost material from a shadowed region of an accretion disc improving the dissipation of a radio jet, can only be obtained by consistently calculating the internal structure of the disc. In this way, we see that small changes in disc material flow can cause very large fluctuations in observed phenomena on kpc scales.

Chapter Four

The vertical transport of angular momentum

4.1 Introduction

The angular momentum within an accretion disc is transported principally by large scale eddies (and energy dissipated mainly by small scale eddies). In the vertical transport of angular momentum, eddies of scale H, the disc scale height, will be deposited in the disc environment. The standard thin disc model developed by Shakura & Sunyaev (1973) and Novikov & Thorne (1973) (see §1) obtain disc solutions using vertically averaged quantities. Thus, in these models the vertical transport of angular momentum is neglected.

Attempts have been made to obtain a self-consistent picture of the internal structure of an accretion disc (Urpin, 1983; Siemiginowska, 1988; Kley & Lin, 1992). Here the effects of the vertical transport of angular momentum must be accounted for. Both Urpin and Kley & Lin have incorporated this vertical transport into their disc models, although Urpin does not include all of the viscous stress tensor components. These models describe surface-less discs extending to infinity.

As discussed in §2, Urpin, using a parameterization similar to Shakura & Sunyaev (1973), found an outwardly directed flow in the equatorial plane and inflow near the surface of the disc. Using the full viscous stress tensor and finite difference method, Kley & Lin found similar results for discs with low α,

but find that for discs with higher values of α (> 0.06), the flow throughout the disc was directed wholly inward. They conclude that a change in direction in the flow can only be obtained by increasing the vertical variation of the azimuthal velocity. A large viscosity increases the stress between mass elements at different heights above the disc midplane and tends to reduce the vertical gradient of the infall velocity. Consequently, flow throughout the disc is directed inwards. However, by using a finite difference method to solve the disc equations it is difficult to gain much insight into the solutions.

In this section we attempt to solve the equations in a gas pressure dominated region with Kramers opacity (2.40) (c.f. zone C; §2.3.2), for a steady state accretion disc, including the vertical transport of angular momentum, analytically as far as possible, resorting to numerical methods for the solution of the final system of ordinary differential equations only. As in §4 we set up the equations of motion of the thin disc under the restrictions that the vertical and horizontal temperature gradients are specified. We find that for consistency the first order correction to Kepler motion must be included.

Following on from the previous chapters, we again define a disc surface through the condition of pressure balance between the disc and its environment (which may be a corona or disc wind; see §2.4). Having a disc surface hampers the transport of angular momentum vertically. As we mentioned previously, eddies of scale H can transport angular momentum vertically by depositing it in the external environment. This produces an external torque (to extract the angular momentum). Therefore in previous chapters we have neglected transport in the vertical direction. In this chapter, to treat the vertical transport of angular momentum correctly, we must impose a boundary condition at the disc surface corresponding to angular momentum loss. Note that we will not consider mass loss in this case.

Our results are similar to those of Kley & Lin (1992). We find that for low α, the internal structure is akin to Urpin (1983), with directional changes of

flow apparent in the disc. At high α, the disc becomes wholly inflowing. However, we expand upon the work done by Kley & Lin and find that for more significant external pressures ($n < n_c$; see §2.2.4), a steady state solution exists, at a given accretion rate, for only one value of surface torque. Alternatively, assuming there exists a fixed external torque generated, for example, by magnetic or viscous interaction with the disc environment, then steady state solutions can be found for one accretion rate only.

4.2 A disc with vertical transport of angular momentum

4.2.1 The disc equations

In this section we will identify the lowest order steady-state equations that describe an accretion disc which includes vertical transport of angular momentum. As in §2 we shall assume that the disc is symmetric about the $z = 0$ midplane. We shall also assume that the disc can be described by the vertically isothermal system of equations (as we did in §3; for an explanation see §2.5.1). This means that the energy equation (2.8) is replaced by a prescribed vertically isothermal temperature distribution $T = T(r)$.

The disc equations are similar to those used in the asymmetric disc model of §3; first

$$V_0 = \frac{1}{\omega^{1/2}} \tag{4.1}$$

$$\sigma_0 = \sigma_{00} \exp(-\frac{\zeta^2}{2c_0^2\omega^3}). \tag{4.2}$$

At zero order the disc material rotates in a Kepler orbit (4.1), and is in hydrostatic equilibrium (4.2). We use the kinematic viscosity prescription

$$\nu = \alpha c_s H \,. \tag{4.3}$$

With the ϕ-equation (2.23), we now differ from §4. Including all viscous stress terms, we have an equation for the zero order radial velocity U_0

$$\sigma_0 U_0 = -\frac{3}{\omega^{\frac{1}{2}}}(\sigma_0 c_0^2 \omega^2)_{,\omega} + 2\sigma_0 c_0^2 \omega^3 V_{1,\zeta\zeta} - 2\sigma_0 \zeta V_{1,\zeta}. \tag{4.4}$$

Here the final two terms represent the corrections from non-Kepler motions; these terms are ignored in the standard treatment when this equation is integrated vertically to give the radial velocity in terms of the surface density. The non-Kepler terms are obtained from the next order correction to the radial equation (2.22):

$$2\sigma_0 V_1 = \alpha^2 c_0^2 \sigma_0 \omega^3 U_{0,\zeta\zeta} + \alpha^2 \sigma_0 \zeta U_{0,\zeta} + \omega^{\frac{3}{2}}(\sigma_0 c_0^2)_{,\omega} - \frac{3\sigma_0}{2\omega^{\frac{5}{2}}}\zeta^2. \tag{4.5}$$

Note that the third term on the right of (4.5) comes from the radial pressure gradients while the first two terms on the right represent the effects of the viscous transport of angular momentum vertically (these terms are not included in the model developed by Urpin, 1983); the final term is from the vertical gradient of the gravitational field. These effects are fed into the radial motion through V_1 in (4.4).

The continuity equation (2.25) is in the same form as in §3:

$$(\sigma_0 U_0 \omega)_{,\omega} + \omega(\sigma_0 W_0)_{,\zeta} = 0. \tag{4.6}$$

Finally, as we mentioned above, we assume that the disc is vertically isothermal and the temperature within the disc is prescribed as $T = T(r)$. The

disc region we are interested in corresponds to gas pressure dominated and Kramers' opacity. We adopt the thin disc temperature dependence (1.22) in the form

$$c_0^2 = \frac{1}{\omega^{3/4}}. \tag{4.7}$$

We showed in §3.6.4 that altering the radial dependence of c_0^2 had little effect on the internal structure of the accretion disc.

4.2.2 Boundary conditions

In §2.2.3 we saw that to obtain the conditions on the surface of the disc we must integrate the momentum equation (2.4) over a pill-box spanning an element of surface (see figure 4 and 2.43). We mentioned in §4.1 that to include the vertical transport of angular momentum correctly, we require an external torque to extract the angular momentum. This is incorporated into the surface integral as

$$\int \rho \upsilon^i \upsilon^j dS_j = -\int \bar{T}^{ij} dS_j - g^{ij} \int P dS_j - \int \rho (\Phi g^{ij})_{;j} dV - \int G_c^{ij} dS_j \tag{4.8}$$

The third term on the right is zero in the limit that the pill-box volume tends to zero, whilst the final term on the right is the external couple. This will introduce vertically transported angular momentum loss at the surface

i.e.

$$\begin{aligned} G_c^{23} &= g_c(r) \\ G_c^{ij} &= 0 \quad \textit{for all other } i \textit{ and } j. \end{aligned} \tag{4.9}$$

$g_c(r)$ represents the couple applied at the disc's surface and its value will be prescribed for specific numerical calculations. Labelling the surface values with the subscript s we obtain

$$[\bar{T}^{ij}n_j + \rho\upsilon^i\upsilon^j n_j + Pn^i - G_c^{ij}n_j]_s = P_{ext}n_s^i \tag{4.10}$$

where P_{ext} is the pressure in the external medium surrounding the disc.

We take from (2.47) the condition of no mass loss from the disc surface

$$\left.\frac{\partial\zeta}{\partial\omega}\right|_s = \left.\frac{W_0}{U_0}\right|_s . \tag{2.47}$$

From (4.10) we get

$$[\bar{T}^{11}n_1 + \bar{T}^{13}n_3 + \rho(\upsilon^1\upsilon^1 n_1 + \upsilon^1\upsilon^3 n_3)]_s = [(P_{ext} - P_+)n^1]_s \tag{4.11}$$

$$[\bar{T}^{21}n_1 + \bar{T}^{23}n_3 + \rho(\upsilon^2\upsilon^1 n_1 + \upsilon^2\upsilon^3 n_3)]_s = [G^{23}n_3]_s \tag{4.12}$$

$$[\bar{T}^{31}n_1 + \bar{T}^{33}n_3 + \rho(\upsilon^3\upsilon^1 n_1 + \upsilon^3\upsilon^3 n_3)]_s = [(P_{ext} - P_+)n^3]_s \tag{4.13}$$

where n_i is the normal vector to the surface of the disc, and hence from (2.47) we get the relation

$$\frac{n_1}{n_3} = -[\frac{\upsilon_z}{\upsilon_r}]_s = -[\frac{W_0}{\tilde{M}U_0}]_s . \tag{4.14}$$

Using the expansions of §2.2.2 we expand (4.11), (4.12) and (4.13) obtaining, respectively

$$\begin{aligned}[\tilde{M}^2\Delta P]_s = &-[c^2\omega^{3/2}\sigma(\frac{4}{3}U_{,\omega} - \frac{2}{3}W_{,\zeta})]_s \\ &+ [c^2\omega^{3/2}\sigma(\tilde{M}^2U_{,\zeta} + W_{,\omega})\frac{U}{W}]_s\end{aligned} \tag{4.15}$$

$$[\tilde{M}^2V_{,\zeta}]_s = [\frac{W}{U}(V_{,\omega} - \frac{1}{\omega}V) - \bar{g}_c(r)]_s \tag{4.16}$$

$$[\tilde{M}^4\Delta P]_s = [c^2\omega^{3/2}\sigma(\tilde{M}^2U_{,\zeta}+W_{,\omega})\frac{W}{U}]_s$$
$$-[c^2\omega^{3/2}\sigma(\frac{4\tilde{M}^2}{3}W_{,\zeta}-\frac{2\tilde{M}^2}{3}U_{,\omega})]_s. \qquad (4.17)$$

Here the external couple $g_c(r)$ is absorbed within $\bar{g}_c(r)=g_c(r)\tilde{M}/(\bar{c}^2\bar{r}\alpha\bar{\rho}\omega^{1/2}c^2\sigma)$. Taking the first order terms of (4.16) and using (2.47), gives us a boundary condition for the correction to Kepler motion at the disc surface:

$$[V_{1,\zeta}]_s = -[\frac{3}{2\omega^{3/2}}\zeta_{s,\omega}+\bar{g}_c(r)]_s. \qquad (4.18)$$

Equating the zero order terms of equations (4.15) and (4.17) gives us another boundary condition, defining the vertical gradient of U_0 at the disc surface

$$[U_{0,\zeta}]_s = 0. \qquad (4.19)$$

Finally, substituting (4.19) back into either (4.15) or (4.17) gives us the definition of the disc surface as a condition of pressure balance between the disc and its surrounding medium through $\Delta P = 0$:

$$P(\omega,\zeta_s) = P_{Ext}(\omega). \qquad (4.20)$$

Once again, to complete the boundary conditions we should specify an inner and an outer radial boundary condition. We therefore expect the disc equations above to yield a two parameter family of solutions.

4.2.3 Solving the disc equations

In §4.2.1 we identified the disc equations that would describe a disc which includes the vertical transport of angular momentum: the hydrostatic

equation (4.2), the equations for the azimuthal velocity (4.1 and 4.5), expressions for the radial velocity (4.4) and disc temperature (4.7), and finally the continuity equation (4.6).

The linearity of equations (4.4) and (4.5) in σ_0 enables us to eliminate σ_∞ from these equations using (4.2). After some manipulation we get

$$\frac{A\alpha^2}{2}U_{0,\zeta\zeta}+\alpha^2\zeta U_{0,\zeta}-V_1=-E-F\zeta^2 \tag{4.21}$$

$$AV_{1,\zeta\zeta}-2\zeta V_{1,\zeta}-U_0=B+C\zeta^2 \tag{4.22}$$

where

$$\begin{aligned}
A &= 2c_0^2\omega^3 \\
B &= 3\omega^{3/2}c_{0,\omega}^2+6\omega^{1/2}c_0^2+3\omega^{3/2}c_0^2\frac{\sigma_{\infty,\omega}}{\sigma_\infty} \\
C &= \frac{3\omega^{3/2}c_0^2A_{,\omega}}{A^2} \\
E &= \omega^{3/2}c_0^2\frac{\sigma_{\infty,\omega}}{\sigma_\infty}+\omega^{3/2}c_{0,\omega}^2 \\
F &= \frac{1}{2\omega^{3/2}c_0^2}c_{0,\omega}^2 \\
c_0^2 &= \frac{1}{\omega^{3/4}}.
\end{aligned} \tag{4.23}$$

Now, to solve the two equations (4.21) and (4.22) for U_0 and V_1, it is helpful to rescale the dimensionless variable for z in terms of A (from 1.7 we see that the disc scale height $H=\sqrt{A/2}$): $\varsigma=\zeta/A^{1/2}$. We also define new variables $V=V_1\lambda$ and $U=U_0$, where $\lambda=\sqrt{2}/\alpha$, and use primes to denote differentiation with respect to ς. The above equations (4.21) and (4.22) become:

$$U''+2\varsigma U'-\lambda V=-\lambda^2E-\lambda^2FA\varsigma^2 \tag{4.24}$$

$$V''-2\varsigma V'-\lambda U=\lambda B+\lambda CA\varsigma^2. \tag{4.25}$$

Note that U and V depend on radius ω only as a parameter - through the ω dependence of A, B, C, E, F in the particular integral and through the dependence on $\varsigma = \zeta / A^{1/2}$. The partial differential equations therefore reduce to a set of ordinary differential equations even when angular momentum is transported vertically.

Particular integrals of this system are readily obtained. For the complementary function we eliminate V to obtain a fourth order homogenous equation for U for which we define four independent solutions, say A_i, $i = 1-4$, by specifying the following conditions at $\varsigma = 0$:

$$\begin{array}{llll} A_1 = 1 & A_1' = 0 & A_1'' = 1 & A_1''' = 0 \\ A_2 = 0 & A_2' = 1 & A_2'' = 0 & A_2''' = 1 \\ A_3 = 1 & A_3' = 0 & A_3'' = -1 & A_3''' = 0 \\ A_4 = 0 & A_4' = 1 & A_4'' = 0 & A_4''' = -1 \end{array} \qquad (4.26)$$

where these conditions determine solutions behaving as $\cosh\varsigma$, $\sinh\varsigma$, $\cos\varsigma$ and $\sin\varsigma$, as ς tends to zero.

From equation (4.24) we can define a similar set of functions, B_i as

$$B_i = \frac{1}{\lambda}(A_i'' + 2\varsigma A_i'). \qquad (4.27)$$

Each of the set A_i and B_i form a complete independent set of complementary functions for (4.24) and (4.25). The general solutions for U and V can now be written as

$$U = \sum_1^4 f_i(\omega) A_i(\varsigma) + p_0 + p_1\varsigma^2 \qquad (4.28)$$

$$V = \sum_1^4 f_i(\omega) B_i(\varsigma) + q_0 + q_1\varsigma^2. \qquad (4.29)$$

If we substitute the particular integral terms of equations (4.28) and (4.29) into (4.24) and (4.25) and equate coefficients of ς^2, we get

$$\begin{aligned} 4p_1 - \lambda q_1 &= -\lambda^2 FA \\ -4q_1 - \lambda p_1 &= \lambda CA. \end{aligned} \tag{4.30}$$

Equating coefficients of ς^0 gives us

$$\begin{aligned} 2p_1 - \lambda q_0 &= -\lambda^2 E \\ 2q_1 - \lambda p_0 &= \lambda B. \end{aligned} \tag{4.31}$$

Solving the simultaneous equations (4.30) and (4.31) gives us the particular integrals of (4.24) and (4.25):

$$p_0 = \frac{2A(F\lambda^2 - 4C)}{(\lambda^2 + 16)} - B \tag{4.32}$$

$$q_0 = -\frac{2A\lambda(4F + C)}{(\lambda^2 + 16)} + E\lambda \tag{4.33}$$

$$p_1 = -\frac{\lambda^2 A(4F + C)}{(\lambda^2 + 16)} \tag{4.34}$$

$$q_1 = \frac{\lambda A(F\lambda^2 - 4C)}{(\lambda^2 + 16)}. \tag{4.35}$$

Turning to the complementary functions, we have assumed that the disc is symmetric around its midplane $\varsigma = 0$. This implies

$$\left.\frac{\partial U}{\partial \varsigma}\right|_{\varsigma=0} = \left.\frac{\partial V}{\partial \varsigma}\right|_{\varsigma=0} = 0. \tag{4.36}$$

These two boundary conditions are substituted into the solutions (4.28) and (4.29). Using the boundary conditions (4.26) and (4.27) we get

$$\begin{aligned} f_2 + f_4 &= 0 \\ 3f_2 - f_4 &= 0 \end{aligned} \quad \Rightarrow f_2 = f_4 = 0. \tag{4.37}$$

Similarly, we substitute the two surface boundary conditions (4.18) and (4.19) into the solutions (4.28) and (4.29) using (4.37) and have

$$\begin{aligned} f_1 &= \frac{1}{C_4}[2q_1\varsigma_s A'_{3(s)} - 2p_1\varsigma_s B'_{3(s)} - WA'_{3(s)}] \\ f_3 &= \frac{1}{C_4}[2p_1\varsigma_s B'_{1(s)} - 2q_1\varsigma_s A'_{1(s)} + WA'_{1(s)}] \end{aligned} \tag{4.38}$$

where

$$W = -\lambda[\frac{3}{2\omega^{3/2}}\zeta_{s,\omega} + \bar{g}_c(r)]_s \tag{4.39}$$

$$C_4 = A'_{1(s)}B'_{3(s)} - A'_{3(s)}B'_{1(s)}. \tag{4.40}$$

If $C_4 = 0$ then (4.38) becomes singular. This can be consistent only if the numerator and denominator of (4.38) vanish at the same point. Using the expressions in (4.23) we can rewrite (4.38) as

$$\begin{aligned} f_1 &= -\frac{\varsigma_s\lambda(42\lambda B'_{3(s)} + (3\lambda^2 + 216)A'_{3(s)}) + WA'_{3(s)}}{4\omega^{1/4}(\lambda^2 + 16)C_4} \\ f_3 &= \frac{\varsigma_s\lambda(42\lambda B'_{1(s)} + (3\lambda^2 + 216)A'_{1(s)}) + WA'_{1(s)}}{4\omega^{1/4}(\lambda^2 + 16)C_4}. \end{aligned}$$

The complementary function solutions A_1 ,A_3, B_1, B_3 can be calculated from (4.24) and (4.25) using a NAG routine such as D02CAF and depend on the value of λ (which is inversely related to the viscosity parameter α). Figures 40 and 41 show how the quantities A'_1, A'_3, B'_1, B'_3 vary with ς for $\alpha = 0.1$ and $\alpha = 1.0$ respectively. These quantities are positive for all ς. Therefore to obtain

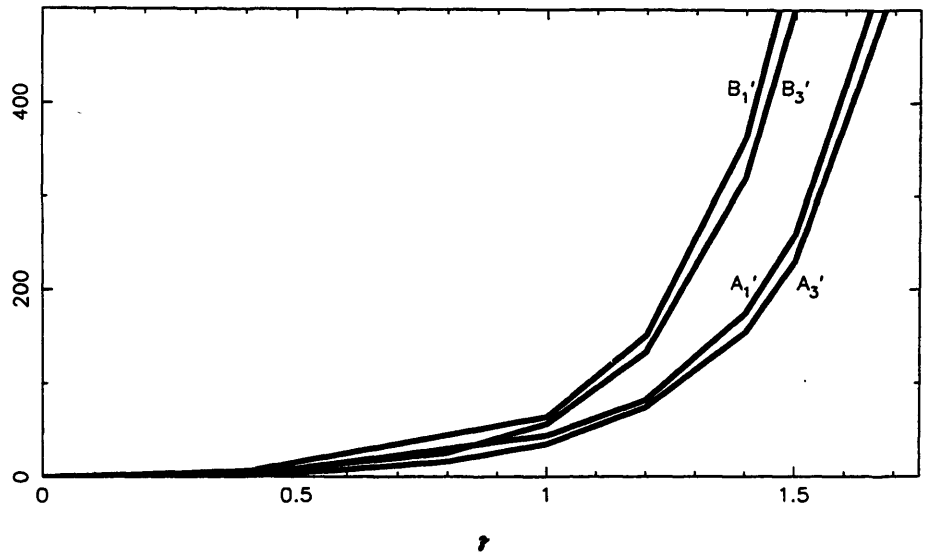

Figure 40
The complementary functions A_1', A_3', B_1', B_3' *as a function of* ς *for* $\alpha = 0.1$.

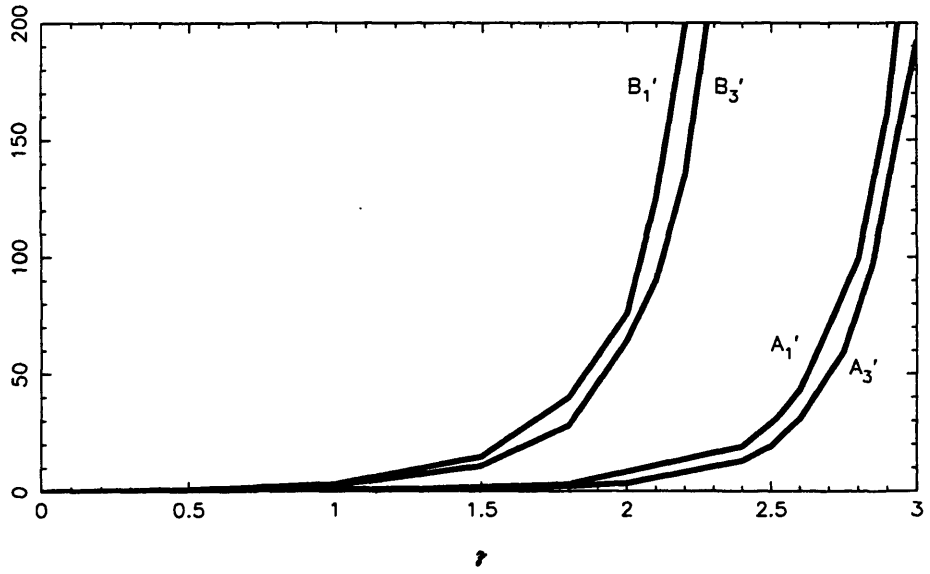

Figure 41
The complementary functions A_1', A_3', B_1', B_3' *as a function of* ς *for* $\alpha = 1.0$.

solutions when $C_4 = 0$, a specific value of g_c must be given to allow the disc to pass smoothly through the 'singularity'.

The form of (4.38) tells us what couple must be applied at the disc surface when $C_4 = 0$ in order to obtain a steady state solution. This arises because the terms f_1 and f_3 are calculated at the disc surface ς_s. The definition of the disc surface (4.20) is one of a pressure balance between the disc and its surrounding medium, where the external pressure is a function of r only. In reality, if the disc surroundings are extracting angular momentum from the disc, then there will be some kind of feedback mechanism which will result in the external pressure becoming dependent on both r and z. This problem does not arise in the surface-less models of Urpin (1983) and Kley & Lin (1992), where angular momentum is transported to infinity.

Because of our lack of knowledge of the feedback processes between the disc and its environment we investigate the disc structure considering a range of power law external pressures

$$P_{Ext} \propto r^{-n}. \tag{4.41}$$

In all examples to follow, the initial value of the external pressure (at r_{in}) will be chosen as $< 10^{-4} P_0$, where P_0 is the disc central pressure. This is so that any disc solutions affected by the external medium will be independent of the initial boundary conditions.

Figure 42 shows how the quantity C_4 varies with ς for differing values of α (0.1, 0.5, 0.7 and 1.0). For high values of α (i.e. $\alpha = 1.0$), C_4 does not pass through zero. From (4.24) and (4.25) we see that when α is large (i.e. small λ), the correction to Kepler motion remains small even when the vertical gradient of the radial velocity is large. In this case, most of the angular momentum is carried away in the radial direction. This is confirmed by the velocity solutions (4.38). If $\alpha >> 0$ ($\lambda \sim 0$) then the correction to Kepler motion $V \sim 0$ and the

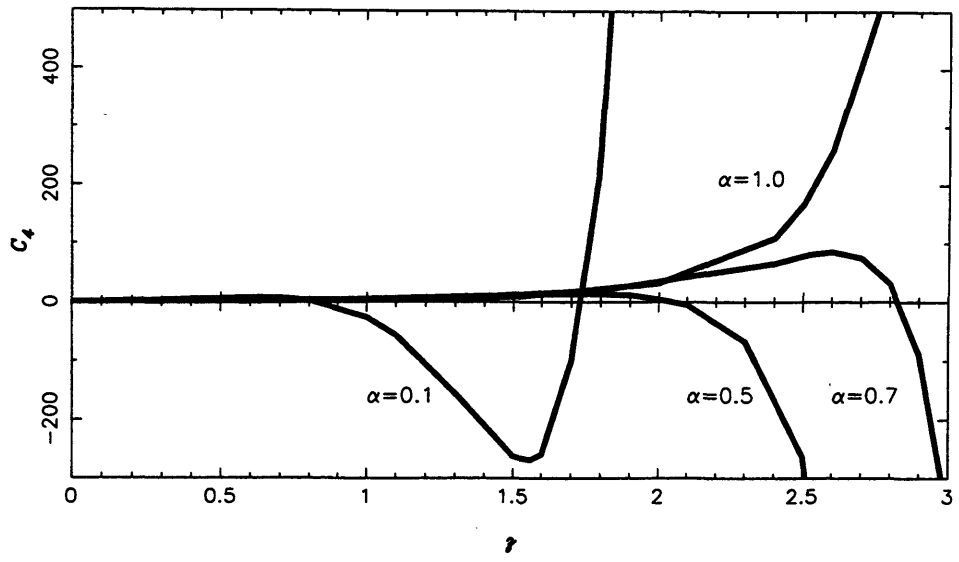

Figure 42
The quantity C_4 as a function of ς for α = 0.1, 0.5, 0.7 and 1.0.

radial velocity is independent of z. All the momentum is carried away radially, and the disc will consist of wholly inflowing material (as found by Kley & Lin, 1992). Note that this result differs from §2 where vertical transport of angular momentum was ignored. Here the radial velocity remained a function of z because Kepler motion was modified by radial pressure gradients and the vertical gradient of the gravitational field (4.5).

For low values of α (high λ), even small gradients in U could lead to large values of V. At certain disc heights (values of ς_s), the vertical transport of angular momentum will become very significant ($C_4 = 0$) and the disc solutions will depend sensitively on the external couple applied at the disc surface.

If the external pressure remains small compared to the central pressure of the disc (c.f. $n > n_c$; §2.2.4), we have seen that the disc surface will increase approximately as a multiple of a scale height (i.e. constant ς; see §2). Therefore, in the case of a small external pressure and fixed α, the quantity C_4 (which depends only on the disc height for fixed α), should remain constant. If α is large, then C_4 will be positive. If α is small, then C_4 could either be

positive or negative, depending on the value of ς_s. However, for an external pressure that becomes more significant with radius ($n < n_c$, i.e. corona or disc wind; §2.4), the disc surface will be 'pushed over' (c.f. results of §2.3.2), lowering ς_s with radius. The value of C_4 will change as ς_s moves to the left on figure 42 and, for discs with low α, possibly move through zero at a some distance. Here, to obtain steady state solutions the value of the couple must allow the solutions to pass smoothly through the $C_4 = 0$ point.

Turn now to the condition of no mass loss at the boundary (2.47). This gives an expression for the vertical velocity at the surface of the disc:

$$W\big|_s = \frac{1}{A^{1/2}}\left(\frac{1}{2}A_{,\omega}\varsigma_s + A\varsigma_{s,\omega}\right)U\big|_s . \tag{4.42}$$

As we showed in §3, the continuity equation can be shown to be a second order differential equation for $\sigma_{00}(\omega)$. Therefore, to solve the disc structure we are going to specify σ_{00} and $\sigma_{00,\omega}$ at some ω and for $\varsigma = 0$ (equivalent to the accretion rate and an inner boundary condition) and integrate with respect ω. To see this we take the continuity equation (4.6) in the form

$$A^{-\frac{1}{2}}(W\sigma_0)' = -U\sigma_{0,\omega} - \sigma_0 U_{,\omega} - U\sigma_0/\omega . \tag{4.43}$$

Integrating from $\varsigma = 0$ to $\varsigma = \varsigma_s$, we get

$$\begin{aligned} A^{-\frac{1}{2}}[u_\gamma\sigma_0]_s = -\sigma_{00}\Big(&\frac{\partial f_1}{\partial\omega}I_1 + \frac{\partial f_3}{\partial\omega}I_3 + \frac{\partial p_0}{\partial\omega}J_1 + \frac{\partial p_1}{\partial\omega}J_2\Big) \\ &- Z_2 - Z_3 - Z_5 \end{aligned} \tag{4.44}$$

where the ς dependent terms are all evaluated at ς_s, and

$$
\begin{aligned}
Z_2 &= \left(\frac{\sigma_{00}}{\omega} + \frac{\partial \sigma_{00}}{\partial \omega}\right)(f_1 I_1 + f_3 I_3 + p_0 J_1 + p_1 J_2) \\
Z_3 &= \frac{\sigma_{00} A_{,\omega}}{A}(f_1 K_1 + f_3 K_3 + p_0 J_2 + p_1 J_4) \\
Z_5 &= \frac{\sigma_{00} A_{,\omega}}{2A}(f_1 L_1 + f_3 L_3 + 2 p_1 J_2)
\end{aligned}
\tag{4.45}
$$

and

$$
\begin{aligned}
I_i &= \int_0^{\varsigma_s} A_i e^{-\varsigma^2} d\varsigma \\
J_1 &= \int_0^{\varsigma_s} e^{-\varsigma^2} d\varsigma \\
J_2 &= \int_0^{\varsigma_s} \varsigma^2 e^{-\varsigma^2} d\varsigma \\
J_4 &= \int_0^{\varsigma_s} \varsigma^4 e^{-\varsigma^2} d\varsigma \\
K_i &= \int_0^{\varsigma_s} A_i \varsigma^2 e^{-\varsigma^2} d\varsigma \\
L_i &= \int_0^{\varsigma_s} A_{i,\varsigma}\, e^{-\varsigma^2} d\varsigma \,.
\end{aligned}
\tag{4.46}
$$

The term $\frac{\partial p_0}{\partial \omega}$ on the right side of (4.44) contains $\sigma_{00,\omega\omega}$ so equation (4.44) is a second order equation for σ_{00}. The coefficients in this equation involve the functions A_i and B_i at the surface $\varsigma = \varsigma_s$ as functions of ω and these must be evaluated by vertical integration of (4.24) and (4.25) at each ω. Thus, we solve (4.44) for $\sigma_{00,\omega\omega}$, and write the resulting equation in the equivalent first order form

$$
\begin{aligned}
y &= \sigma_{00} \\
y_{,\omega} &= Y \\
Y_{,\omega} &= \bar{F}(y, Y, \omega)
\end{aligned}
\tag{4.47}
$$

where the form of $\bar{F}$, obtained from (4.44), is

$$\bar{F} = (3\omega^{3/2}c_0^2 J_1)^{-1}\{Z_1 + Z_2 + Z_3 + Z_4 - Z_5 + \sigma_\infty(\frac{2}{\lambda}\frac{\partial q_1}{\partial \omega} - (3\omega^{3/2}c_0^2{}_{,\omega} + 6\omega^{1/2}c_0^2)_{,\omega} - \sigma_{\infty,\omega}(\frac{3\omega^{3/2}c_0^2}{\sigma_\infty})_{,\omega})J_1\} \qquad (4.48)$$

where Z_2, Z_3 and Z_5 are given by (4.45) and

$$Z_1 = [\sigma_0 W]_s A^{-1/2}$$
$$Z_4 = \sigma_\infty(\frac{\partial f_1}{\partial \omega}I_1 + \frac{\partial f_3}{\partial \omega}I_3 + \frac{\partial p_1}{\partial \omega}J_2). \qquad (4.49)$$

The radial system (4.47) is solved by the NAG library routine D02CAF which integrates a system of first-order ordinary differential equations over a range with suitable initial conditions, using a variable-order variable-step Adams method. Rather than using the integrals in (4.46) directly, we append the ς-derivatives of these quantities to the equivalent first order system from (4.24) and (4.25) giving a total of 17 first order equations and boundary conditions which are integrated with respect to ς, again using the NAG library routine D02CAF whenever $\bar{F}$ is called by the radial integration routine. In addition we check the accuracy of the integration by computing the accretion rate at each radius. This is found to be constant, as it should be, to at worst, within 1% over a factor 10^2 in radius.

4.3 Disc solutions

4.3.1 Testing the code

The code has been run for various values of accretion rate, external pressure and disc radius. It is essentially a modified version of the code developed in §3, and as such requires the same starting parameters, namely, $\sigma_\infty(\omega)$ and $\sigma_{\infty,\omega}(\omega)$ (4.46) which corresponds to the mass flux within the disc, and the height of the disc ς_s. The choice of ς_s has little effect on the disc

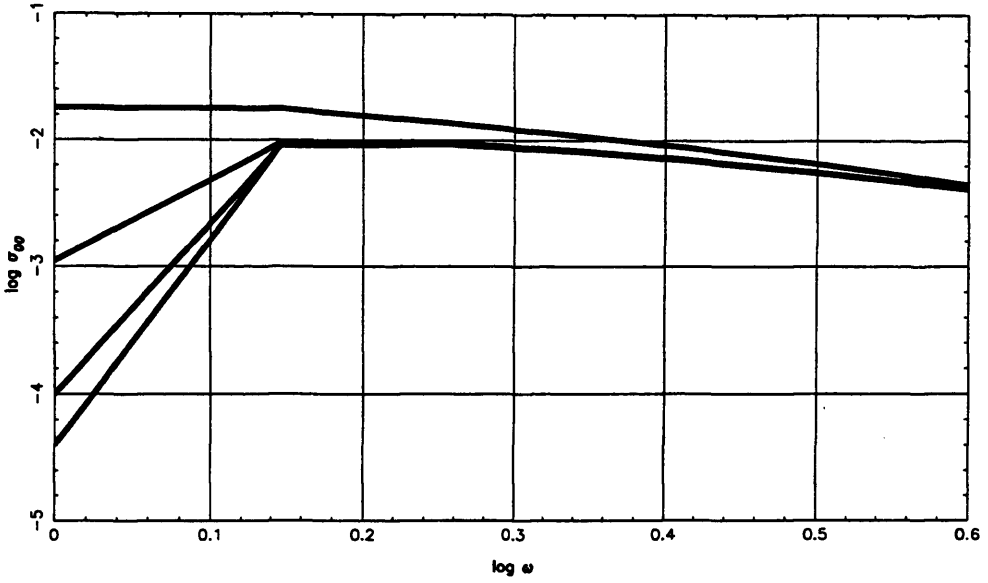

Figure 43

The evolution of the central density $\sigma_{00}(\omega)$ *with respect to the dimensionless radial variable* ω *for a range of initial disc heights (with increasing* $\sigma_{00}(\omega)$*:* $\varsigma_s = 1.5,\ 2.0,\ 2.5,\ 3.0$*).*

Disc system: $M = 10^8 M_0$, $\dot{M} = 0.1 M_0 yr^{-1}$, $\alpha = 0.1$.

solutions away from r_{in} (for a given $\dot{M}$). Figure 43 shows the evolution of the disc quantity $\sigma_{00}(\omega)$ with radial distance ω for a choice of initial disc heights ($\varsigma_s = 1.5,\ 2.0,\ 2.5,\ 3.0$, corresponding to $z_s \sim 1.5\sqrt{2}H$, $2.0\sqrt{2}H$, $2.5\sqrt{2}H$, $3\sqrt{2}H$, where H is the disc scale height (1.7) at the starting radius). The solutions correspond to a symmetric disc (i.e. equal external pressure applied to both sides of the disc) with $M = 10^8 M_0$, $\dot{M} = 0.1 M_0 yr^{-1}$ and $\alpha = 0.1$. The function $\sigma_{00}(\omega)$ rapidly converge towards equilibrium solutions. The two most extreme choices of ζ_s are within 95% of the 'average' solution by $\sim 1.3 r_{in}$. This computation has been repeated using various permutations of accretion rate, alpha parameter and external pressure with similar results.

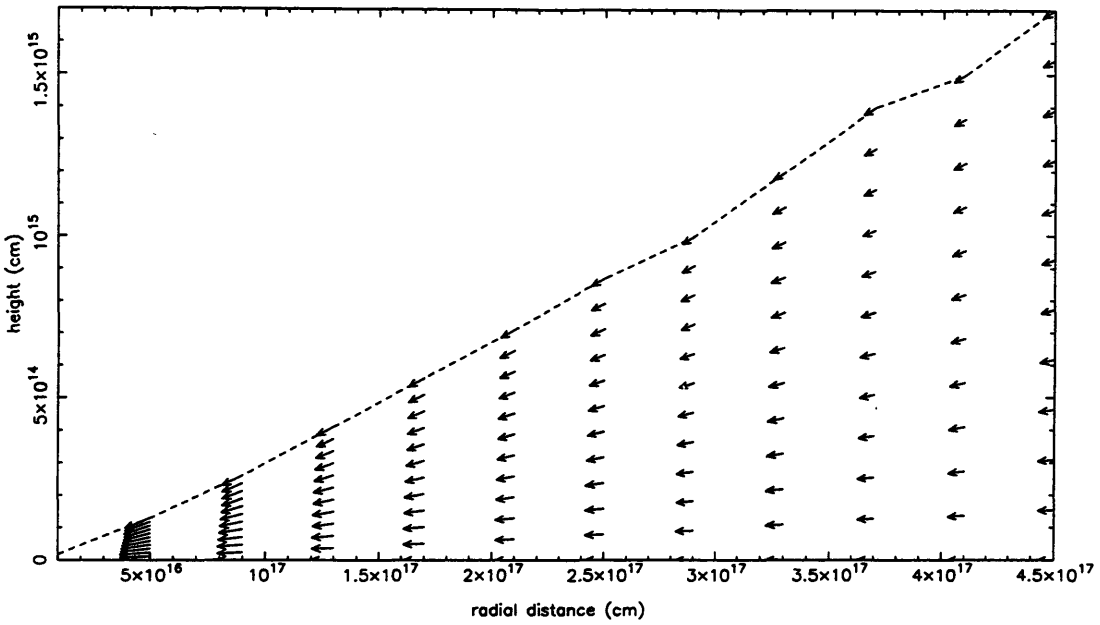

Figure 44

The r-z velocity field for a disc with $\alpha = 1.0$, $\dot{M} = 0.5 M_0 yr^{-1}$ *and* $n = 2.7$.

4.3.2 Discs subjected to small external pressures

In §2 we investigated the effect of external pressures on an optically thick accretion discs with vertical temperature gradients. We showed that, for consistency, a disc surface calculated by a pressure balance between the disc and its environment, should be at the same height as the photospheric ($\tau = 1$) surface. If the external pressure is small compared to the disc central pressure, the surface will have a (thin disc) radial dependence of $r^{9/8}$ in a disc zone which is gas pressure dominated and has Kramers' opacity. This corresponds to a disc with ς_s =constant and C_4 =constant. The value of both ς_s and C_4 will depend on the value of the viscous parameter α, the accretion rate, and the magnitude of the external pressure.

Figure 42 showed that the quantity C_4 took a variety of different forms as α was varied. The high α solutions did not pass through the $C_4 = 0$ line as ς was increased, whilst the low α solutions crossed the line several times. In this section we will investigate the internal structures of discs with different α,

subjected to small external pressures (approximately constant ς_s). In §4.2.2 we showed that to correctly consider the vertical transport of angular momentum, an external couple must be placed at the disc surface to extract the angular momentum. We have seen that because we do not know the physical processes involved at the surface, the external pressure is given as a function of r only. As a result the value of the external couple is unknown (except at $C_4 = 0$, where only one value for the couple will give a steady state solution). Therefore, in this section where ς_s and C_4 are constant (but non-zero) over the range of r, we will choose the unphysical $g_c = 0$.

Figure 44 shows the r-z velocity field for a disc with high α ($\alpha = 1.0$), $\dot{M} = 0.5 M_0 yr^{-1}$ and $n = 2.7$. For this value of α, C_4 is positive for all ς_s beyond $\varsigma_s = 3.0$ (figure 42). In this example the numerical computations give $\varsigma_s \sim 2.1$. It was shown in §4.2.3, that when α is high (low λ) the disc transports the majority of its angular momentum in the radial direction. There is no correction to Kepler motion, $V = 0$, and the radial velocity is independent of z. This is shown by the wholly inflowing disc structure of figure 44. Similar solutions were found by Kley & Lin (1992).

If the viscosity parameter is reduced to $\alpha = 0.5$, then the quantity C_4 has a zero at $\varsigma_s \sim 2.05$. Figure 45 shows the r-z velocity field for a disc with $\alpha = 0.5$ and $\varsigma_s \sim 2.3$ (negative C_4). The flow pattern is similar to those found by Urpin (1983), the low α solutions of Kley & Lin (1992), and the solutions of §2 where the vertical transport of angular momentum was ignored. There is an outflow of material near the equatorial plane, and inflow near the disc surface. The magnitude of transport of angular momentum in the vertical direction leads to values of V similar to those found in models where vertical transport is ignored (where V is non-zero, because of radial pressure gradients and the vertical gradient of the gravitational force). If ς_s is lowered, by decreasing $\dot{M}$ or increasing the external pressure, then C_4 becomes positive. This results in the velocities changing sign. Figure 46 shows the disc with $\alpha = 0.5$, but with a

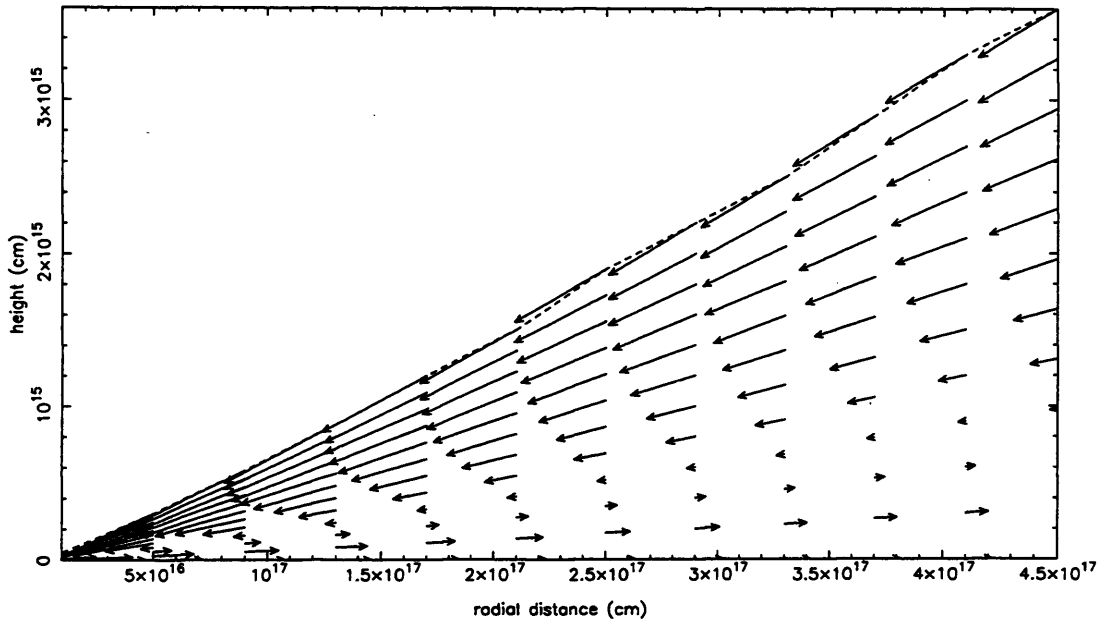

Figure 45
Same as figure 44, but with $\alpha = 0.5$ *and* $\varsigma_s \sim 2.3$ *(negative* C_4*).*

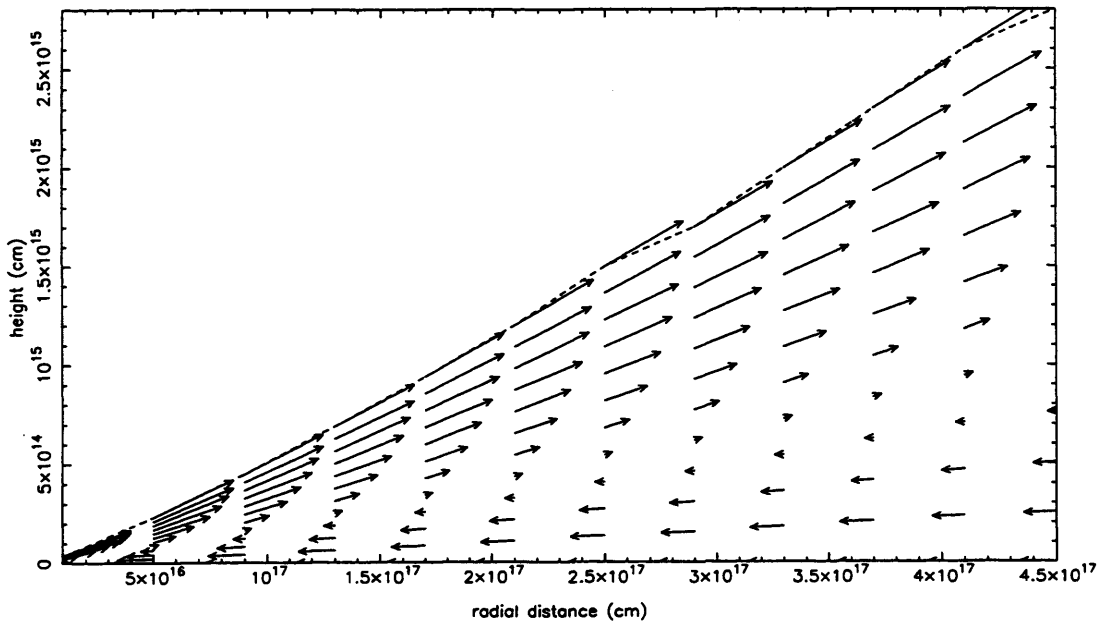

Figure 46
Same as figure 45, but with $\varsigma_s \sim 1.8$ *(positive* C_4*).*

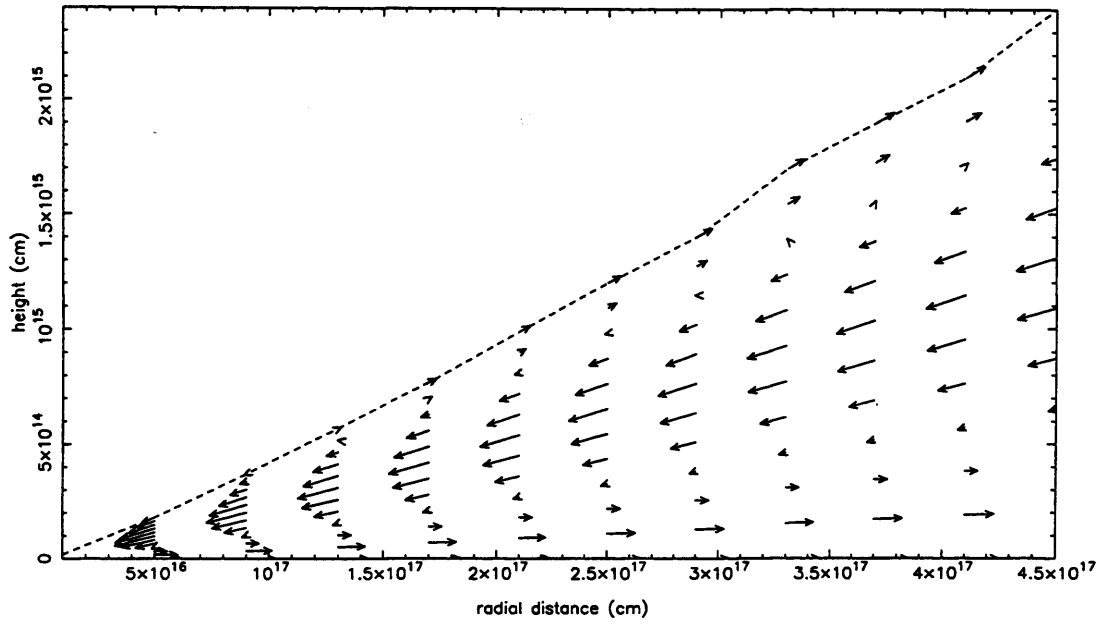

Figure 47
Same as figure 44, but with $\alpha = 0.1$ *and* $\varsigma_s \sim 1.3$ *(negative* C_4*).*

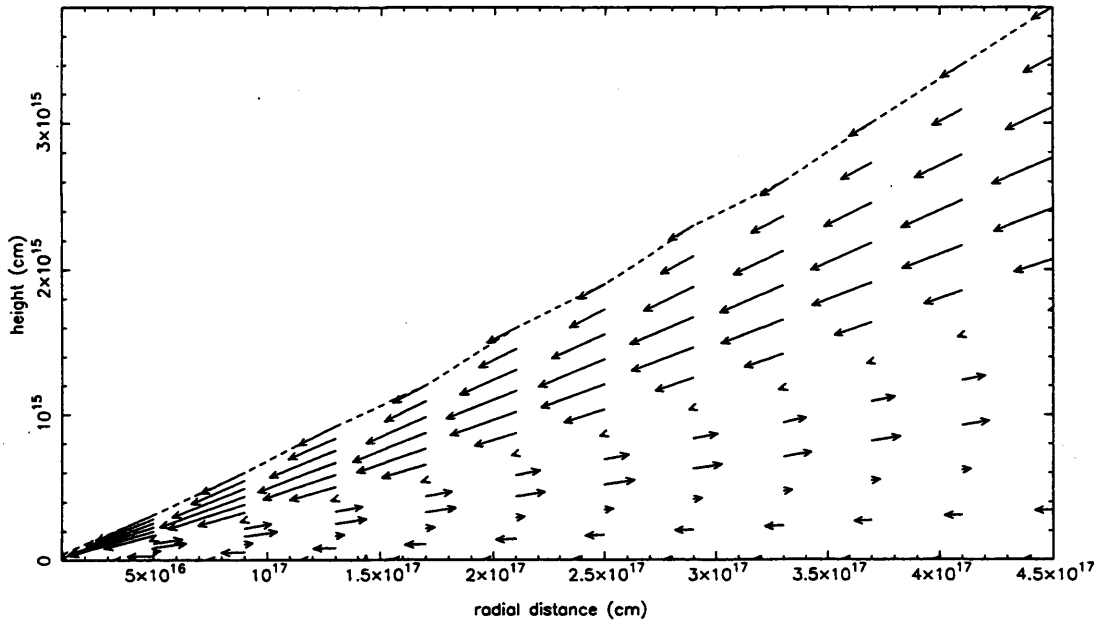

Figure 48
Same as figure 47, but with $\varsigma_s \sim 1.9$ *(positive* C_4*).*

reduced disc height of $\varsigma_s \sim 1.8$ (i.e. lower $\dot{M} = 0.2 M_0 yr^{-1}$). Now there is inflowing material near the equatorial plane and outflow near the disc surface.

Finally we look at disc solutions with low values of α. Equation (4.29), along with (4.33), (4.35) and (4.37), shows that when $\alpha << 1$ (high λ), the correction to Kepler motion, and therefore the vertical transport of angular momentum, becomes significant. Figure 47 shows the *r-z* velocity field for a disc with $\alpha = 0.1$ and $\varsigma_s \sim 1.3$. This corresponds to a negative value for C_4 (with $\alpha = 0.1$, C_4 has two zeros residing at $\varsigma_s \sim 0.8$ and $\varsigma_s \sim 1.7$). We see that the large vertical transport of angular momentum induces a flow pattern where there is outflow at both the equatorial plane and disc surface, but inflow in the middle. Altering ς_s (corresponding to changing $\dot{M}$) to make the value of C_4 positive generates the opposite velocity field. Figure 48 illustrates this with a disc whose surface is at $\varsigma_s \sim 1.9$. The equatorial plane and disc surface consist of inflowing material whilst inbetween there is outflow.

4.3.3 Discs subjected to power-law external pressures with $n < n_c$

In §2.2.4 we proposed that if a disc is subjected to an external pressure, where the external pressure takes the form of a power law (4.42), with $n < n_c$ (where $n = 21/8$ for a gas pressure dominated / Kramers' opacity disc) then the disc surface (and photospheric surface) will be 'pushed' over and begin to deviate from its thin disc radial dependence $r^{9/8}$. In this situation the value of ς_s will decrease with *r*. This corresponds to a variation in the value of C_4 with *r* (for a given α, the value of C_4 will change as ς_s moves to the left on figure 42). Therefore there is likely to be a radius at which the disc surface will move through the $C_4 = 0$ axis. We have seen in §4.2.3 that when $C_4 = 0$, the external couple g_c must be sufficient to allow (4.38) to pass through the point smoothly, if there is to be a steady state solution for the disc.

Figure 49 shows the *r-z* velocity flow for a disc with $\alpha = 0.5$, with a starting height of $\varsigma_s \sim 2.5$, being subjected to an external pressure with $n = 1$.

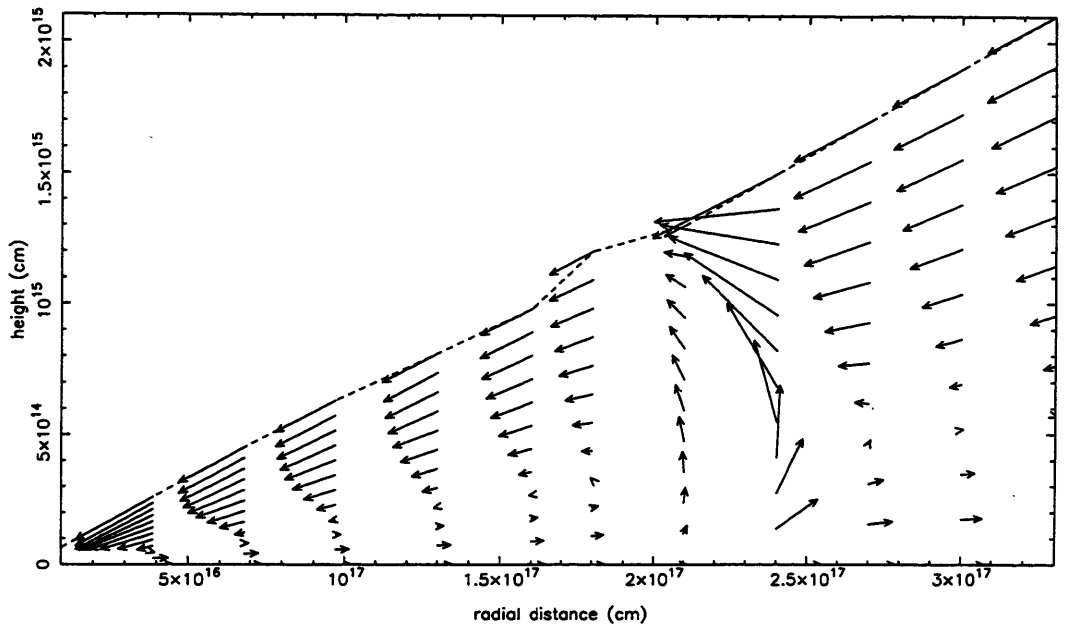

Figure 49
The r-z velocity field of a disc with $\alpha = 0.5$, $n = 1$ *and starting height* $\varsigma_s \sim 2.5$. *The disc passes through* $C_4 = 0$ *at* $\sim 2.3\times10^{17} cm$.

The starting conditions mean that C_4 is initially negative (see figure 42), with outflow near the equatorial plane and inflow near the disc surface. However, the external pressure is such that at large r it becomes significant enough to lower ς_s. At $\sim 2.3\times10^{17} cm$ the disc surface has been pushed down to such an extent that $\varsigma_s \sim 2.05$ and C_4 passes through zero, becoming positive. We saw in figure 46, that when $\alpha = 0.5$ and C_4 is positive, the velocity field shows inflow near the equatorial plane and outflow near the disc surface. To pass smoothly through the $C_4 = 0$ singularity, the correct couple is applied at the surface. Its effect on the internal structure of the disc, is to keep the flow pattern within the disc intact. There is outflow near the equatorial plane and inflow near the surface for both positive and negative values of C_4. This contrasts with the results found in §2, where the vertical transport of angular momentum was ignored, and where the velocity flow in a disc changed if the external pressure became significant compared with the central pressure of the disc. The slight

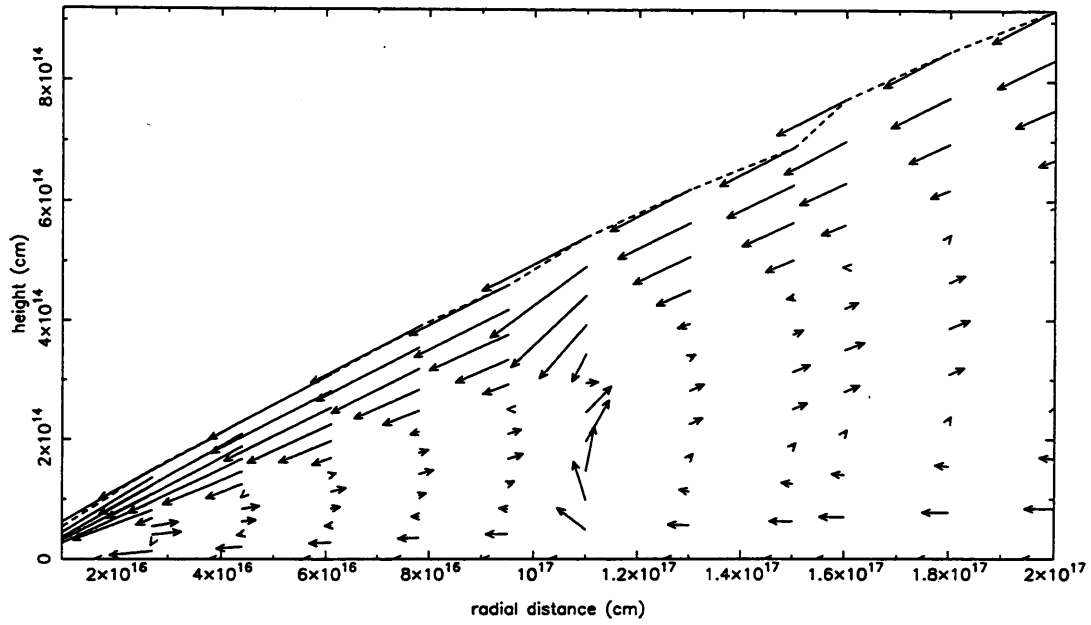

Figure 50
The r-z velocity field of a disc with $\alpha = 0.1$, $n = 1$ *and starting height* $\varsigma_s \sim 1.9$. *The disc passes through* $\varsigma_s \sim 1.9$ *at* $\sim 1.1\times10^{17} cm$.

disturbance in the velocity field in figure 49 at $\sim 2.3\times10^{17} cm$, is due to the numerical error in running the model through the $C_4 = 0$ point. If the computation were to be done more accurately then the velocity field would show a smoother transition between positive and negative values of C_4.

Figure 50 illustrates a similar transition across $C_4 = 0$. In this example $\alpha = 0.1$, the starting height is $\varsigma_s \sim 1.9$, and the external pressure power law has $n = 1$. From figure 42, we see that with these starting conditions C_4 is positive. There is inflow at both the equator and disc surface, and outflow inbetween (figure 48). The external pressure suppresses the disc surface from its thin disc radial dependence and at $\sim 1.1\times10^{17} cm$, $\varsigma_s \sim 1.7$ the value of C_4 changes from being positive to negative. As with figure 49, the external couple needed to allow the equations (4.38) to pass smoothly through $C_4 = 0$, also maintains the velocity field of the disc. Therefore we have the scenario, that even if the external pressure becomes significant, a steady state disc with vertical transport

of angular momentum will maintain the same flow pattern if α and $\dot{M}$ remain constant.

It should be noted that by changing the accretion rate, and thereby ς_s, the radius at which $C_4 = 0$ can be altered. Therefore, if the external couple and α are fixed for a given disc, steady state solutions that pass smoothly through $C_4 = 0$ can be found by specifying the correct accretion rate.

4.4 Conclusions

In this chapter we have attempted to investigate the internal structure of an accretion disc which includes the vertical transport of angular momentum. Although similar studies have been done (i.e. Urpin, 1983; Kley & Lin, 1992), these have assumed surface-less discs where angular momentum can be deposited at arbitrary heights. It is unlikely that accretion discs sit in vacuua. The surrounding medium could consist of a corona or a radially, or thermally, driven wind from the central disc regions or radio jets. In this case, a surface between the disc and its surroundings can be defined and the vertically transported angular momentum is extracted by coupling to these surroundings.

Our model simplifies the physics involved in the interaction between the disc and its environment, by assuming the external pressure varied as a fixed given function of radius only. In reality, if the disc's environment extracts angular momentum from the disc then this will in turn influence the environment and its effect on the disc, resulting in an (r, z) dependence. The magnitude of the couple extracting angular momentum from the disc is unspecified. However, if the disc surface reaches a height such that the term $C_4 = 0$ (4.40), then, if $\dot{M}$ is fixed, there is only one value for the couple, g_c which will allow a steady state solution (4.38). Alternatively, if g_c is fixed for a given disc, then there is only one value for the accretion rate $\dot{M}$, which will

allow steady-state solutions. Inclusion of feedback to the environment is unlikely to alter these conclusions.

Our results can be compared with those by Kley & Lin (1992). Discs with high viscous parameter α, consist of wholly inflowing material and all angular momentum is transported radially (i.e. figure 44). As α is reduced, the vertical transport of angular momentum increases. This is manifested by a change in the flow direction within the disc (i.e. figure 47) as the correction to Kepler motion grows. The greater the vertical transport of angular momentum, the more changes in fluid flow within the disc.

The direction of flow depends on the sign of C_4. When C_4 is negative, there is outflow along the equatorial plane, whilst if it is positive, there is inflow. When the vertical transport of angular momentum is ignored (as in §2), the equatorial fluid velocity can change sign if the disc is subjected to a significant external pressure compared with the central pressure of the disc. However when vertical transport is allowed, this directional change does not occur because the external couple required at $C_4 = 0$ is sufficient to maintain a constant flow pattern (i.e. figure 50). Therefore there is a bifurcation of flow patterns for a disc with constant α, consisting of inflow and outflow along the equatorial plane, where the direction of flow is chosen by the initial conditions.

If an $\alpha << 1$ disc is subjected to an external pressure power law such that $n < n_c$ (see §2.2.4) then the quantity C_4 will pass through zero at some radial point. As we have mentioned above, if g_c is fixed for a given disc, then there is only one value for the accretion rate $\dot{M}$, which will allow steady-state solutions. Thus, if (a) the external environment has a significant effect on the disc, and (b) there is vertical transport of angular momentum, then the steady state accretion rate is determined by the external torque on the disc. Conversely, for a general accretion rate and where the torque on the disc is fixed by the conditions in the environment, there is no steady state solution.

Chapter Five

Conclusions

In this thesis we have developed a mathematical model that describes the internal structure of an α-accretion disc. Our method is to consider the standard thin disc (Shakura & Sunyaev, 1973; Novikov & Thorne, 1973; Lynden-Bell & Pringle, 1974; §1.2) as a zero order approximation to a disc with vertical structure. The order of the approximation is controlled by the parameter $1/M^2$, where M is the Mach number of the azimuthal flow at a fiducial point. The method develops the theory of the disc analytically as far as possible, resorting to numerical methods for the final system of ordinary differential equations only.

Our model expands upon the work of other authors (i.e. Urpin, 1983; Kley & Lin, 1992) by assuming a disc surface defined by the condition of pressure balance between the disc and its environment in a special case of zero net torque at the boundary. Vertically transported angular momentum is extracted by coupling to these surroundings. In the absence of an external couple, the vertical transport of angular momentum should be ignored, as is the case in the standard thin disc.

If the external pressure is assumed to follow a radial power law dependence, i.e.

$$P_{Ext}(r) \propto r^{-n},$$

where the external pressure is small compared to the disc central pressure at the inner boundary, then a critical external pressure can be defined when $n = n_c$ (c.f. §2.2.4). If $n > n_c$ then the disc environment has little influence on the disc solutions. If $n < n_c$ then the surroundings will effect the structure of the disc at large radii. The value of n_c is found to be the predicted radial dependence of the thin disc central pressure. Sources of external pressure are discussed in §2.4.

When $n > n_c$ and the vertical transport of angular momentum is ignored, we find that the disc solutions closely resemble those of Urpin (1983) and have thin disc radial dependencies. There is an outflow of material near the equatorial plane and inflow near the disc surface. In solving the disc equations Urpin used a vertically isothermal approximation (c.f. §2.5.1). The closeness between our results and those of Urpin suggests that when investigating the velocity structure of accretion discs a vertically isothermal prescription can be adopted. This is confirmed by results in §3.6.4.

If the disc environment provides an external pressure with $n < n_c$, then at large radii the pressure can become significant enough to 'surpress' the disc, and photospheric ($\tau = 1$), surface. Our disc model predicts a lowering of the surface and a reduction in the emitted flux, and therefore the disc temperature. This could be of importance in the inner radiation pressure dominated regions. The observed collimation of radio jets would suggest that large external pressures are apparent in the inner regions of discs. The disc surface adjusts itself against the surroundings which cools the disc, thereby preventing thermal (but not viscous) instabilities. Since we have only treated a special case (zero net torque boundary condition) a more formal investigation into the stability of radiation pressure dominated discs subjected to large external pressures would be needed to establish these results conclusively.

If the observed UV variability in AGN spectra is caused by instabilities in the radiation pressure dominated regions, and can therefore give a guide to

the value of the viscous parameter α, as proposed by Siemiginowska & Czerny (1989) (c.f. §2.5.6), then disc cooling by its surroundings could imply that all AGN have a similar value of α. The observed short timescale UV variability could be due to thermal instabilities in disc systems experiencing little external pressure, whilst the longer term variability would be due to viscous instabilities in systems with significant external pressures.

If the environment exerts a pressure such that within the disc

$$\frac{P_{0,\omega}}{P_0} < -\frac{2}{\omega},$$

assuming no vertical transport of angular momentum, then the outflow of material near the equatorial plane will cease and the disc will become wholly inflowing. This means that for a given accretion rate, the surface density of the disc at a particular radius depends on the external pressure being applied by the disc environment. This could be of importance when determining the stability of the disc equilibrium solutions (see §2.5.4). By investigating discs that are partially ionised (where an S-shaped $\dot{M}(\Sigma)$ curve has been predicted; Clarke, 1988), the ability of the external pressure to influence the evolution of the disc (either limit-cycle or thermal runaway) could be studied.

A limitation of our model is that it can only describe optically thick accretion discs (i.e. where the (pressure balance) disc surface is at the same height as the photospheric surface). This results from our use of the NAG routine D02HBF to solve the disc equations (see §2.2.4). By using the NAG routine D02SAF, a modified blackbody condition could be applied at the photospheric surface, and a flux limiting diffusion equation (i.e. 2.12) used. This would allow us to investigate optically thick discs with optically thin atmospheres (c.f. §1.9). Attempts were made to use this routine, but it has proved difficult to apply.

When the vertical transport of angular momentum is included, our results can be compared with those of Kley & Lin (1992). Discs with high α consist of wholly inflowing material, and all angular momentum is transported radially. As α is reduced, the vertical transport of angular momentum increases. This manifests itself by changing the flow direction within the disc as the correction to Kepler motion grows. The greater the vertical transport of angular momentum, the greater the changes in fluid flow. We find a bifurcation of flow patterns for a disc with constant α, consisting of inflow and outflow along the equatorial plane, where the direction of flow is determined by the initial conditions. If $n < n_c$ then the steady state accretion rate is determined by the external torque on the disc. Therefore, for a given accretion rate and an applied torque that is fixed by the conditions in the environment, there is no steady state solution. Investigating the time dependency of such discs could be undertaken at a future date.

Finally, in §3 we proposed a possible model for intrinsically one-sided radio sources. This assumed that the inner disc solutions could be described by a series of steady state systems and depended on assuming a finite perturbation to generate asymmetric states. To obtain a complete picture we should follow a dynamically evolving disc over the full mass losing region and include the effects of mass and angular momentum loss consistently.

We have attempted to show in this thesis the potential importance of considering the internal structure of thin accretion discs. In particular the possibility of spontaneous breaking of symmetry may depend on the velocity field in the disc. Further problems that must involve the internal structure are: inclusion of magnetic fields (for applications to radio galaxies), surface advection of entropy (for the possible generation of mass outflows in the inner disc), general relativistic effects (although it is not clear that these can be incorporated consistently in the present expansion scheme) and two temperature discs or ion-tori (for the prediction of spectral properties).

References

Abramowicz, M.A. (1981) *Nature*, **294**, 235.

Abramowicz, M.A., Czerny, B., Lasota, J.P. & Szuszkiewicz, E. (1988) *Ap.J.*, **332**, 646.

Alexander, D.R., Johnson, H.R. & Rypma, R.L. (1983) *Ap.J.*, **272**, 773.

Arnaud K.A.et al. (1985) *Mon.Not.R.Astr.Soc.*, **217**, 105.

Bath, G.T.& Pringle, J.E. (1982) *Mon.Not.R.Astr.Soc.*, **199**, 267.

Begelman, M.C., McKee, C.F. & Shields, G.A. (1983) *Ap.J.*, **271**, 70.

Begelman, M.C. & McKee, C.F. (1983) *Ap.J.*, **271**, 89.

Begelman, M.C., Blandford, R.D. & Rees, M.J. (1984) *Rev.Mod.Phys.*, **56**, 255-351.

Betchtold, J. et al. (1984) *Ap.J.*, **281**, 76.

Betchtold, J., Czerny, B., Elvis, M., Fabbiano, G. & Green, R.F. (1987) *Ap.J.*, **314**, 699.

Blandford, R.D. (1979) in *Active Galactic Nuclei* ed. by C.Hazard & S.Mitton, Cambridge, p241.

Blandford, R.D. & Znajek, R.L. (1977) *Mon.Not.R.Astr.Soc.*, **179**, 433.

Blumenthal, G.R., Yang, L.T. & Lin, D.N.C. (1984) *Ap.J.*, **287**, 774.

Bridle, A.H. & Perley, R.A. (1984) *Ann.Rev.Astr.Ap.*, **22**, 319.

Bridle, A.H., Perley, R.A. & Henriksen, R.N. (1986) *Astron.J.*, **92**, 534.

Caditz, D. (1993) *Ap.J.*, **411**, 103.

Callahan, P.S. (1977) *Astr. and Ap.*, **59**, 127.

Canizares, C.R. & White, J.L. (1989) *Ap.J.*, **339**, 27.

Cannizzo, J.K. & Wheeler, J.C. (1984) *Ap.J.Suppl.*, **55**, 367.

Cannizzo, J.K. & Reiff, C.M. (1992) *Ap.J.*, **385**, 87.

Cannizzo, J.K. (1992) *Ap.J.*, **385**, 94.

Cao, X. (1992) *Astr. and Ap.*, **262**, 350.

Celotti, A., Fabian, A.C., Rees, M.J. (1992) *Mon.Not.R.Astr.Soc.*, **255**, 419.

Chakrabarti, S.K. & Khanna, R. (1992) *Mon.Not.R.Astr.Soc.*, **256**, 300.

Chen, X. & Taam, R.E. (1993) *Ap.J.*, **412**, 254.

Chen, X. (1994) *submitted.*

Chen, X. (1995) *Ap.J.*, **448**, 803.

Chen, X., Abramowicz, M.A., Lasota, J-P., Narayan, R. & Yi, I. (1995) *Ap.J.Letter*, **443**, L61.

Chevalier, R.A. & Klein, R.I. (1979) *Ap.J.*, **234**, 597.

Christianen, W.A., Pacholcyzk, A.G. & Scott, J.S. (1982) *IAU Circ.*, **97**, 51.

Clarke, D., Karpik, S. & Henriksen, R.N. (1985) *Ap.J.Suppl.*, **58**, 81.

Clarke, C.J. (1988) *Mon.Not.R.Astr.Soc.*, **235**, 881.

Clavel, J. et al. (1992) *Ap.J.*, **393**, 113.

Collin-Souffrin, S. (1994) in *Theory of Accretion Discs - 2*, ed. by J. Wolfgang et al., Kluwer, p 195.

Collin-Souffrin, S. & Dumont, A.M. (1990) *Astr. and Ap.*, **229**, 292.

Coppi, P., Blandford, R.D. & Rees, M.J. (1993) *Mon.Not.R.Astr.Soc.*, **262**, 603.

Cox, A.N. & Stewart, J.N. (1970) *Ap.J.Suppl.*, **19**, 243.

Cunningham, C. (1975) *Ap.J.*, **202**, 788.

Cunningham, C. (1976) *Ap.J.*, **208**, 534.

Czerny, B., Czerny, M. & Grindlay, J.E. (1986), *Ap.J.*, **311**, 241.

Czerny, B. & Elvis, M. (1987) *Ap.J.*, **321**, 305.

de Kool, M. & Begelman, M.C. (1989) *Nature*, **338**, 484.

Dermer, C.D., Liang, E.P. & Canfield,E. (1991) *Ap.J.*, **369**, 410.

Eardley, D.M, Lightman, A.P., Payne, D.G. & Shapiro, S.L. (1978) *Ap.J.*, **224**, 53.

Eddington, A.S. (1925) *Observatory*, **48**, 73.

Eggum, G.E., Coroniti, F.V. & Katz J.I. (1985) *Ap.J. Letter*, **298**, L41.

Eggum, G.E., Coroniti, F.V. & Katz J.I. (1987) *Ap.J.*, **323**, 634.

Ekers, R.D. (1982) *IAU Circ.*, **97**, 465.

Elvis, M., Wilkes, B.J. & Tanabaum, H. (1985) *Ap.J.*, **292**, 357.

Elvis, M. et al., (1986) *Ap.J.*, **310**, 291.

Fanaroff, B.L. & Riley, J.M. (1974) *Mon.Not.R.Astr.Soc.*, **167**, 31.

Fabian, A.C., Guilbert, P., Arnaud, K., Shafer, R., Tennant, A & Ward, M. (1986) *Mon.Not.R.Astr.Soc.*, **218**, 457.

Feretti, L., Comorette, G., Giovannini, G., Venturi, T. & Wehrle, A.E. (1993) *Ap.J.*, **408**, 446.

Ferland, G.J., Korista, K.T. & Peterson, B.M. (1990) *Ap.J. Letter*, **363**, 121.

Frank, J., King, A.R. & Raine, D.J. (1992) in *Accretion Power in Astrophysics*, Cambridge.

Garrington, S.T. & Conway, R.G. (1991) *Mon.Not.R.Astr.Soc.*, **250**, 198.

Garrington, S.T., Conway, R.G. & Leahy, J.P. (1991) *Mon.Not.R.Astr.Soc.*, **250**, 171.

George, I.M., Warwick, R.S. & Bromage, G.E. (1988) *Mon.Not.R.Astr.Soc.*, **232**, 793.

Glatzel, W. (1992) *Mon.Not.R.Astr.Soc.*, **257**, 572.

Grindlay, J.E. (1976) *Comments on Astrophys.*, **VI**, 165.

Guilbert, P.W. & Stepney, R. (1985) *Mon.Not.R.Astr.Soc.*, **212**, 523.

Hargrave, P.J. & Ryle, M. (1976) *Mon.Not.R.Astr.Soc.*, **175**, 481.

Hjellming, R.M. & Rupen, M.P. (1995) *Nature*, **375**, 464.

Hummel, C.A. et al. (1992) *Astr. and Ap.*, **257**, 489.

Jones, B.C. & Raine, D.J. (1980) *Astr. and Ap.*, **81**, 128.

Jones, D.L. (1986) *Ap.J.*, **309**, L5.

Kapahi, V.K. (1981) *J.Ap.Astr.*, **2**, 43.

Kato, S. (1978) *Mon.Not.R.Astr.Soc.*, **185**, 629.

Kato, S., Honma, F. & Matsumoto, R. (1988) *Mon.Not.R.Astr.Soc.*, **231**, 37.

Kippenhahn, R. & Thomas, H. C. (1982) *Astr. and Ap.*, **114**, 77.

Kley, W. & Lin, D.N.C. (1992) *Ap.J.*, **397**, 600.

Kley, W. (1994) in *Theory of Accretion Discs - 2*, ed. by J. Wolfgang et al., Kluwer, p 175.

Krautter, A., Henriksen, R.N. & Lake, K. (1983) *Ap.J.*, **269**, 81.

Kumar, S. & Coleman, C.S. (1993) *Mon.Not.R.Astr.Soc.*, **260**, 323.

Kumar, S., Coleman, C.S. & Kley, W. (1994) *Mon.Not.R.Astr.Soc.*, **266**, 379.

Kusonose, M. & Takshara, F. (1988) *Publ.Astron.Soc.Jpn.*, **40**, 435.

Kusunose, M. & Mineshige, S. (1992) *Ap.J.*, **392**, 653.

Kusonose, M. & Mineshige, S. (1994) *Ap.J.*, **423**, 600.

Laor, A. & Netzer, H. (1989) *Mon.Not.R.Astr.Soc.*, **238**, 897.

Lasota, J.P. (1994) in *Theory of Accretion Discs - 2*, ed. by J. Wolfgang et al., Kluwer, p 341.

Levermore, D.C & Pomraning, G.C. (1981) *Ap.J.*, **248**, 321.

Liang, E.P.T. (1977) *Ap.J.Letter*, **211**, L67.

Liang, E.P.T. & Thompson, K.A. (1980) *Ap.J.*, **240**, 271.

Lightman, A.P. (1974) *Ap.J.*, **194**, 429.

Lightman, A.P. & Eardley, D.M. (1974) *Ap.J. Letter*, **187**, L1.

Lin, D.N.C. & Pringle, J.E. (1987) *Mon.Not.R.Astr.Soc.*, **225**, 607.

Lin, D.N.C. & Shields, G.A. (1986) *Ap.J.*, **305**, 28.

Litchfield, S.J., King, A.R. & Brooker, J.R. (1989) *Mon.Not.R.Astr.Soc.*, **237**, 1067.

Lovelace, R.V.E., Wang, J.C.L. & Sulkanen, M.E. (1987) *Ap.J.*, **315**, 504.

Lynden-Bell, D. & Pringle, J.E. (1974) *Mon.Not.R.Astr.Soc.*, **168**, 603.

Macklin, J.T. (1981) *Mon.Not.R.Astr.Soc.*, **196**, 967.

Madau, P. (1988) *Ap.J.*, **327**, 116.

Malkan, M.A. & Sargent, W.L.W. (1982) *Ap.J.*, **254**, 22.

Malkan, M.A. (1983) *Ap.J.*, **268**, 582.

Malkan, M.A. (1991), in *Physics of Active Galactic Nuclei*, ed. by Holt, Neff & Urry, AIP.

Maraschi, L. & Molendi, S. (1990) *Ap.J.*, **353**, 452.

Mathews, N.G. & Ferland, G.J. (1987) *Ap.J.*, **232**, 456.

Meier, D.L. (1979) *Ap.J.*, **223**, 664.

Meyer, F. & Meyer-Hofmeister (1983) *Astr. and Ap.*, **128**, 420.

Miley, G. (1980) *Ann.Rev.Astr.Ap.*, **18**, 165.

Milsom, J.A., Chen, X. & Taam, R.E. (1994) *Ap.J.*, **421**, 668.

Mineshige, S. & Shields, G.A. (1990) *Ap.J.*, **351**, 47.

Molendi, S., Maraschi, L. & Stella, L. (1992) *Mon.Not.R.Astr.Soc.*, **255**, 27.

Muchotrzeb-Czerny, B. (1986) *Acta Astr.*, **36**, 1.

Narayan, K. & Goodman J. (1989) in *Theory of Accretion Discs*, F.Meyer et al. eds., Kluwer, p 231.

Narayan, R. & Popham, R. (1993) *Nature*, **362**, 820.

Narayan, R. & Yi, I. (1994) *Ap.J.Letter.*, **428**, L13.

Neff, S.G. & Rudnick, L. (1980) *Mon.Not.R.Astr.Soc.*, **192**, 531.

Novikov, I.D. & Thorne, K.S. (1973) in *Black Holes*, ed. by C. DeWitt & B. DeWitt, New York: Gordon & Breach, p 343.

O'Reilly, M.D. & Raine, D.J. (1991) in *Structure and Emission Properties of Accretion Discs*, ed. by C. Bertout et al. Edition Froni'eres, Gif sur Yvette p 509.

Okazaki, A.T., Kato, S. & Fukue, J. (1987) *Publ.Astron.Soc.Jpn.*, **39**, 457.

Paczynski, B. & Wiita, P.J. (1980) *Astr. and Ap.*, **88**, 23.

Payne, D.G. & Eardley, D.M. (1977) *Astrophys.Letter*, **19**, 39.

Perley, R.A., Bridle, A.H. & Willis, A.G. (1984) *Ap.J.Suppl.*, **54**, 291.

Perley, R.A., Dreher, J.W. & Cowan, J.J. (1984) *Ap.J.*, **285**, L35.

Pollack, J.B., McKay, C.P. & Chritofferson, B.M. (1985) *Icarus*, **64**, 471.

Pounds, K.A., Strange, V.J., Turner, T.J. King, A.R. & Czerny, B. (1984) *Mon.Not.R.Astr.Soc.*, **224**, 443.

Pounds, K.A., Nandra, K., Stewart, G.C. & Leighly, K. (1989) *Mon.Not.R.Astr.Soc.*, **240**, 769.

Pringle, J.E. (1981) *Ann.Rev.Astr.Ap.*, **19**, 137.

Pringle, J.E., Rees, M.J. & Pacholczyk, A.G. (1973) *Astr. and Ap.*, **29**, 179.

Rees, M.J., Begelman, M.C. & Blandford, R.D. (1981) *Ann.N.Y.Acad.Sci.*, **375**, 254.

Robson, D.W. (1981) *Nature*, **294**, 59.

Ross, R.R., Fabian, A.C. & Mineshige, S. (1992) *Mon.Not.R.Astr.Soc.*, **258**, 189.

Ross, R.R. & Fabian, A.C. (1993) *Mon.Not.R.Astr.Soc.*, **261**, 74.

Roxburgh, I.W. (1966) *Mon.Not.R.Astr.Soc.*, **132**, 261.

Rudnick, L. (1982) in *IAU Symposium 97, Extragalactic Radio Sources*, ed. D.S. Heeschen & C.M. Wade (Dordrecht: Reidel), p211.

Rudnick, L. & Edgar, B.K. (1984) *Ap.J.*, **279**, 74.

Rybicki, G.B. & Lightman, A.P. (1979) in *Radiative Processes in Astrophysics*, New York: Wiley.

Ryle, M. & Longair, M.S. (1967) *Mon.Not.R.Astr.Soc.*, **136**, 123.

Saikia, D.J., Jenor, W., Muxlow, T.W.B. & Tzioumis, A.K. (1989) *Nature*, **339**, 286.

Saikia, D.J. & Wiita, P.J. (1982) *Mon.Not.R.Astr.Soc.*, **200**, 83.

Saxton, R.D., Turner,M.J.L., Williams, O.R., Stewart, G.C., Ohashi, T. & Kii, T. (1993) *Mon.Not.R.Astr.Soc.*, **262**, 63.

Schilizzi, R.T. & de Bruyn, A.G. (1983) *Nature*, **303**, 26.

Shakura, N.I. & Sunyaev, R.A. (1973) *Astr. and Ap.*, **24**, 337.

Shakura, N.I. & Sunyaev, R.A. (1976) *Mon.Not.R.Astr.Soc.*, **175**, 613.

Shakura, N.I., Sunyaev, R.A. & Zilitinkevich, S.S. (1978) *Astr. and Ap.*, **62**, 179.

Shapiro, N.I., Lightman, A.P. & Eardley, D.M. (1976) *Ap.J.*, **204**, 187.

Shimura, T. & Takahara, F. (1993) *Ap.J.*, **419**, 78.

Shklovsky, I.S. (1977) *Astr.Zh.*, **53**, 713.

Siemiginowska, A. (1988) *Acta Astr.*, **38**, 21.

Siemiginowska, A. & Czerny, B. (1989) *Mon.Not.R.Astr.Soc.*, **239**, 289.

Silk, J. & Arons, J. (1975) *Ap.J.Letter*, **200**, L131.

Smith, M.D. & Raine, D.J. (1985) *Mon.Not.R.Astr.Soc.*, **212**, 425.

Sun, W.H. & Malkan, M.A. (1989) *Ap.J.*, **246**, 38.

Szuszkiewicz, E., Malkan, M.A. & Abramowicz, M.A. (1995) *submitted.*

Tribble, P.C. (1992) *Mon.Not.R.Astr.Soc.*, **256**, 281.

Tritz, B.G. (1990) *PhD Thesis.*

Urpin, V.A. (1983) *Astro. & Space Sci.*, **90**, 79.

van Groningen, E., Miley, G.K. & Norman, C. (1980) *Astr. and Ap.*, **90**, L7.

Vogt, H. (1925) *Astron. Nachr*, **223**, 229.

Wandel, A. & Petrosian, V. (1988) *Ap.J.Letter*, **329**, L11.

Wang, J.C.L., Sulkanen, M.E. & Lovelace, R.V.E. (1990) *Ap.J.*, **355**, 38.

Wang, J.C.L., Sulkanen, M.E. & Lovelace, R.V.E. (1992) *Ap.J.*, **390**, 46.

Wiita, P.J. (1978a) *Ap.J.*, **221**, 42.

Wiita, P.J. (1978b) *Ap.J.*, **221**, 436.

Wiita, P.J. & Siah, M.J. (1981) *Ap.J.*, **243**, 710.

White, T.R. & Lightman A.P. (1989) *Ap.J.*, **340**, 1024.

Wu, X., Yang, L. & Yang, P. (1994) *Mon.Not.R.Astr.Soc.*, **270**, 465.

Yu, W., Yang, L. & Wu, X. (1994) *Mon.Not.R.Astr.Soc.*, **270**, 131.

Zdziarski, A.A. & Coppi, P.S. (1991) *Ap.J.*, **376**, 480.